Neurodevelopmental Alterations in Idiopathic and Isogenic iPSC-derived Psychiatric Disease Models

Dissertation

der Mathematisch-Naturwissenschaftlichen Fakultät

der Eberhard Karls Universität Tübingen

zur Erlangung des Grades eines

Doktors der Naturwissenschaften

(Dr. rer. nat.)

vorgelegt von

Johanna Heider

aus Bergisch-Gladbach

Tübingen

2024

Gedruckt mit Genehmigung der Mathematisch-Naturwissenschaftlichen Fakultät der Eberhard Karls Universität Tübingen.

Tag der mündlichen Qualifikation:	23.09.2024
Dekan:	Prof. Dr. Thilo Stehle
1. Berichterstatter/-in:	Prof. Dr. Hansjürgen Volkmer
2. Berichterstatter/-in:	Prof. Dr. Andrea Burgalossi

Table of contents

List of Figures

List of Tables

Abbreviations

AD2	Ascl1 + Dlx2
ASCL1	Achaete-scute homolog 1
AUC	Area under the curve
BDNF	Brain-derived neurotrophic factor
bFGF	Basic fibroblast growth factor
CDK1	Cyclin-dependent kinase 1
CNS	Central nervous system
CNTF	Ciliary neurotrophic factor
CNV	Copy number variant
CRISPR	Clustered regularly interspaced short palindromic repeats
crRNA	CRISPR RNA
CTR	Control
DISC1	Disrupted in schizophrenia 1
DIV	Day in vitro
DLX2	Distal-less homeobox 2
DMEM	Dulbecco's Modified Eagle Medium
DMSO	Dimethyl sulfoxide
dNTP	Deoxynucleotide triphosphate
DPBS	Dulbecco's Phosphate-Buffered Saline
DSB	Double strand break
E-I	Excitatory-inhibitory
FACS	Fluorescence-activated cell sorting
FCS	Fetal calve serum
FGAs	First-generation antipsychotics
FWHM	Full width at half maximum
GABA	Gamma-aminobutyric acid
GAD	Glutamate decarboxylase
GAPDH	Glyceraldehyde 3-phosphate dehydrogenase
gDNA	Genomic DNA
GDNF	Glial cell line-derived neurotrophic factor
GFP	Green fluorescent protein
gRNA/sgRNA	(single) guide RNA
GWAS	Genome-wide association study
HCA	High-content analysis
IL	Interleukin
Indel	Insertion-deletion
iPSC	Induced pluripotent stem cells
LEF1	Lymphoid enhancer-binding factor 1
LPS	Lipopolysaccharide
NEHJ	Non-homologous end joining

NeuM	Neuronal medium
NGN2	Neurogenin 2
NPC	Neural progenitor cell
OCT4	Octamer-binding transcription factor 4
PAM	Protospacer adjacent motif
PBS	Phosphate-buffered saline
PCR	Polymerase chain reaction
PET	Positron emission tomography
PFA	Paraformaldehyde
PFC	Prefrontal cortex
PI	Propidium iodide
PLO	Poly-L-ornithine
PSD	Postsynaptic density
PV	Parvalbumin
ROI	Region of interest
RT	Room temperature
RT-PCR	Reverse transcription polymerase chain reaction
SCF	Stem cell factor
SCZ	Schizophrenia spectrum disorder
SEM	Standard error of the mean
SGAs	Second-generation antipsychotics
SNP	Single nucleotide polymorphism
SOX	SRY related HMG box transcription factor
SSEA-4	Stage-specific embryonic antigen 4
SST	Somatostatin
STR	Short tandem repeat
TGF	Transforming growth factor
TPO	Thrombopoietin
tracrRNA	Trans-activating CRISPR RNA
VEGF	Vascular endothelial growth factor
vGAT	Vesicular GABA transporter
vGLUT	Vesicular glutamate transporter
WT	Wild-type

Abstract

Deregulated synaptic connectivity and neuronal activity are suggested to play an important role in the pathology of neuropsychiatric disorders. According to a popular hypothesis in the field, an imbalance between excitatory and inhibitory neurotransmission in the prefrontal cortical microcircuitry contributes to a disruption of neuronal network activity, which is involved in higher cognitive processing and affected in neuropsychiatric diseases such as schizophrenia spectrum disorder (SCZ). SCZ is a spectrum of severe and highly complex neurodevelopmental diseases, characterized by a variety of symptoms including hallucinations, emotional and cognitive deficits. Genetic risk, as well as adverse environmental impacts to the developing brain (e.g. neuroinflammation) are thought to contribute to the manifestation of the disease. To date, there is no curative treatment for SCZ, which can partially be attributed to the lack of functional insight into the underlying cellular and molecular mechanisms.

To investigate excitation-inhibition imbalance in SCZ and related neuropsychiatric diseases, an optimized human *in vitro* model of the developing cortical microcircuitry, composed of induced pluripotent stem cell (iPSC)-derived glutamatergic and GABAergic cortical neurons was employed (E-I co-cultures). Two approaches of *in vitro* disease modeling were explored: both iPSC derived directly from patients with idiopathic SCZ, as well as an isogenic disease model in which mutations in iPSC were introduced into the neuropsychiatric risk gene *DISC1*, were studied.

Patient-derived neural progenitor cells revealed decreased neuronal differentiation efficiency and altered cell cycle control. For the first time, cell-type specific analysis was employed in patient-derived E-I co-cultures, which identified aberrant synapse formation and altered neuronal single-cell and network activity in SCZ. To investigate the impact of neuroinflammation on synapse formation, patient-derived microglia were added to E-I co-cultures. Here, a reduction of inhibitory synaptic terminals was observed, suggesting a cell-type specific aberrant microglia-neuron interaction.

To generate an isogenic disease model, mutations were introduced into the neuropsychiatric risk gene *DISC1* in a healthy iPSC line using CRISPR-Cas9 gene-editing. In mutant E-I co-cultures, synaptic excitation-inhibition imbalance was shifted due to increased inhibitory input, which was linked to increased differentiation efficiency of mutant neurons towards the GABAergic lineage.

Overall, the E-I co-culture system provided novel insights into synaptic connectivity and neuronal functionality in psychiatric diseases. Idiopathic and isogenic disease models shared

synaptic excitation-inhibition imbalance as an overarching phenotype, although different types of neurons were primarily affected in the two models.

Zusammenfassung

Aberrante synaptische Konnektivität und neuronale Aktivität spielen eine zentrale Rolle in der Pathologie neuropsychiatrischer Störungen. Einer weit verbreiteten Hypothese zufolge trägt ein Ungleichgewicht zwischen exzitatorischer und inhibitorischer Neurotransmission in den Mikroschaltkreisen des präfrontalen Kortex zu einer Störung der neuronalen Netzwerkaktivität bei, welche wesentlich bei der Verarbeitung komplexer, kognitiver Prozesse beteiligt ist und bei neuropsychiatrischen Erkrankungen wie der Schizophrenie-Spektrum-Störung (SCZ) beeinträchtigt ist. SCZ ist ein Spektrum schwerer und hochkomplexer neurologischer Entwicklungskrankheiten, die durch eine Vielzahl von Symptomen wie Halluzinationen, emotionalen und kognitiven Defiziten gekennzeichnet sind. Es wird angenommen, dass genetische Risikofaktoren sowie negative Umwelteinflüsse auf das sich entwickelnde Gehirn (z. B. Neuroinflammation) zur Manifestation der Krankheit beitragen. Bis heute gibt es keine Kausaltherapie für SCZ, was zum Teil auf den Mangel an bisherigen Erkenntnissen bezüglich der zugrunde liegenden zellulären und molekularen Mechanismen der Erkrankung zurückgeführt werden kann.

Um das Ungleichgewicht zwischen neuronaler Exzitation und Inhibition bei SCZ und verwandten neuropsychiatrischen Erkrankungen zu untersuchen, wurde ein optimiertes humanes *in-vitro*-Modell der sich entwickelnden kortikalen Mikroschaltkreise verwendet, das sich aus glutamatergen und GABAergen kortikalen Neuronen, differenziert aus induzierten pluripotenten Stammzellen (iPSC), zusammensetzt (E-I Co-Kulturen). Es wurden zwei Ansätze zur *in-vitro*-Krankheitsmodellierung untersucht: iPSC die direkt von Patienten mit idiopathischer SCZ reprogrammiert wurden, als auch ein isogenes Krankheitsmodell, bei dem Mutationen in das neuropsychiatrische Risikogen *DISC1* der iPSC eingebracht wurden.

Patientenabgeleitete neuronale Vorläuferzellen wiesen eine verminderte neuronale Differenzierungseffizienz und eine veränderte Zellzykluskontrolle auf. Zum ersten Mal wurde eine zelltypspezifische Analyse in von Patienten stammenden E-I Co-Kulturen durchgeführt, die Störungen der Synapsenbildung und eine veränderte neuronale Einzelzell- und Netzwerkaktivität in SCZ ergab. Um den Einfluss neuroinflammatorischer Prozesse auf die Synapsenbildung zu untersuchen, wurden aus Patientenzellen differenzierte Mikroglia mit E-I Co-Kulturen kombiniert. Hier zeigt sich eine Verringerung der inhibitorischen synaptischen Terminale, was auf eine zelltypspezifische aberrante Mikroglia-Neuron-Interaktion hindeutet.

Um ein isogenes Krankheitsmodell zu generieren, wurden Mutationen in das *DISC1*-Gen einer gesunden iPSC-Linie mit Hilfe von CRISPR-Cas9 eingebracht. In E-I-Co-Kulturen mit *DISC1* Mutation wurde eine Verschiebung der E-I Balance beobachtet, welche auf erhöhten

inhibitorischen Input zurückzuführen war. Dies konnte mit einer erhöhten Differenzierungseffizienz der Zellen mit DISC1 Mutation in Richtung der GABAergen-Linie in Verbindung gebracht werden.

Zusammenfassend konnten durch das E-I Co-Kultursystem neue Erkenntnisse über die synaptische Konnektivität und die neuronale Funktionalität bei psychiatrischen Erkrankungen gewonnen werden. Idiopathische und isogene Krankheitsmodelle wiesen als übergreifenden Phänotyp ein Ungleichgewicht zwischen Exzitation und Inhibition auf, auch wenn diese sich in unterschiedlichen neuronalen Zelltypen manifestierte.

1. Introduction

1.1. Schizophrenia spectrum disorders

1.1.1 Symptoms

Schizophrenia spectrum disorders (SCZ) are a group of highly complex neuropsychiatric diseases, which are characterized by psychotic, emotional and cognitive disturbances. The term ‘Schizophrenia spectrum disorders’ was introduced to replace the formerly used term ‘Schizophrenia’ in the latest version of the Diagnostic and Statistical Manual of Mental Disorders (DSM-V), due to the notion that SCZ is not a single unique disease, but rather comprises a spectrum of closely related psychiatric diseases (1, 2).

It is estimated that ~4 in 1,000 people develop SCZ during their lifetime (3), the majority of which start experiencing the first disease symptoms in adolescence (4). The incidence of SCZ is slightly higher in men than in women (5). Tragically, patients with SCZ lose an average of 14.5 years of life (6) due to an increased overall mortality risk and an especially high risk increase of death by suicide (7).

Symptomatically, SCZ overlaps with other neuropsychiatric diseases such as autism spectrum disorder (ASD), bipolar disorder and depressive disorder (2). To facilitate a clinical distinction from these diseases, diagnostic criteria are specified in the DSM-V, according to which SCZ symptoms can be divided into three main categories: positive symptoms (hallucinations, delusions), negative symptoms (social withdrawal, apathy, emotional blunting) and cognitive symptoms (deficits in attention, memory and concentration). As SCZ is such a heterogeneous disease, some, but not all of these symptoms have to be present for diagnosis (2).

1.1.2 Genetic and environmental risk factors

Adding to this complexity, the etiology of SCZ is diverse and there is no single cause of the disease. Based on findings from twin and population studies, the heritability of SCZ is estimated to be as high as 80-85 % (8, 9). To date, five major genome-wide association studies (GWAS) have identified >200 SCZ risk loci, the majority of which has been linked to genes involved in synaptic neurotransmission, neurodevelopment and the immune system (10-14). Large exome sequencing data sets confirmed many of the risk loci from GWAS studies and their strong association with synapses and glutamatergic neurotransmission (15). Most of the

identified variants are common in the general population and, if regarded individually, have low effect sizes. Exome sequencing and family studies have been conducted in the search of rare genetic variants with larger effect sizes, which led to the identification of multiple additional SCZ risk genes. The most prominent and most extensively studied amongst these genes is Disrupted-in-Schizophrenia 1 (*DISC1*) (16, 17), which will be addressed in section **1.4** in more detail. Another previously identified SCZ risk gene is *SETD1A*, which is involved in chromatin remodeling (18), and thereby might contribute to the unique gene methylation profile that is associated with SCZ (19). Finally, several copy number variants (CNVs) have also been linked to an increased risk of developing SCZ (20, 21).

Despite the large genetic component, it is well established that gene-environment interactions play a crucial role in disease etiology and that early insults to the developing brain can increase the risk for SCZ. The notion of SCZ as a neurodevelopmental disorder was supported by the observation of cerebral atrophy and lateral ventricular enlargement in patients (22, 23), which in monozygotic twin studies was found to be only present in the twin affected by SCZ (24). It was therefore concluded that these anatomical alterations were mainly caused by environmental influences. Since then, several environmental risk factors related to prenatal and obstetric complications were linked to SCZ, such as maternal infection during pregnancy, birth during winter and advanced parental age (25-27). Additionally, trauma, low socioeconomic status, substance abuse and urban environments are associated with the disease (28-31).

1.1.3 The dopaminergic hypothesis and antipsychotic treatment

Arguably the most well-known theory of the etiology of SCZ is the dopaminergic (DA) hypothesis. Initially, the discovery that antipsychotic drugs can block dopamine D2 receptors and effectively treat psychosis led to the conclusion, that excess dopaminergic neurotransmission (hyperdopaminergia) could be one molecular driver underlying SCZ pathology (32-34). Supported by new findings from patient and animal studies, a modified version of the dopamine hypothesis emerged later on, which postulated distinctive aberrations of DA transmission in different brain regions. According to this reconceptualization, hyperdopaminergia is specific for subcortical areas (striatum), while in the frontal cortex, DA levels are reduced (hypodopaminergia) (35).

Based on the DA hypothesis, the most common drugs used to treat SCZ are antipsychotics, which show good efficacy in alleviating the positive symptoms of the disease. The major target of common antipsychotics is the DA receptor D2, which is antagonized by the drugs to block the effects of hyperdopaminergia (36). The major downside of these first-generation

antipsychotic drugs (FGAs) are the extrapyramidal side-effects, which result from the non-selective blockage of dopaminergic pathways in the brain (37), as well as their inability to address negative and cognitive symptoms (38). To circumvent these disadvantages, second-generation antipsychotics (SGAs) targeting the serotonergic receptor 5-HT2A, as well as dopamine D2 receptors, were developed. Following their discovery, it was believed that SGAs were more efficient in treating the negative and cognitive symptoms of SCZ, a belief which could not be validated through further studies (39). In addition, as many as ~ 20 % of patients do not respond to the treatment or show only a small reduction of symptoms (~ 43 %) (40). The SGA Clozapine is the only known antipsychotic so far which is effective in the treatment of about 70 % of non-responding patients (36, 39). Overall, the currently available treatment options are ineffective for a large group of patients, inefficient in treating the broad range of disease symptoms and often lead to major side effects. Consequently, there is an urgent need to identify and evaluate new drug targets in SCZ, possibly addressing other neurotransmitter systems in the brain.

1.2 Alterations of the prefrontal cortical microcircuitry in SCZ

An alternative approach for the treatment of SCZ is targeting neurons in the prefrontal cortex (PFC), as there is substantial evidence for aberrant neuronal network function in this brain region. Approximately 20 % of identified risk loci in GWAS studies are associated with the dorsolateral PFC (41), a brain region involved in higher cognitive functions such as planning and decision making (42). Anatomically, a reduction of cortical gray matter volume in patients with SCZ has been reported by multiple studies (43). Cortical thinning can already be observed in individuals at high risk of developing SCZ (44), indicating that these anatomical changes can precede the onset of symptoms and are not merely a result of antipsychotic medication. The reduction of grey matter volume in the PFC seems to be mainly attributable to reduced spine density and dendritic complexity (45). A recent PET imaging study, for example, reported synapse loss in the cortical areas of seven out of eight SCZ patients using a PET tracer against synaptic vesicle glycoprotein 2A (SV2A) (46). This finding was supported by a meta-analysis of post-mortem studies showing a reduction of synaptophysin expression in the frontal cortex in SCZ (47).

1.2.1 Phenotypes of glutamatergic and GABAergic neurons in SCZ

The human PFC is composed of two major neuronal populations: ~ 80 % excitatory, glutamatergic pyramidal neurons and ~ 20 % inhibitory, GABAergic interneurons (48, 49).

Interneurons can be further subdivided into different subgroups based on their morphology, biochemical and functional properties, as well as their connectivity with pyramidal neurons. The most abundant class of interneurons in the human cortex are Parvalbumin (PV)-expressing interneurons, followed by the second-largest class of Somatostatin (SST)-expressing interneurons (50).

In SCZ, both glutamatergic and GABAergic neurons are affected. In line with the findings from genetic studies reporting aberrant gene expression related to glutamatergic neurotransmission (see section 1.1.2), one of the most consistently reported phenotypes of cortical glutamatergic neurons is synaptic loss and impaired synaptic function. Multiple SCZ risk genes are associated with the glutamatergic synapse, and include AMPA and NMDA receptors subunits, postsynaptic scaffolding proteins (PSD95, Homer, SHANK), calcium signaling proteins, vesicle trafficking proteins and cell adhesion proteins (51-53). The NMDA receptor has become a particular focus of SCZ research, ever since it was discovered that application of Ketamine, a NMDA receptor antagonist, reproduces positive, negative and cognitive disease symptoms (54). Subsequently, it was discovered that there is a reduction of NR1 mRNA expression, a subunit of the NMDA receptor, in the PFC of SCZ patients (55). Finally, elevated levels of glutamate were reported in patients (56). These findings led to the formulation of the glutamate hypothesis of SCZ, according to which a hypofunction of the NMDA receptor leads to a compensatory increase in glutamate levels (57). Besides the strong synaptic phenotype, additional morphological alterations reported in glutamatergic neurons include a reduction in neurite length, complexity, and soma volume (58, 59).

Research on cortical interneurons in SCZ suggests that PV interneurons seem to be most strongly affected, with the most consistent finding being a reduction of PV mRNA and protein levels in these neurons (60-62). The density of PV interneurons however is likely unaffected (62-64). There is also evidence for altered inhibitory synaptic function, as mRNA levels of the $GABA_A$ receptor α1 subunit (65) and of the GABA-synthesizing enzyme glutamate decarboxylase (GAD67) were reported to be reduced in SCZ (66-68). There are only few studies so far on other types of interneurons, however lower levels of SST mRNA have also been linked to SCZ (69, 70).

1.2.2 Excitation-inhibition imbalance in SCZ

As outlined above, both glutamatergic and GABAergic cortical neurons are affected in SCZ, and morphological studies primarily demonstrate synaptic alterations of these neurons. During

development, the formation of refined synaptic connections is crucial for proper network function of the cortical circuitry. In the human cortex, the interplay of excitatory and inhibitory neurons underlies the generation of cortical oscillations, which are rhythmic pattern of neuronal network activity and can occur in different frequency ranges (71). *In vivo*, fast spiking PV interneurons are the major driver of these oscillations by pacing the activity of principal pyramidal neurons (72). In patients with SCZ, high-frequency cortical gamma-oscillations (30-100 Hz) are disturbed (73, 74). Y-oscillations play an important role in working memory and sensory information processing, which are both processes impaired in patients with SCZ (75). Based on this evidence, it has been proposed that the synaptic deficits of cortical neurons might result in an imbalance of excitation and inhibition (E-I imbalance), which consequently leads to impaired network synchronicity in SCZ (75). Besides SCZ, E-I imbalance has also been associated with other neurodevelopmental disorders, including ASD (76) and Rett Syndrome (77).

1.3 Neuroinflammation in SCZ

A further central hypothesis in SCZ research describes the influence of elevated neuroinflammation as a contributing factor to the synaptic pathology of the disease. Evidence supporting this theory has been obtained from various studies which identified elevated levels of pro-inflammatory cytokines in the cerebrospinal fluid and blood from patients (78-80). Microglia are the innate immune cells of the brain and can release pro-inflammatory cytokines and chemokines in response to inflammation or infection in the CNS (81, 82). In this activated state, microglia can also phagocytose pathogens or cell debris, release reactive oxygen species and can interact with the complement system (83). In SCZ, PET imaging and postmortem studies have demonstrated elevated activation of microglia (84, 85), supporting the notion that microglia substantially contribute to the increased neuroinflammatory state in patients.

A further important function of microglia is their involvement in synaptic pruning during brain development, a critical process during which the initially excess number of synaptic connections is reduced by the removal of weak or redundant synapses to refine the neuronal network (84, 86). Synaptic pruning is primarily mediated through complement signaling. Complement components such as C1q can be expressed at the synapse to ‘tag’ weak synapses and induce formation of complement component C3 via C4/C2, which can be recognized by the microglial complement receptor CR3 to induce engulfment of the synapse (87).

As the number of synapses is reportedly reduced in SCZ, the neuroinflammatory hypothesis proposes that aberrant interactions between activated microglia and neurons during synaptic pruning might contribute to the loss of synapses observed in patients (88). In line with this, the strongest genetic association with SCZ was reported for the major histocompatibility complex (MHC) (13), which has been linked to genetic variation in the complement gene *C4* (89).

1.4 DISC1: a risk gene for neuropsychiatric disorders

In 1990, a balanced chromosomal translocation between chromosomes 1 and 11 (t(1;11)(q42.1;q14.3) was identified in a Scottish family, where the mutation co-segregated with cases of SCZ, bipolar disorder and major depression (17). 10 years later, two genes were identified at the translocation breakpoint on chromosome 1, which were named disrupted-in-Schizophrenia 1 and 2 (*DISC1, DISC2*) (16). While *DISC1* is a protein coding gene, *DISC2* encodes for a non-coding RNA antisense to *DISC1* and could thereby regulate the expression of the latter (16). Therefore, *DISC1* became the primary focus of research in the following decades and further genetic studies were able to identify mutations in the gene in individuals with psychiatric illness. In an American family, a 4bp deletion in exon 12, resulting in a C-terminal frameshift, was identified in patients diagnosed with SCZ, but was absent in healthy controls (90). Additionally, multiple heterozygous ultra-rare single-nucleotide polymorphisms (SNPs) in *DISC1* were identified by linkage analysis and shown to be associated with SCZ, bipolar disorder and major depression (91-94).

1.4.1 The DISC1 protein

In its full-length version, the DISC1 protein consists of 854 amino acids and encompasses 13 exons. Structurally, DISC1 consists of an N-terminal head domain and a coiled-coil C-terminal region (16, 95). The pre-translational processing of DISC1 is highly complex, and there are more than 50 previously reported differentially spliced isoforms (96). DISC1 is ubiquitously expressed in the brain and shows a peak of expression during development, which declines after birth (97). On a subcellular level, DISC1 is also expressed throughout the cell and is localized, for example, at the membrane, cytoskeleton, synapses and mitochondria (98). Concordant with its high expression during development, DISC1 is involved in important processes in developing neurons, such as neurite outgrowth (99, 100), axon outgrowth (101), intracellular transport, neural progenitor proliferation (102), spine formation; maturation and

synaptic plasticity (98). The notion of DISC1 as a hub protein is further underlined by its large interactome, of which several interacting proteins have themselves been associated with SCZ (103).

1.4.2 Neuronal phenotypes associated with DISC1 mutation: animal models

Phenotypes associated with mutations in DISC1 have been extensively studied in mice. For this purpose, different mutant models have been developed to interfere with the function of the protein (90, 104). One of these rodent models mimics the truncating exon 12 patient mutation (90), which was shown to result in fewer excitatory synapses, impaired synaptic plasticity and memory deficits (105). In a second commonly used model, two stop codons were introduced into exons 7 and 8, leading to elimination of the full-length isoform of DISC1 (104). Using this model, researchers have identified a loss of granule cell spines, reduced dendritic length in cortical neurons, decreased PFC volume, altered synaptic plasticity, and working memory deficits in mutant mice (104, 106). In missense mutation models (e.g. L100P and Q31L), similar phenotypes were identified, including reduced brain volume, dendritic complexity, and behavioral alterations (107-109). In summary, mutations in *DISC1* which have been studied in rodents converge on common phenotypes such as altered synaptic morphology and function, dendritic structure, and behavioral deficits.

1.5 iPSC-based *in vitro* model systems for the study of SCZ

1.5.1 Reprogramming and characteristics of iPSC

One promising approach for the identification of new drug targets is *in vitro* disease modeling, using iPSC. Most of our current knowledge about cellular and molecular mechanisms involved in SCZ stems from post-mortem and animal studies. However, post-mortem studies only represent the end point of the disease, and the results can be heavily influenced by confounding factors such as primary cause of death and the effects of life-long treatment with antipsychotic medication. While animal models are very valuable to establish a link between cellular mechanisms and behavior, the rodent brain is less complex than the human brain, often limiting translatability of the findings and contributing to the significant failure rate of drug candidates in clinical trials (110).

The generation of iPSC was first achieved almost two decades ago in 2006 by Yamanaka and colleagues through introduction of the four transcription factors OCT3/4, SOX2, c-Myc and KLF4 into fibroblasts (111). The thereby generated cells were able to theoretically self-renew indefinitely (stemness) and were pluripotent, which describes their potential to differentiate into cells of the three germ layers ectoderm, mesoderm and endoderm (112). Until today, many different somatic source cell types and reprogramming strategies for the generation of iPSC have been identified. iPSC can, for example, be reprogrammed from fibroblasts, blood cells and melanocytes by both viral and non-viral, integrative and non-integrative overexpression of different pluripotency factors (113). In the past years, researchers have made enormous progress in using iPSC to generate cell types from various tissues, with the aim to model diseases in 2D or 3D culture systems with a human genetic background (114).

1.5.2 Strategies of *in vitro* disease modeling with iPSC

There are two main strategies which are employed to model diseases *in vitro* using iPSC: reprogramming of iPSC directly from patients, or the introduction/correction of disease-associated mutations by gene-editing. A major advantage of using patient-derived iPSC is that the genetic background of the individual donor is preserved, which is especially relevant for the study of complex genetic diseases like SCZ, which are caused by an interplay of multiple genetic variants. However, there is considerable inter-individual variation between lines from different donors in idiopathic cohorts, making it difficult to identify overarching phenotypes with smaller samples sizes (115). These difficulties can be circumvented by using isogenic pairs of iPSC to study the influence of one or few risk variants on a disease. Using gene editing, mutations can either be introduced into healthy control iPSC lines, or can be corrected in patient-derived lines, the latter bearing the advantage that other genetic disease-influencing factors of the patient are preserved.

1.5.3 CRISPR-Cas9 gene editing

There are various possibilities to interfere with the function of a gene or RNA, including RNA interference or gene editing by zinc-finger nucleases or transcription activator–like effector nucleases (TALENs) (116, 117). Today, the state-of-the-art method for site-specific gene-editing is the CRISPR-Cas9 (clustered regularly interspaced short palindromic repeats (CRISPR)–CRISPR-associated protein 9 (Cas9)) system. The system was originally discovered in bacteria, where it serves as an adaptive defense system against infections (118). The CRISPR array is a specialized region in the bacterial genome, in which sequences of

foreign DNA (e.g. from invading phages), are integrated as spacers between palindromic repeat sequences. The CRISPR array can be transcribed into CRISPR-RNA (crRNA), consisting of both spacers and repeats. A tracrRNA, complementary to the repeat sequence, can bind the crRNA, and forms a complex with the enzyme Cas9. In mammalian cells, crRNAs typically have a length of 20 nucleotides and can be fused to the tracrRNA to generate a guide RNA (gRNA). The Cas9/guide-RNA complexes can recognize and cleave the DNA or RNA of the previous invader during subsequent infections. To do so, Cas9 recognizes a short conserved genomic sequence, the protospacer adjacent motif (PAM), and will induce a double strand break (DSB) 2-5 base pairs (bp) upstream of the sequence (119).

Once a DSB has been introduced, there are two main cellular repair mechanisms which researchers can exploit to introduce the desired genetic mutation: non-homologous end joining (NHEJ) and homology-directed repair (HDR) (**Figure 1**). During NHEJ, endogenous DNA repair mechanisms repair the broken strand. This is however an error-prone process and can lead to the introduction of small insertions or deletions of a few nucleotides (Indel mutations). Indel mutations can then cause frameshifts, which might result in premature termination codons and protein truncation (120). HDR is a precise repair mechanism, for which the cell uses a DNA template strand to repair the break. This template strand can be introduced into the cell by researchers to either knock-in a gene or replace an existing gene (120).

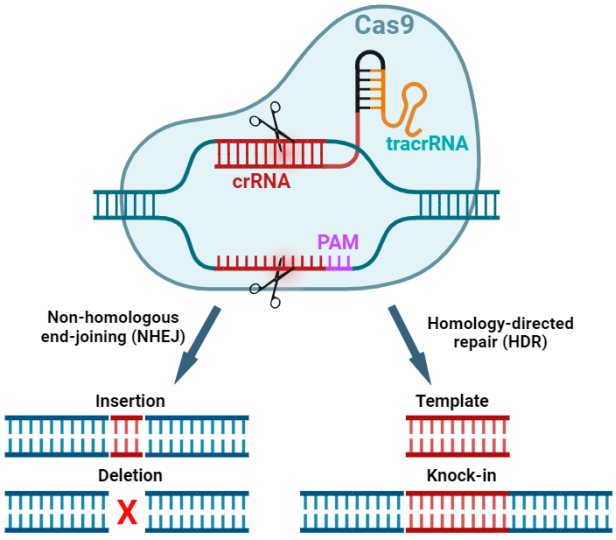

Figure 1 Strategies for CRISPR-Cas9 gene editing.
The enzyme Cas9 is guided to the DNA target sequence by a homologous gRNA (crRNA+tracrRNA). Cas9 then induces double strand breaks upstream of the PAM sequence. During error-prone NHEJ, small insertions or deletions (Indel mutations) can be generated. For HDR, a DNA template is provided and can be used by the cell to repair the break (knock-in). Figure created with BioRender.com.

1.5.4 Differentiation of iPSC into neuronal cell types

To model a CNS disease *in vitro*, an ideal model should contain multiple neuronal cell types of interest to recapitulate the cell-cell interactions *in vivo* as closely as possible. Until today, various differentiation protocols for the generation of different types of neurons, astrocytes and microglia have been established. For the differentiation of iPSC, two main approaches can be pursued. The first is undirected differentiation, which aims to recapitulate the developmental patterning *in vivo* by timed addition of growth factors and cytokines as cues for cell type/tissue-specific differentiation. The second approach is directed differentiation via the forced overexpression of lineage-specific transcription factors (121). Although undirected differentiation protocols follow physiological processes more closely, they often take considerably longer than the more artificial process of accelerated directed differentiation. Additionally, the cultures obtained by growth factor-based differentiation are often heterogeneous, containing a mixture of neuronal and glial cell types. While this can be beneficial to study cell-cell interactions, the ratios of cell types often varies between individual differentiations. In contrast, directed differentiation protocols allow the generation of more homogenous populations of single cell types and are often combined with antibiotic selection to increase the purity of the resultant cultures (121).

Directed differentiation protocols have been established to generate different types of neurons, including cortical glutamatergic (122) and cortical GABAergic neurons (123), by overexpression of the lineage-specific transcription factors Neurogenin 2 (NGN2) and ASCL1+DLX2 (AD2), respectively. Transient overexpression of the transcription factors in these protocols is achieved by doxycycline-dependent induction via the tetON-system. The tetON-system allows controlled initiation of gene expression by binding of the co-transduced reverse tetracycline transactivator (rtTA) to the tetracycline response element (TRE) in the presence of the tetracycline derivate doxycycline (124). After as little as 3-5 weeks of differentiation, induced neurons were demonstrated to express cell-type specific markers and generate spontaneous neuronal activity (122, 123, 125). For the differentiation of microglia and astrocytes from iPSC, protocols were optimized to allow accelerated differentiation within ~30 days (126, 127). Most glial differentiation protocols rely on growth-factor based undirected differentiation (81), however, attempts have been made to generate astrocytes and microglia by transcription factor overexpression (128, 129).

Overall, a plethora of protocols has been established to achieve the robust and efficient generation of neuronal and glial cell types from iPSC, which resemble their *in vivo* counterparts as closely as possible. Nevertheless, an important aspect that needs to be considered is that iPSC-derived cell types still depict immature characteristics and are comparable to human

neurons at the fetal or embryonic stage (130). While this characteristic might limit the directed translatability of the findings to the adult brain, it can be beneficial for the study of neurodevelopmental diseases such as SCZ, in which it is hypothesized that disruptions of neuronal circuit formation during early brain development lead to the manifestation of the disease at later stages (131).

1.6 Aim of this thesis

As outlined above, SCZ is a highly heterogenous, complex and multifactorial disease. Aberrations during early neurodevelopment, as well as neuroinflammation, likely contribute to alterations of synapse formation and neuronal functionality in the cortical microcircuitry. The aim of this thesis is to identify and characterize phenotypic signatures of neuropsychiatric diseases using iPSC-derived idiopathic and isogenic models of the developing cortical circuitry.

To cover a broad spectrum of potential disease-influencing mechanisms, the following aspects will be addressed in this thesis:

1) *Analysis of early neurodevelopmental aberrations in SCZ*

Using SCZ patient-derived neural progenitor cells (NPC), it will be investigated whether healthy and diseased cells can already be distinguished at this early developmental stage. This is of particular interest as potential alterations in NPC might translate to aberrations in differentiating neurons.

2) *Analysis of aberrant synaptic connectivity in the cortical microcircuitry in SCZ*

The focus of previous iPSC-based research has been the study of glutamatergic neurons. On the other hand, there is very little evidence on disease-related alterations of GABAergic neurons and the interaction of both cell types. As cortical E-I imbalance is suggested to contribute to the pathology of various neuropsychiatric disorders, a co-culture system comprising both glutamatergic and GABAergic neurons at defined ratios will be employed for the study of synaptic phenotypes underlying E-I imbalance in SCZ. Cell-type specific analysis in E-I co-cultures will be used to help decipher the cellular origin of potential aberrations.

3) *Analysis of aberrant neuronal activity as a consequence of synaptic phenotypes*

To study the functional implication of aberrant synaptic connectivity in SCZ patient-derived neurons, measurements of cell-type specific single-cell and network activity will be conducted in E-I co-cultures.

4) *Analysis of the impact of neuroinflammation in SCZ*

The interaction of microglia and neurons will be explored to shed light on the impact of neuroinflammation on the activity and synapse formation of developing neurons. E-I co-cultures will additionally allow to investigate, whether microglia exert a preferential influence on either glutamatergic or GABAergic neurons. Finally, the potential of anti-inflammatory treatment of patient microglia will be explored.

5) Comparison of idiopathic and isogenic DISC1 mutant disease models

In addition to the idiopathic patient-derived model, an isogenic disease model for the study of highly penetrant risk variants will be generated by introduction of mutations in the neuropsychiatric risk gene *DISC1*. Synapse formation of mutant neurons will be studied to evaluate whether phenotypes can be observed that are solely attributable to the mutation in a single risk gene. By comparing the phenotypes of the patient-derived and the *DISC1* model system, common and diverging phenotypes will be discussed with the aim to identify shared disease mechanisms of SCZ and other neuropsychiatric disorders.

2. Material and Methods

2.1 Material

2.1.1 iPSC lines

Table 1 iPSC lines used in this study.

Unique cell line identifier = registry number in Human Pluripotent Stem Cell Registry (Charité, Berlin, www.hpscreg.eu).

iPSC line (internal name)	Unique cell line identifier	Gender	Source cell type	Age at donation
CTR1	TMOi001-A	female	cord blood-derived CD34+ progenitors	neonate
CTR2	NMIi010-A	male	peripheral-blood derived CD34+ hematopoietic stem/progenitor cells	49
CTR3	NMIi001-A	female	skin fibroblasts	28
CTR4	n/a	male	skin fibroblasts	70
SCZ1	NMIi002-A	male	skin fibroblasts	37
SCZ2	NMIi003-A	female	skin fibroblasts	54
SCZ4	NMIi004-A	male	skin fibroblasts	50
SCZ5	NMIi006-A	female	skin fibroblasts	27

2.1.2 General materials

Table 2 General Materials

Materials	Manufacturer
37 µm Reversible Strainers	STEMCELL Technologies, Canada
96 well µClear® half-area plate, black	Greiner Bio-One, Germany
96 well µClear® plate, black	Greiner Bio-One, Germany
96-well microplate, V-bottom, PS, clear	Greiner Bio-One, Germany
AggreWell™800	STEMCELL Technologies, Canada
Cell culture flasks (25, 75, 175 cm2)	Corning Inc., USA
Cryo tubes	Greiner Bio-One, Germany
Eppendorf Tubes (1.5, 2 ml)	Eppendorf AG, Germany
Falcon Tubes (15, 50 ml)	Greiner Bio-One, Germany
Mr. Frosty™ Freezing Container	Thermo Fisher Scientific, USA
Parafilm	Pechiney Plastic Packaging
Pipette boy ROTILABO®	Carl Roth GmbH + Co. KG, Germany

Pipettes (0.1-2.5 µl; 0.5-10 µl; 10-200 µl; 100-1000 µl)	Eppendorf AG, Germany
Plastic pipettes	Greiner Bio-One, Germany
Protein LoBind® Tubes	Eppendorf AG, Germany
Well plates (96, 48, 24, 12, 6 well)	Corning Inc., USA

2.1.3 Instruments/devices

Table 3 Instruments/devices

Instrument	Manufacturer
Amaxa 4D Nucleofector® system	Lonza, Germany
Cell Observer SD	Zeiss, Germany
Centrifuge 5804 R	Eppendorf AG, Germany
CO2 incubator	WTC Binder, Germany
FACS LSRFortessa™	BD Biosciences, USA
FACS Melody™	BD Biosciences, USA
Gel electrophoresis chamber HU13	Thermo Fisher Scientific, USA
GelDoc Go Imaging System	Bio-Rad Laboratories, USA
ImageXpress Micro Confocal High-Content Imaging System	Molecular Devices, USA
IncuCyte	Sartorius AG, Germany
Nanodrop, Spectrophotometer ND-100	Thermo Fisher Scientific, USA
Nucleocounter NC-200	Chemometech A/S, Denmark
pH meter	Mettler Toledo, Germany
Thermocycler Biometra TOne	Analytic Jena AG, Germany
Thermomixer (comfort)	Eppendorf AG, Germany
Ultracentrifuge Sorvall™ MX Plus Mikro	Thermo Fisher Scientific, USA
Vortex Genie 2	Scientific Industries Inc., USA
Water bath WBT 6	Carl Roth GmbH + Co. KG, Germany

2.1.4 Chemicals and reagents

Table 4 Chemicals and reagents

Reagent	Manufacturer	Catalogue number
1 kb Plus DNA Ladder	New England Biolabs, USA	N3200
Accutase	Sigma-Aldrich, USA	A6964
Agarose Broad Range	Carl Roth GmbH + Co. KG, Germany	T846
Alt-R CRISPR-Cas9 crRNA	Integrated DNA Technologies, USA	Design-ID: Hs.Cas9.DISC1.1.AC
Alt-R® CRISPR-Cas9 tracrRNA, ATTO 550	Integrated DNA Technologies, USA	1072532

Alt-R® S.p. Cas9 Nuclease V3	Integrated DNA Technologies, USA	1081058
Ascorbic Acid 2 Phosphate	Sigma-Aldrich, USA	A8960
B27 Plus™ supplement	Thermo Fisher Scientific, USA	A3582801
B-27™ Supplement (50x), minus Vitamin A	Thermo Fisher Scientific, USA	12587010
Blocking Reagent BMB	Roche, Switzerland	11112589001
Bovine Serum Albumin (BSA) Fraction V	Carl Roth GmbH + Co. KG, Germany	1ETA.4
Cal-520™ AM	AAT Bioquest Inc., USA	ABD-21130
Calbyrte™ 590 AM	AAT Bioquest Inc., USA	ABD-20701
Chemically-Defined Lipid Concentrate	Thermo Fisher Scientific, USA	11905031
CHIR99021	Tocris Bioscience, UK	4423
CloneR™ 2	STEMCELL Technologies, Canada	100-0691
Dimethylsulfoxid (DMSO)	Carl Roth GmbH + Co. KG, Germany	A994.1
DNase Stop Solution	Promega GmbH, Germany	Z312C-C
dNTPs	New England Biolabs, USA	N0447
Doxycycline	Sigma-Aldrich, USA	D9891
Dulbecco's phosphate buffered saline	Thermo Fisher Scientific, USA	14190094
G418	Carl Roth GmbH + Co. KG, Germany	2039
Gel Loading Dye, Purple (6X)	New England Biolabs, USA	B7024S
Glucose solution	Thermo Fisher Scientific, USA	A2494001
GlutaMAX	Thermo Fisher Scientific, USA	35050038
HEPES (1M)	Thermo Fisher Scientific, USA	15630056
Hygromycin B solution	Carl Roth GmbH + Co. KG, Germany	1287
Insulin-Transferrin-Selenium-Ethanolamine (ITS-X)	Thermo Fisher Scientific, USA	51500056
Laminin	Sigma-Aldrich, USA	L2020
L-Ascorbic Acid	Sigma-Aldrich, USA	A2078
LDN193189	STEMCELL Technologies, Canada	72147
L-Glutamine	Thermo Fisher Scientific, USA	25030024
Lipofectamine™ 2000	Thermo Fisher Scientific, USA	11668019
Matrigel ® hESC-qualified Matrix	Corning Inc., USA	354277
Midori Green Advance	NIPPON Genetics EUROPE GmbH, Germany	MG04
M-MuLV Reverse Transcriptase, 1X M-MuLV Reverse Transcriptase Reaction Buffer	New England Biolabs, USA	M0253S
N2 Supplement	Thermo Fisher Scientific, USA	17502048
Non-essential amino acids	Thermo Fisher Scientific, USA	11140035
Nuclease-free Water	New England Biolabs, USA	B1500S
Paraformaldehyd (PFA)	Carl Roth GmbH + Co. KG, Germany	0335
Penicillin/Strepomycin	Thermo Fisher Scientific, USA	15140122

Platinum II Taq Hot-Start DNA Polymerase, 5X Platinum II PCR Buffer, Platinum GC Enhancer	Thermo Fisher Scientific, USA	14966001
Poly Vinyl Alcohol (PVA)	Sigma-Aldrich, USA	P8136
Poly-L-Ornithine Solution	Sigma-Aldrich, USA	P4957
Primer „random“ (dN6-Primer)	Roche, Switzerland	11034731001
Propidium Iodide Solution	BioLegend, USA	421301
Puromycin	Thermo Fisher Scientific, USA	11113803
Ready-to-Use Packaging Plasmid Mix (pCPack2 Lentiviral Packaging Plasmid Mix)	Cellecta, Inc., USA	CPCP-K2A
RNAse A	New England Biolabs, USA	T3018L
RQ1 DNase 10x Reaction Buffer	Promega GmbH, Germany	M198A-C
RQ1 RNase-free DNase	Promega GmbH, Germany	M6101
SB431542	Bio-Techne, USA	1614
Sodium Pyruvate (100 mM)	Thermo Fisher Scientific, USA	11360070
STEMdiff™ Neural Rosette Selection Reagent	STEMCELL Technologies, Canada	05832
Triton-X-100	Carl Roth GmbH + Co. KG, Germany	3051
TrypLE	Thermo Fisher Scientific, USA	12604054
Trypsin/EDTA 0.025 %	Thermo Fisher Scientific, USA	25300054
Virusgenerierungsstuff		
XAV939	Sigma-Aldrich, USA	X3004
Y-27632	STEMCELL Technologies, Canada	72304
α-Monothioglycerol	Sigma-Aldrich, USA	M6145

2.1.5 Cytokines and growth factors

Table 5 Cytokines and growth factors

Cytokine	Manufacturer	Catalogue Number
Human Activin A	Miltenyi Biotec, Germany	130-115-008
Human bFGF	Bio-Techne, USA	233-FB-025
Human BMP-4	PeproTech, Inc., USA	120-05ET
Human GM-CSF	Miltenyi Biotec, Germany	130-093-864
Human IL-3	PeproTech, Inc., USA	200-03
Human IL-34	PeproTech, Inc., USA	200-34
Human IL-6	Miltenyi Biotec, Germany	130-095-352
Human SCF	PeproTech, Inc., USA	300-07
Human TGF-β1	PeproTech, Inc., USA	100-21
Human TPO	Miltenyi Biotec, Germany	130-095-747
Human VEGF	PeproTech, Inc., USA	100-20
Recombinant Human BDNF	PeproTech, Inc., USA	450-02
Recombinant human CNTF	PeproTech, Inc., USA	450-13

Recombinant Human GDNF	PeproTech, Inc., USA	450-10

2.1.6 Commercially available kits

Table 6 Commercially available kits

Kit	Manufacturer	Catalogue Number
Lenti-X p24 Rapid Titer Kit	Takara Bio Inc., Japan	632200
P3 Primary Cell 4D-Nucleofector X Kit L	Lonza Sales AG, Switzerland	V4XP-3012
QIAamp DNA Mini Kit	Qiagen, Germany	51304
QIAquick PCR Purification Kit	Qiagen, Germany	28104
RNeasy Mini Kit	Qiagen, Germany	74104
STEMdiff™ SMADi Neural Induction Kit	STEMCELL Technologies, Canada	08581
STEMdiff™ Trilineage Differentiation Kit	STEMCELL Technologies, Canada	05230

2.1.7 Basal media for cell culture

Table 7 Basal media for cell culture

Medium	Manufacturer	Catalogue Number
DMEM, high glucose, GlutaMAX™ Supplement	Thermo Fisher Scientific, USA	10566016
DMEM/F12, no glutamine	Thermo Fisher Scientific, USA	21331020
Fetal Bovine Serum	Thermo Fisher Scientific, USA	10270
Ham's F-12 Nutrient Mix	Thermo Fisher Scientific, USA	21765029
IMDM, no phenol red	Thermo Fisher Scientific, USA	21056023
mTeSR™ Plus	STEMCELL Technologies, Canada	100-0276
Neurobasal Plus™ Medium	Thermo Fisher Scientific, USA	A3582901
Neurobasal™ medium	Thermo Fisher Scientific, USA	21103049
Opti-MEM™, Reduced Serum Medium	Thermo Fisher Scientific, USA	31985070
STEMdiff™ Neural Progenitor Medium	STEMCELL Technologies, Canada	05833

2.1.8 Astrocyte medium

Table 8 Astrocyte medium

Component	Final concentration
DMEM, high glucose, GlutaMAX™ Supplement	1x
FCS	10 %
Penicillin/Streptomycin	1 %

Sodium Pyruvate	1 % (1mM)

2.1.9 Neuronal Medium (NeuM)

Table 9 Neuronal Medium (NeuM)

Component	Final concentration
Neurobasal Plus™ Medium	1x
B27 Plus™ supplement (50x)	1x
N2 Supplement (100x)	1x
Laminin	1 mg/ml
BDNF	50 µg/ml
GDNF	50 µg/ml
L-Ascorbic Acid	35 µg/ml
Penicilin/Streptomycin	1 %

2.1.10 Microglia differentiation/cultivation media

Table 10 Microglia differentiation/cultivation media

Component	Final concentration
a) basal medium	
IMDM, no phenol red	50 %
Ham's F-12 Nutrient Mix	50 %
Poly Vinyl Alcohol (PVA)	10 µg/ml
Ascorbic acid 2 phosphate (AA2P)	64 µg/ml
Chemically defined lipid concentrate	0.1 %
IST-X	2 %
αMTG (in IMDM)	0.0039 % (stock: 1.3 %)
GlutaMAX	1 %
Non-essential amino acids	1 %
Penicillin/Streptomycin	1 %
b) myeloid differentiation medium 1 (DIV 0-1)	
BMP4	50 ng/ml
Activin A	15 ng/ml
CHIR99021	1.5 µM
c) myeloid differentiation medium 2 (DIV 2-4)	
VEGF	50 ng/ml
bFGF	50 ng/ml
SCF	50 ng/ml
SB431542	10 µM
d) myeloid differentiation medium 3 (DIV5-9)	
VEGF	50 ng/ml
bFGF	50 ng/ml

SCF	50 ng/ml
IL-6	50 ng/ml
TPO	50 ng/ml
IL-3	50 ng/ml
e) microglia culture medium (from day 9)	
IL-34	100 ng/ml
TGF-β	50 ng/ml
GM-CSF	25 ng/ml

2.1.11 HEK293FT media

Table 11 HEK293FT media

Component	Final concentration
a) culture medium	
DMEM, high glucose, GlutaMAX™ Supplement	1x
FCS	10 %
Non-essential amino acids	1 %
G418	500 µg/ml
Penicillin/Streptomycin	1 %
b) transfection medium	
Opti-MEM™	1x
FCS	5 %
Penicillin/Streptomycin	1 %

2.1.12 N2 Neurite outgrowth medium

Table 12 N2 Neurite outgrowth medium

Component	Final concentration
DMEM/F12	1x
HEPES	15 mM
Non-essential amino acids	1 %
GlutaMAX	1 %
Glucose	1.5 %
N2 supplement (100x)	1x
SB431542	10 µM
XAV939	1 µM
LDN193189	100 nM

2.1.13 Primary antibodies

Table 13 Primary antibodies

Antibody target	Host Species	Manufacturer	Catalouge Number	Dilution
Aurora A/AIK (1G4)	rabbit	Cell Signaling Technology, USA	4718	1:100
Beta-catenin	rabbit	Cell Signaling Technology, USA	8480	1:400
Brachyury	rabbit	Abcam, UK	Ab209665	1:100
Cyclin B1 [Y106]	rabbit	Abcam, UK	ab32053	1:100
DISC1 (C-terminus, ICC analysis)	rabbit IgG	Thermo Fisher Scientific, USA	40-6800	1:250
Gephyrin	mouse IgG1, hybridoma supernatant, clone mAb7a	Synaptic Systems, Germany	147021	1:400
GFAP	rabbit	Agilent Technologies, USA	Z0334	1:500
Hoechst 33258	-	Sigma-Aldrich, USA	861405	1:800
Iba1	rabbit	Wako Pure Chemical Industries, USA	019-19741	1:1000
LEF1 (C12A5)	rabbit	Cell Signaling Technology, USA	2230	1:200
MAP2	chicken IgY	Thermo Fisher Scientific, USA	PA1-10005	1:2000
NANOG	rabbit	Cell Signaling Technology, USA	4903	1:200
NCAM (CD56)	mouse	Cell Signaling Technology, USA	3576	1:500
OCT4A	rabbit	Cell Signaling Technology, USA	2840	1:400
Pax-6	mouse	BioLegend, USA	862001	1:200
Phalloidin-Alexa Fluor 488	-	Santa Cruz Biotechnology Inc., USA	SC-363791	1:1000
PSD95 (PDZ domain)	rabbit IgG1	Synaptic Systems, Germany	124008	1:500
Somatostatin	rat IgG2b clone YC7	Sigma-Aldrich, USA	MAB354	1:500
SOX17	rabbit IgG	Cell Signaling Technology, USA	81778S	1:3200
SOX2	rabbit	Cell Signaling Technology, USA	3579	1:400
SSEA-4	mouse IgG	Cell Signaling Technology, USA	4755	1:500

TRA-1-81	mouse IgM	Cell Signaling Technology, USA	4749	1:500
vGAT cytoplasmic domain	rabbit	Synaptic Systems, Germany	131003	1:500
vGLUT1	mouse IgG	Synaptic Systems, Germany	135511	1:300
Vimentin	rabbit	Cell Signaling Technology, USA	5741	1:200
β-III-tubulin	mouse IgG2a	STEMCELL Technologies, Canada	60100	1:250

2.1.14 Secondary antibodies

Table 14 Secondary antibodies

Fluorophore	Host and target species	Manufacturer	Catalogue Number	Dilution
Alexa Fluor 405	goat anti-mouse IgY (H+L) Alexa Fluor 405	Thermo Fisher Scientific, USA	A-31553	1:150
AlexaFluor 488	goat anti-chicken IgY (H+L)	Thermo Fisher Scientific, USA	A-11039	1:400
Cy3-AffiniPure	goat anti-mouse IgG (H+L)	Jackson ImmunoResearch, UK	115-165-146	1:500
Cy3-AffiniPure	goat anti-rabbit IgG (H+L)	Jackson ImmunoResearch, UK	111-165-144	1:500
Cy5-AffiniPure	goat anti-mouse IgG (H+L)	Jackson ImmunoResearch, UK	115-175-146	1:500
Cy5-AffiniPure	goat anti-rabbit IgG (H+L)	Jackson ImmunoResearch, UK	111-175-144	1:500

2.1.15 Plasmids

Table 15 Plasmids

Plasmid	Distributor	Catalogue Number	Reference
DLX2-hygro	Addgene	97330	doi: 10.1038/nmeth.4291. 10.1038/nmeth.4291
FUdelta GW-rtTA	Addgene	19780	doi: 3(3):340-5. 10.1016/j.stem.2008.08.003

pLV-TetO-hNGN2-eGFP-Puro	Addgene	79823	doi: 10.1016/j.ymeth.2015.11.019. 10.1016/j.ymeth.2015.11.019
pLV-TetO-hNGN2-Puro	Addgene	79049	doi: 10.1016/j.ymeth.2015.11.019. 10.1016/j.ymeth.2015.11.019
TetO-Ascl1-puro	Addgene	97329	doi: 10.1038/nmeth.4291. 10.1038/nmeth.4291

2.1.16 Oligonucleotides

Table 16 Oligonucleotides

Name	Sequence (3'-5')	Amplicon length (bp)
crRNA DISC1 exon 2	CCAAGAGGCCTCTCGAGTCA	-
DISC1 Exon2_fw	GGCTACATGAGAAGCTCGA	324
DISC1 Exon2_rev	ATCCATGGCTGCAAACTCT	
hOCT3/4-S1165_fw	GAC AGG GGG AGG GGA GGA GCT AGG	144
hOCT3/4-AS1283_rev	CTT CCC TCC AAC CAG TTG CCC CAA AC	
hSOX2-S1430_fw	GGG AAA TGG GAG GGG TGC AAA AGA GG	151
hSOX2-AS1555_rev	TTG CGT GAG TGT GGA TGG GAT TGG TG	
GAPDH_fw	TCA CCA TCT TCC AGG AGC G	572
GAPDH_rev	CTG CTT CAC CAC CTT CTT GA	
ECAT4-macaca-968S_fw	CAG CCC CGA TTC TTC CAC CAG TCC C	391
ECAT4-macaca-1334AS rev	CGG AAG ATT CCC AGT CGG GTT CAC C	

2.1.17 Software

Table 17 Software

Software	Company	Version used
Fiji (based on Image J2)	National Institutes of Health, USA (Image J)	2.9
FlowJo 10	BD Biosiences,, USA	10
GraphPad Prism	GraphPad Software, USA	10.2
Imaris Bitplane	Oxford Instruments, UK	10
IncuCyte® Basic Analyzer	Sartorius AG, Germany	-

MetaXpress	Molecular Devices, USA	-
Origin	OriginLab Corporation, USA	2015G
ZEN (blue edition)	Zeiss, Germany	3.0

2.2 Methods for cell culture

2.2.1 iPSC line information

The majority of iPSC lines used in this study was previously generated from skin fibroblasts of one healthy volunteer (CTR3) and four patients with Schizophrenia spectrum disorder (SCZ1, SCZ2, SCZ4, and SCZ5) in the Molecular Neurobiology group at the NMI in Reutlingen in cooperation with the University Hospital in Tübingen (Department of Psychiatry), with positive ethical vote from the Ethics Committee of the University Hospital and Faculty of Medicine Tübingen. Reprogramming of dermal fibroblasts was achieved with a non-integrative approach by nucleofection of five plasmids expressing SOX2, OCT3/4, L-MYC, KLF4 and LIN28 (132). The CTR1 iPSC line was purchased from Thermo Fisher Scientific and was reprogrammed from umbical cord blood-derived CD34-positive progenitor cells by non-integrative transfection of OCT3/4, SOX2, KLF4, MYC, NANOG, LIN28 and SV40T-expressing plasmids (133). The CTR2 iPSC line was a gift from the Tumorbiology group at the NMI in Reutlingen, where the cells were reprogrammed from peripheral blood hematopoetic stem cells by non-integrative overexpression of OCT3/4, SOX2, KLF4, MYC, LIN28, EBNA1 and mp53DD (134). The CTR4 iPSC line was a gift from Dr. Julia Fitzgerald at the Hertie Institute for Clinical Brain Research in Tübingen and was reprogrammed from dermal fibroblasts by non-integrative nucleofection of the plasmids hOCT4, hSOX2 and hKLF4, and hL-MYC and hLIN28 (135). All iPSC lines used in this study are fully characterized and chromosomally intact (132-135). For more detailed information on all iPSC lines, see **Table 1**. For information on SCZ patient diagnosis, clinical symptoms and medication, see (136).

2.2.2 Matrigel coating

iPSC cultures were maintained on the murine basement membrane extract Matrigel to ensure consistent growth and maintenance of a pluripotent state. According to the lot-specific protein concentration, Matrigel aliquots were prepared so that one aliquot is sufficient to prepare 6 ml of coating solution. For plate coating, Matrigel was diluted 1:100 in ice-cold DMEM/F12 to prevent gelling. 1 ml of Matrigel solution was used for coating of a single well of a 6-well plate. Coated plates were incubated at 37 °C for 30 minutes before usage and could be stored for up to one week at 4 °C.

2.2.3 iPSC cultivation and propagation

iPSC were cultured in mTeSR Plus medium + 1 % Penicillin/Streptomycin on Matrigel-coated 6-well plates. Full medium changes were performed daily, on the weekends the medium was changed once. Once a week, single cell passaging of iPSC was performed using enzymatic dissociation with Accutase. The culture medium was removed and Accutase was added to the wells. Cell were then incubated for 2-3 minutes at 37°C, 5 % CO_2 until they started to detach. DMEM/F12 was added to the wells to terminate the enzymatic reaction and the resulting single cell suspension was centrifuged at 300 xg for 3 minutes. Cells were counted using the Nucleocounter NC-200 and $1.05x10^4$ viable iPSC/cm^2 were seeded per well of a 6-well plate for cultivation. iPSC were used for differentiations until passage 30.

2.2.4 iPSC cryopreservation and thawing

For cryopreservation, single cell suspensions of iPSC were obtained as described in 2.2.3. $1x10^6$ viable cells were centrifuged at 300 xg for 3 minutes, resuspended in 1 ml of mTeSR Plus + 10 % DMSO and transferred into a cryovial. Cryovials were frozen at – 80 °C in Mr. Frosty™ freezing containers overnight and kept at -150 °C for long-term storage.

Cryopreserved iPSC were thawed in a water bath at 37°C for a few minutes and transferred to Falcons containing 5 ml of DMEM/F12. Cells were centrifuged at 300 xg for 3 minutes, resuspended in mTeSR Plus with 10 µM of Y-27632 to enhance cell survival, and plated on Matrigel-coated 6-well plates.

2.2.5 Poly-L-ornithine/laminin coating

For culturing of NPC and neurons, plates were coated with Poly-L-Ornithine (PLO) and laminin. PLO was diluted 1:5 in DPBS and plates were incubated with the solution for 2h at RT. 1 ml of coating solution was used per well of a 6-well plate. Next, wells were washed once with DPBS and once with DMEM/F12, followed by incubation with 10 µg/ml laminin diluted in DMEM/F12 overnight at 37°C in the incubator. Coated plates were stored at 4 °C for up to one week.

2.2.6 NPC differentiation

NPC were differentiated from iPSC following the embryoid body (EB) protocol of the STEMdiff™ SMADi Neural Induction Kit. $2x10^6$ iPSC were seeded per well of an AggreWell™ 800 plate in 2 ml of STEMdiff™ SMADi Neural Induction medium. Prior to cell seeding, AggreWell™ plates were pre-treated with 1 ml of Anti-Adherence Rinsing Solution for 5 minutes at RT and washed once with DPBS to prevent cells from adhering to the plate bottom. AggreWell™ plates were centrifuged for 1 minute at 100 xg to make the cells condense in the microwells and facilitate EB generation. Daily 75 % medium changes were performed for 7 days with SMADi Neural Induction medium before EBs were harvested with a 37 µm reversible strainer to filter out remaining single cells. EBs from one AggreWell™ were re-plated in one well of a PLO/laminin-coated 6-well plate in 2 ml of SMADi Neural Induction medium. EBs should have adhered to the plate the following day. EBs were then cultivated for another 7 days in SMADi Neural Induction medium with daily 100 % medium changes. Afterwards, the emerging neural rosette clusters were selected with a 1.5 h treatment at 37 °C with STEMdiff™ Neural Rosette Selection Reagent. The rosette-containing clusters were selectively dislodged by pipetting with DMEM/F12, centrifuged for 3 minutes at 300 xg and re-plated into one well of a PLO/laminin-coated 6-well plate in SMADi Neural Induction medium. Once ~ 90 % confluence was reached, NPC were dissociated with Accutase and re-plated in STEMdiff™ Neural Progenitor Medium at a density of $1.05x10^4$ cells/cm^2 per well of a PLO/laminin-coated 6-well plate.

2.2.7 NPC cultivation and propagation

NPC were maintained on PLO/laminin-coated 6-well plates in STEMdiff™ Neural Progenitor Medium + 1 % Penicillin/Streptomycin. Full medium changes were performed on Mondays, Wednesdays, and Fridays. Once a week, NPC were passaged enzymatically using Accutase (as described in 2.2.3). For routine passaging, $1.05x10^4$ cells/cm^2 were seeded per well of a 6-well plate. NPC were used for differentiations until passage 10.

2.2.8 NPC thawing and cryopreservation

For cryopreservation, single cell suspensions of NPC were obtained by dissociation with Accutase. $1x10^6$ viable cells were centrifuged at 300 xg for 3 minutes, resuspended in 1 ml of Neural Progenitor Medium + 10 % DMSO and transferred into a cryovial. Cryovials were frozen

at – 80°C in Mr. Frosty™ freezing containers overnight and kept at -150 °C for long-term storage.

Cryopreserved NPC were thawed in a water bath at 37°C for a few minutes and transferred to Falcons containing 5 ml of DMEM/F12. Cells were centrifuged at 300 xg for 3 minutes, resuspended in Neural Progenitor Medium and plated on PLO/laminin-coated 6-well plates.

2.2.9 Astrocyte cell culture

Mouse astrocytes used in this study were prepared from postnatal day 1 pups by Sophia-Marie Hartmann and Sabrina Vogel. After preparation, astrocytes were cultivated in flasks until confluent and then cryopreserved (p1). Astrocytes were maintained on 6-well plates in astrocyte medium (**Table 8**). Full medium changes were performed on Mondays, Wednesdays, and Fridays. For passaging, astrocytes were enzymatically dissociated with trypsin-EDTA (0.25 %) for 5 minutes and the reaction stopped by the addition of DMEM/F12. Cells were centrifuged at 300 xg for 3 minutes and split at a ratio of 1:2-1:5. For neuronal differentiations, astrocytes were used up to passage 2. Either frozen p1 astrocytes were thawed and directly added to the cultures, or p2 astrocytes in culture were dissociated with trypsin-EDTA (0.25 %) and added to the neurons.

2.2.10 Differentiation of glutamatergic neurons by overexpression of Neurogenin 2

Differentiation of NPC into glutamatergic neurons was achieved by lentiviral overexpression of human Neurogenin 2 (NGN2), based on the protocol developed by Ho et al. with slight modifications (122). On day *in vitro* (***DIV) -1***, NPC were dissociated by Accutase treatment, and $4.21x10^4$ cells/cm^2 were seeded per well of a PLO/laminin-coated 12-well or 6-well plate in Neural Progenitor Medium, depending on the final number of neurons required. On ***DIV 0***, 24h after seeding, NPC were transduced with two lentiviral constructs, to induce the overexpression of NGN2-Puro (puromycine resistance) or NGN2-GFP-Puro under a tetracycline operator sequence (tetO) and of the reverse tetracycline transactivator protein (rtTA) (**Table 15**). On ***DIV 1***, 24h after transduction, the medium was changed to Neural Progenitor Medium containing 1 µg/ml of doxycycline, to induce doxycycline-dependent overexpression of NGN2. After 24h (***DIV 2***), the medium was changed to Neural Progenitor Medium + 1 µg/ml of doxycycline + 2 µg/ml of puromycin to select for transgene-expressing cells. Cells were selected for 24h. For assays involving NGN2 neurons in monocultures, immature neurons were detached by Accutase treatment on ***DIV 3***, resuspended in neuronal

medium (NeuM, **Table 9**) supplemented with 1 µg/ml of doxycycline, and plated at a density of $1.25x10^5$ cells/cm^2 on PLO/laminin-coated 96-half-well plates. After 2-3 h, immature neurons should have attached to the plates and mouse astrocytes were co-seeded at a ratio of 1:4 (astrocytes: neurons, see 2.2.9 for details). On Mondays, Wednesdays, and Fridays, 50 % of the medium was replaced by medium without doxycycline for sequential dilution of doxycycline. On ***DIV25***, a full medium change with NeuM + 1 µg/ml of doxycycline was performed. This additional doxycycline treatment was introduced to ensure a high expression level of GFP, which was important to distinguish NGN2 from AD2 neurons in co-culture experiments. Calcium imaging and synapse quantification experiments were performed on ***DIV28***.

2.2.11 Differentiation of GABAergic neurons by overexpression of Ascl1 and Dlx2

Differentiation of NPC into GABAergic neurons was achieved by lentiviral overexpression of mouse *Ascl1* and *Dlx2* based on the protocol developed by Barretto et al. with some additional modifications (123). On ***DIV -1***, NPC were dissociated by Accutase treatment, and $4.21x10^4$ cells/cm^2 were seeded per well of a PLO/laminin-coated 12-well or 6-well plate in Neural Progenitor Medium, depending on the final number of neurons required. On ***DIV 0***, 24h after seeding, NPC were transduced with three lentiviral constructs, to induce the overexpression of *Ascl1* and *Dlx2* under a tetO sequence and of the rtTA (**Table 15**). On ***DIV 1***, 24h after transduction, the medium was changed to Neural Progenitor Medium containing 1 µg/ml of doxycycline, to induce overexpression of the transgenes. After 24h (***DIV 2***), the medium was changed to Neural Progenitor Medium + 1 µg/ml of doxycycline + 2 µg/ml of puromycin + 250 µg/ml of hygromycin. Puromycin resistance is encoded by the Ascl1 plasmid and hygromycin resistance by the Dlx2 plasmid. Therefore, only cells expressing both transgenes were selected. For assays involving AD2 neurons in monocultures, immature neurons were detached by Accutase treatment after 24h of selection (***DIV3***), resuspended in NeuM (**Table 9**) with 1 µg/ml of doxycycline, and plated at a density of $1.25x10^5$ cells/cm^2 on PLO/laminin-coated 96-half-well plates. After 2-3 h, immature neurons should have attached to the plates and mouse astrocytes were added at a ratio of 1:4 (astrocytes: neurons). On Mondays, Wednesdays, and Fridays, 50 % of the medium was replaced by medium without doxycycline for sequential dilution of doxycycline. On ***DIV25***, a full medium change with NeuM + 1 µg/ml of doxycycline was performed. Calcium imaging and synapse quantification experiments were performed on ***DIV28***.

2.2.12 NGN2/AD2 co-culture (E-I co-culture)

To generate co-cultures of glutamatergic and GABAergic neurons (**Figure 2**), NGN2 and AD2 neurons were differentiated as described in sections 2.2.10 and 2.2.11. NGN2 and AD2 neurons which were combined into co-cultures were always derived from the same donor. NPC seeding, transduction, and selection for both types of neurons was simultaneously performed in separate wells. On ***DIV3***, NGN2 and AD2 neurons were dissociated by Accutase treatment and counted. Viable neurons were seeded into co-cultures comprising 80 % NGN2 and 20 % AD2 neurons in 96-well plates in NeuM medium (**Table 9**) + 1 µg/ml of doxycycline. For example, $2x10^4$ neurons in total were seeded per well of a 96-half-well plate, $1.6x10^4$ of which were NGN2 and $4x10^3$ of which were AD2 neurons. After 2-3 h, immature neurons should have attached to the plates and mouse astrocytes were co-seeded at a ratio of 1:4 (astrocytes: neurons). On Mondays, Wednesdays, and Fridays, 50 % of the medium was replaced by medium without doxycycline for sequential dilution of doxycycline. On ***DIV25***, a full medium change with NeuM + 1 µg/ml of doxycycline was performed. Calcium imaging and synapse quantification experiments were performed on ***DIV28***.

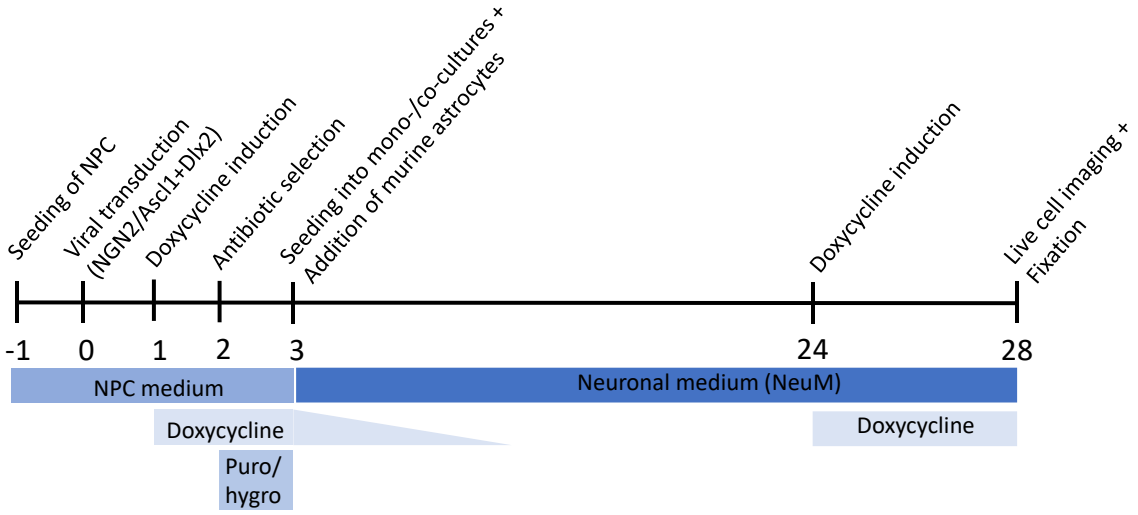

Figure 2 Schematic overview of the generation of monocultures and co-cultures of NGN2 and AD2 neurons.
NPC are transduced with lineage-specific transcription factors by lentiviral infection. Doxycycline was added to the media to induce transgene expression and transgene-expressing cells were selected by addition of suitable antibiotics for 24h (puro= puromycin, hygro= hygromycin). NGN2 and AD2 neurons were seeded into mono- or co-cultures and murine astrocytes were added for improved viability and network maturation. Neurons were cultured in NeuM media with 50 % medium changes every other day. Doxycycline was again added to the media for improved maturation four days prior to the end of the cultivation period (DIV28).

2.2.13 Microglia differentiation

Microglial cells were differentiated from iPSC by timed addition of growth factors and cytokines, following the protocol previously developed in our group and published by Breitmeyer et al. (136). Briefly, iPSC were dissociated by Accutase treatment and seeded at a density of $5x10^4$ cells/cm^2 (***DIV-2***). On ***DIV0***, the medium was replaced by basal medium + myeloid differentiation medium 1 (basal medium + supplements, see Table 10 for all microglia differentiation media) to initiate mesodermal differentiation. At ***DIV2***, SMAD inhibition was initiated by changing the medium to myeloid differentiation medium 2. At ***DIV5***, medium was changed to myeloid differentiation medium 3 to induce hematopoietic patterning. At **DIV9**, cells should be confluent besides a few hematopoietic stem cells present in the supernatant. At this point, the supernatant was collected, the adherent cells dissociated with Accutase and both cell suspensions were combined. The cells were centrifuged, resuspended in microglia cultivation medium and plated onto 12-well plates. Before seeding, plates were pre-treated with Anti-Adherence Rinsing Solution for 5 minutes and washed once with PBS to avoid cells attaching to the well bottom. From then on, microglial cells were cultured in suspension and a medium change was performed with microglia cultivation medium every other day. At **DIV18** of microglial differentiation, microglia were seeded into co-cultures with neurons.

2.2.14 Microglia- NGN2/AD2 neuron co-culture

Differentiation of NGN2 and AD2 neurons was started one week in advance of microglial differentiation. NGN2 and AD2 neurons were differentiated from NPC as described in 2.2.10 and 2.2.11 and seeded into co-cultures with murine astrocytes at a ratio of 80:20, as described in 2.2.12. Microglia were differentiated from iPSC as described in 2.2.13. Microglia, NGN2 and AD2 neurons which were combined into co-cultures were always derived from the same donor. At ***DIV24*** of neuronal differentiation, microglia were seeded into E-I co-cultures. First, ***DIV18*** microglial suspension cultures were centrifuged for 3 minutes at 300 xg, counted and resuspended in fresh microglia culture medium (**Table 10**). For $4x10^4$ neurons initially seeded per well of a standard 96-well plate, $1.5x10^4$ microglia were added in 200 µl of microglia medium/well. Neurons and microglia were co-cultured in this setup for 72 h until ***DIV28***, without further medium changes. For calcium imaging, the cultures were recorded in NeuM medium as this was found to improve neuronal activity in comparison to microglia medium.

2.2.15 LPS/Minocycline stimulation of microglia

For some experiments, microglial cells were stimulated with either LPS or minocycline before seeding into co-culture with neurons. For stimulation, the required number of microglial cells to be seeded was resuspended in 500 µl of microglia cultivation medium **Table 10**, containing either 100 ng/ml of LPS, 10 µM of minocycline or DMSO. Cells were stimulated for 60 minutes at 37 °C, 5 % CO_2, afterwards washed with PBS, resuspended in microglia medium an added to the neuronal cultures. Neurons and microglia were co-cultured for 72 h.

2.3 Molecular biology methods

2.3.1 Lentivirus production

The highly transfectable HEK293FT cell line was used for lentivirus production. The cells stably express a neomycin resistance gene and are therefore routinely cultured under G418 selection (500 µg/ml) in HEK293FT culture medium (**Table 11**). Four days prior to transfection (***DIV4***) HEK293FT cells were washed with DPBS and incubated with EDTA-Trypsin at 37 °C until they started to detach. The cells were centrifuged for 3 minutes at 300 xg, counted, and $5x10^5$ viable cells were seeded per T175 cell culture flask in HEK culture medium without G418. Two T175 flasks were used per lentivirus that was generated. The cells were cultured at 37 °C, 8 % CO_2 until ***DIV0***, without further medium changes. On ***DIV0***, cells should be > 90 % confluent. For transfection of the cells, the following mixes were prepared:

a) 27 µg lentiviral packaging mix + 18 µg plasmid DNA + 4.5 ml Opti-MEM™
b) 108 µl Lipofectamine™ 2000 + 4.5 ml Opti-MEM™

Both solutions were incubated separately for 5 minutes at RT. Next, the plasmid mix (a) was transferred into the Lipofectamine mix (b) without resuspension, and further incubated for 20 minutes at RT. HEK cell medium was changed to HEK transfection medium (**Table 11,** 20 ml per T175 flask) and the transfection mix (9 ml) was added to the medium. Transfected cells were incubated for 24h at 37 °C, 5 % CO_2. On ***DIV1,*** a 100 % medium change with 30 ml of HEK transfection medium was performed. Starting DIV1, all work was performed under biological safety level 2 conditions. On ***DIV2***, the medium, now containing lentiviral particles, was collected and frozen at -80 °C. 30 ml of fresh transfection medium was added to the flasks. The medium was again collected and frozen 24h later (***DIV3***). At this point the cells were discarded.

The frozen lentiviral suspensions were thawed in a water bath at 37 °C and subsequently ultracentrifuged at 50,000 xg for 80 minutes at 4°C. The supernatant was carefully discarded by pouring and the tubes air-dried for a few minutes. Remaining liquid was removed with sterilized tissue paper. 100 µl of PBS + 1 % BSA was added to the viral pellets, without resuspension. Tubes were sealed with Parafilm and stored over night at 4°C. The next day, pellets were resuspended, aliquoted and stored at -80 °C.

2.3.2 Determination of lentiviral titers

Titers of the generated lentiviruses were determined using the Lenti-X^{TM} p24 Rapid Titer Kit, according to the manufacturer's instructions. Viral suspensions were diluted to a concentration of 10^{-5} and 10^{-10} and quantified against a p24 standard curve. The expected yields range between $5x10^{10}$ to $5x10^{11}$. For infections, 10 ng/ml or $2x10^{8}$ particles/ml were used.

2.3.3 Immunocytochemistry

For immunocytochemical analysis, cells were fixed with 4 % PFA in PBS for 15 minutes at RT and afterwards washed 3x with PBS. To block unspecific antibody binding and permeabilize the cells, incubation in PBS + 1x Blocking Reagent BMB + 0.1 % Triton-X-100 (blocking solution) was performed for a minimum of 30 minutes at RT. Primary antibodies were diluted in blocking solution and incubated over night at 4 °C. Cells were washed 3x with PBS and secondary antibodies, diluted in blocking solution, incubated for 2 h at RT on an orbital shaker in the dark. Next, cells were again washed 3x with PBS. If nuclear staining was required, Hoechst dye was diluted in PBS and incubated for 30 minutes at RT in the dark, followed by washing with PBS.

2.4 Generation and characterization of DISC1 mutant iPSC

2.4.1 Generation of Indel mutations in DISC1 exon 2 with CRISPR/Cas9

The Alt-R® CRISPR-Cas9 system from Integrated DNA Technologies was used to generate indel mutations in *DISC1* exon 2. The system makes use of a functional gRNA duplex, consisting of crRNA and tracrRNA. The crRNA targeting exon 2 was selected using the IDT predesigned gRNA library (https://eu.idtdna.com/site/order/designtool/index/CRISPR_CUS

TOM, Design ID: Hs.Cas9.DISC1.1.AC). The crRNA with highest on-target specificity and lowest off-target score, both provided by IDT, was chosen. A tracrRNA labelled with an Atto 550 fluorescent dye was used to identify successfully electroporated cells.

crRNA and tracrRNA oligonucleotides were diluted in IDT buffer to yield a concentration of 200 µM. 3 µl of crRNA and 3 µl of tracrRNA were combined, heated at 95 °C for 5 minutes to form a gRNA complex, and subsequently cooled to 15-20°C at RT. 30 µM of gRNA complex, 9.2 µM of Alt-R® S.p. Cas9 Nuclease V3 and PBS (to a total volume of 20 µl per $2x10^6$ iPSC) were mixed and incubated for 20 minutes at RT to form a ribonucleoprotein (RNP) complex. $2x10^6$ iPSC were dissociated with Accutase, washed once with PBS, centrifuged and resuspended in 100 µl of nucleofection buffer P3. The RNP complex was added to the cells, resuspended, and the entire solution transferred to a nucleofection cuvette. 1 µg of MaxGFP plasmid (included in the Lonza P3 Primary Cell 4D-Nucleofector X Kit) was electroporated separately as a positive control. Nucleofection was performed with the 4D-Nucleofector™ System, using the program CA-137. The cells were pulsed twice to increase RNP delivery efficiency and subsequently seeded into Matrigel-coated 6-well plates with pre-warmed mTeSR Plus medium + 10 µM Y-27632. Starting the following day, daily 50% medium changes without Y-27632 were performed.

2.4.2 Sequencing of monoclonal iPSC for assessment of successful mutation

Genomic DNA (gDNA) was isolated from WT and *DISC1 +/-* iPSC using the QIAamp DNA Mini Kit, according to the manufacturer's instructions. DNA concentration was measured with a Nanodrop Spectrophotometer. Using a pair of primers surrounding the region targeted by the sgRNA (DISC1 Exon2_fw + DISC1 Exon2_rev, **Table 16**), a polymerase chain reaction (PCR) was performed. See **Table 18** and **Table 19** for the PCR reaction setup and temperature profile used. PCR products were mixed with 1x gel loading dye and were run on a 1 % Agarose gel for 60 minutes at 120 V to confirm that the PCR was successful. In-gel staining of DNA was performed with Midori Green Advance DNA stain, which was added to the gels before solidification (4 µl/100 µl gel) and can be visualized using the blue/green LED illumination of the GelDoc Go imaging system. The remaining PCR product was purified using the QIAquick PCR Purification Kit. Sanger sequencing of the amplicon was performed by 4base lab AG (Reutlingen), using the forward primer (DISC1 Exon2_fw).

Table 18 PCR reaction setup

Reagent	Amount
5X platinum II PCR Buffer	4.8 µl
Platinum GC Enhancer	4.8 µl
Platinum II Taq Hot-Start DNA Polymerase	0.19 µl
Forward primer	1 µl
Reverse primer	1 µl
dNTP mix	0.48 µl
Template DNA	200 ng
Nuclease-free water	fill up to 24 µl

Table 19 PCR temperature profile

Process	Temperature	Time
Initial denaturation	94 °C	2 min.
Denaturation	94 °C	30 sec.
Annealing	60 °C	30 sec.
Extension	68 °C	30 sec./kilobase
Final extension	72 °C	5 min.
Hold	3 °C	∞

2.4.3 Expansion of monoclonal iPSC

After the presence of a mutation in *DISC1* exon 2 was confirmed, iPSC were FACS-sorted to generate monoclonal lines, derived from a single cell with a unique genetic background. A minimum of $1x10^6$ iPSC were dissociated with Accutase, centrifuged, and resuspended in an appropriate volume of DPBS + 2 % FCS (2 ml per $1x10^6$ cells). A Matrigel-coated 96-well plate containing pre-warmed mTeSR Plus medium, supplemented with 10 % FCS and 10 µM of Y-27632, was prepared to improve cell survival after FACS sorting. Single cells were sorted into individual wells of the 96-well plate using the BD FACSMelody™ Cell Sorter. After sorting, the cells were cultured in the IncuCyte live cell imaging incubator, to ensure that only wells in which colonies emerged from a single cell were considered. The following day, the medium was changed to mTeSR Plus + 10 % CloneR™ 2 supplement. Daily medium changes with mTeSR Plus + 10 % CloneR™ 2 were performed until colonies were visible, which can take up to two

weeks. Once colonies reached 30-50 % confluence, they were detached using Accutase and transferred to 6-well plates. Sanger sequencing of monoclonal lines was performed as described in **2.4.2** to identify mutation-carrying clones. Deconvolution analysis of heterozygous mutations was performed using DSDecodeM (https://skl.scau.edu.cn/dsdecode/).

2.4.4 Array CGH analysis

The introduction of genetic modifications in iPSC increases the risk of chromosomal aberrations due to unwanted off-target effects. For this reason, array-CGH analysis of *DISC1+/-* iPSC was performed. $2x10^6$ iPSC per clone were pelleted, washed with DPBS, and frozen at -80 °C. Array CGH analysis with a resolution of 50-100 kilobases was performed by CeGaT GmbH, Tübingen.

2.4.5 Validation of pluripotency gene expression by RT-PCR

RNA was isolated from iPSC using the RNeasy Mini Kit, according to the manufacturer's instructions. To digest residual DNA, 8 µl of isolated RNA were combined with 1 µl of RQ1 RNase-free DNase, 1 µl of RQ1 DNase 10x Reaction Buffer and incubated for 30 minutes at 37 °C. 1 µl of DNase stop solution was added and incubated for 10 minutes at 65°C to terminate the reaction. RNA was stored at -80 °C.

For cDNA synthesis, 10 µl of DNA-free RNA, 0.3 µl of dN_6-primers, 0.5 µl of 25 mM dNTPs and 2.2 µl of nuclease-free H_2O were combined and incubated for 10 minutes at 70 °C. 1 µl of MuLV Reverse Transcriptase and 2 µl of Reverse Transcriptase Reaction Buffer were added and incubated for 70 minutes at 42 °C. Afterwards, the mixture was incubated for 5 minutes at 80 °C to terminate the enzymatic reaction. cDNA concentration was measured with the Nanodrop Spectrophotometer.

A PCR reaction (**Table 18, Table 19**) was run to detected endogenous expression of the pluripotency genes NANOG, OCT3/4, and SOX2 (for primers, see **Table 16**). PCR products were run on an Agarose gel as described in **2.4.2.**

2.4.6 Analysis of DISC1 protein expression

DISC1 protein expression in iPSC and NPC was analyzed by immunocytochemical staining. iPSC and NPC were seeded into 96-well plates at a density of $1x10^4$ cells per well and cultivated until 60-80 % confluence. Cells were fixed and stained with a DISC1 antibody directed to the C-terminus of DISC1 (Thermo Fisher Scientific, # 40-6800). Imaging was performed using the spinning disk confocal microscope Cell Observer SD with a plan-apochromatic 20 x objective. From 3 independent experiments, 3-5 microscopic fields (containing multiple cells) were imaged per well. 2 wells were imaged for each condition in every biological replicate. From each microscopic field, DISC1 mean fluorescence intensity of 4 individual cells was measured by hand-drawn regions of interest (ROI) using the software ZEN 3.0 (Zeiss). Background intensities were measured in each microscopic field and subtracted from DISC1 intensity values. These were afterwards normalized to mean WT fluorescence intensities within individual replicates.

2.5 Cellular assays

2.5.1 Imaging and analysis of iPSC/NPC markers with HCA

NPC or iPSC from alle donors, with the same passage for all donors in each replicate, were seeded into 96-well µClear plates at a density of $1.5x10^4$ cells per well. Once 70-80 % confluence was reached, the cells were fixed with PFA (see 2.3.3) and immunocytochemical staining of proteins of interest was performed. Images were acquired with the ImageXpress Micro Confocal High-Content Imaging System (Molecular Devices). Z-stacks were obtained from four sites per well, which contained multiple cells each. All acquisition parameters for individual antibodies were kept constant within biological replicates. For image analysis, the software MetaXpress (Molecular Devices) was used. First, 2D projection images were generated. Thresholds for intensity and size (only for spot-like or nuclear signals) were defined for each marker, which were then applied to generate a mask covering the fluorescent signal. Depending on the expression pattern of the respective marker (nuclear vs. cytosolic expression), different parameters were used for analysis. For nuclear stains and markers for which cells were either clearly positive or negative, the mean stained area was analyzed per image. For stainings, which were present in all cells but varied in intensity between different cells, the mean intensity per image was analyzed. Values from one well were averaged and

data was obtained from three biological replicates. Afterwards, data was normalized to WT mean within individual biological replicates.

2.5.2 Proliferation assay NPC

NPC of alle donors, matched in passage, were seeded into transparent 96-well plates at a density of $2x10^4$ cells/well in Neural Progenitor Medium. For 72 h, the cells were cultivated in the IncuCyte® Live Cell Analysis System without further medium changes. Whole-well brightfield images were acquired every 4h with a 10x objective from three wells per line. Cell proliferation was analyzed with the IncuCyte® Basic Analyzer at every time point and values at t=0 h were set to 1. Data was obtained from three biological replicates.

2.5.3 Neurite outgrowth assay – directed differentiation (HCA)

On ***DIV -1***, NPC were seeded into 96-well µClear plates in Neural Progenitor Medium. For infection with NGN2, $8x10^3$ NPC were seeded per well and for AD2 infection, $1x10^4$ cells were seeded per well, as NGN2 neurons grew more densely in a shorter period of time. On ***DIV 0***, NPC were transduced with lentiviral constructs to separately overexpress NGN2 or Ascl1+Dlx2 under a doxycycline-inducible tet-ON promotor, as described in sections 2.2.10 and 2.2.11. On ***DIV 1***, 1 µg/ml of doxycycline was added to the medium to induce transgene expression. On ***DIV 2***, NGN2-expressing cells were selected with 2 µg/ml of puromycin, and AD2-expressing cells were selected with 2 µg/ml of puromycin + 250 µg/ml of hygromycin, which were supplemented to doxycycline-containing Neural Progenitor Medium. On ***DIV 3***, outgrowing neurites were visible in the cultures and to ensure that networks did not grow too dense to detect individual neurites, the experiment was terminated, and the cultures were fixed. Cells were stained for β-III-tubulin to visualize the neuronal cytoskeleton and Hoechst for nuclear staining as described in 2.3.3. For three independent differentiations per line, 4 wells were imaged per type of neuron and 9 images were acquired per well, using the ImageXpress Micro Confocal High-Content Imaging System with a 20x objective. Using the software MetaXpress, images were analyzed with the built-in analysis module ‘Neurite outgrowth’. The module detects cell numbers by quantification of Hoechst-positive nuclei and creates a mask of the β-III-tubulin signal to measure the length of neurites. Thresholds for nuclei and neurite detection were kept constant for all lines within individual replicates. Mean values were calculated from each well and normalized to CTR mean.

2.5.4 Neurite outgrowth assay – undirected differentiation (Incucyte)

On ***DIV -1***, passage-matched NPC were seeded into transparent 48-well plates at a density of $1x10^4$ cells per well in Neural Progenitor Medium. After 24 h (***DIV0***), the medium was changed to N2-medium (**Table 12,** t=0 h). From then on, cells were cultured in the IncuCyte® Live Cell Analysis System and were imaged every 4 h in brightfield mode with a 10x objective. Two wells were imaged per line, with 4 sites imaged per well. On ***DIV1***, a complete medium change with N2 medium was performed and cells were imaged without further medium changes until t=40 h. Neurite length (mm) per number of cell body clusters was determined for each time point, using the IncuCyte® NeuroTrack analysis module. Analysis parameters were kept constant for all replicates analyzed and were defined as follows: cell body clusters with a minimum area of 200 µm, containing cells with a minimum width of 7 µm, were counted. Neurite width was defined as 1 µm. These parameters were analyzed for each of the four sites imaged and then averaged per well. Data was obtained from four biological replicates. Values at t= 0 h were set to 1.

2.5.5 Flow cytometry cell cycle analysis

NPC in the same passage for all donors, were seeded on 12-well plates at a density of $8.5x10^4$ cells/cm^2 to ensure exponential growth until fixation. When cells reached ~ 70% confluence, they were detached with Accutase and counted. $6x10^5$ cells per condition were fixed with 4% PFA in PBS for 15 min at RT. Cells were washed three times with PBS and treated with 100 µg/ml RNAse A and 0.1% Triton X-100 in TrypLE express at 37 °C for 30 minutes to remove RNA and permeabilize the cells while remaining cells in a single-cell suspension. Next, $3x10^5$ cells were transferred per well of a 96-well plate and cells were stained with 2 µg/ml propidium iodide (PI) solution, diluted in TrypLE express for 30 min at 37 °C. Without further washing, analysis of PI staining was performed using the FACS Fortessa™ Cell Analyzer (BD Biosciences). A minimum of 15,000 events was recorded per well, from two wells per line. Analysis of flow cytometry data was performed using FlowJo 10 (BD Biosciences). G0/G1, S and G2/M cell cycle phases were identified automatically using the build-in univariate cell cycle analysis tool of the FlowJo software (Dean-Jett-Fox model, (137)).

2.5.6 Calcium imaging

At DIV28, neurons in NGN2/AD2 co-cultures were stained with 2 µM of the red fluorescent calcium indicator Calbryte™ 590 AM or the green fluorescent calcium indicator Cal-520™ AM, diluted in NeuM medium for 30 minutes at 37 °C, 5 % CO_2. Afterwards, cells were washed with DMEM/F12 and incubated for 15 minutes at 37 °C in NeuM medium to recover. To record spontaneous single-cell calcium activity, neurons were imaged at 37 °C, 5 % CO_2 with the spinning disc confocal microscope Cell Observer SD. Microscopic fields containing multiple cells were recorded for 3-5 minutes, depending on the experiment, with a 20x objective at a frame rate of 20 frames/second. For cell type-specific analysis of calcium activity, a snapshot of the Calbryte™ signal (staining all neurons) and GFP signal of NGN2 neurons was obtained for each microscopic field, to distinguish NGN2 and AD2 neurons. For each individual differentiation, 2-3 wells with 2 videos per well were recorded per donor. Data was obtained from a minimum of 3 biological replicates per donor.

2.5.7 Analysis of single-cell calcium traces and network activity

For the analysis of neuronal network activity, cultures were regarded as synchronous if either a larger fraction of cells showed synchronized neuronal activity (minimum of $\sim 1 / 4$ of cells per well) or if there was network activity observed throughout the whole well that was recorded from.

To analyze single-cell calcium activity in E-I co-cultures, somatic calcium signals were measured from individual neurons by drawing regions of interest with the Fiji freehand tool and extracting the mean fluorescence intensity for each frame over time. A minimum of 3 spontaneously active neurons (= minimum of one calcium peak per recording period) of both subtypes (NGN2, AD2) were analyzed per recording.

Extracted traces were further analyzed with the Origin 2015G Peak Analyzer module (OriginLab Corporation). In cultures in which network activity was observed, synchronously active and neurons with unsynchronized activity were analyzed in parallel. To distinguish between synchronously active and unsynchronized neurons, the calcium traces of individual neurons were compared as stacked lines in a y-offset graph. Neurons which shared a minimum of one synchronized calcium peak per recording period were regarded as neurons with synchronized activity.

Traces were normalized to a baseline of 0 and a minimum peak amplitude threshold as well as minimum inter-peak distance were defined. These thresholds were kept constant across all

biological replicates. Peak amplitude ($\Delta F/F_0$), full width at half maximum (FWHM), area under the curve (AUC) and peak frequency (n peaks/seconds recorded) were extracted for each peak. These values were averaged across all peaks of a single neuron. Next, data from all recorded neurons within each well or recording was averaged. For peak amplitude, AUC and FWHM values, data was normalized to the mean of CTR1 values within each biological replicate.

2.5.8 Synapse quantification with IMARIS

At DIV28, neurons in monocultures or co-cultures were fixed and stained for pre- and postsynaptic markers, as well as the neuronal cytoskeletal protein MAP2. Imaging of synaptic markers was performed using the spinning disk confocal microscope Cell Observer SD with a plan-apochromat 63 x oil immersion objective. 4-5 z-stack images per well from 2 wells per donor were imaged for each differentiation. Images were acquired in regions with comparable MAP2-network density. Data was obtained from a minimum of 3 independent neuronal differentiations per donor.

Analysis of synaptic densities was performed using IMARIS Bitplane 10 (Oxford Instruments), as depicted in **Figure 3**. For each image, a 3D mask of the MAP2 signal, staining all neurons in the culture, was created to filter all synaptic signals lying within the MAP2 volume. Synapse numbers within the MAP2 volume were then quantified using the spot detection tool. Intensity thresholds for spot detection and spot size limits (in x, y and z direction) were kept constant within biological replicates for each synaptic marker. To analyze the co-localization of pre- and postsynaptic spots, the MATLAB-based IMARIS XTension plugin ‘Spots Colocalize’ was used. Pre- and postsynaptic spots with a distance of ≤ 0.2 µm were defined as a synapse, as this distance corresponds to the resolution limit of the Cell Observer SD microscope.

To distinguish between synapses on either NGN2 or AD2 neurons in co-cultures, a 3D mask of the GFP signal of NGN2 neurons was created. Synaptic marker channels were again filtered to exclude spots localized outside the GFP mask. The number of synapses and the number of pre- and postsynaptic spots in apposition within the GFP mask were quantified as described above. Synapse densities on AD2 neurons were derived mathematically by subtraction of synapse numbers on NGN2 neurons from the total synapse number in the MAP2 network. To account for differences in neuronal network density, synapse numbers were normalized to the volume of either the MAP2 mask (all neurons), GFP mask (NGN2 neurons), or the difference of both (AD2 neurons). The values obtained from one well were averaged. Within individual differentiations, data was normalized to the mean of CTR values.

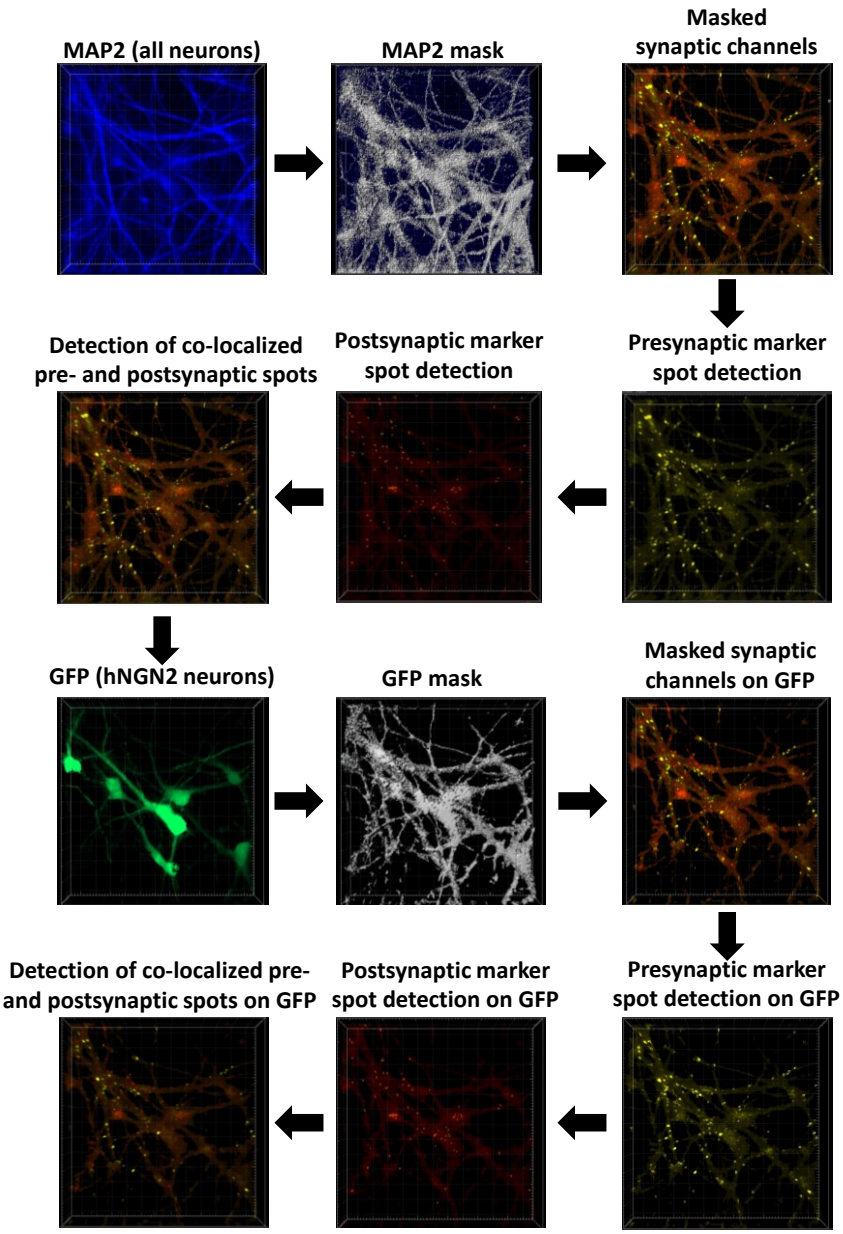

Figure 3 Workflow of synapse analysis with IMARIS software.
Confocal z-stack images are analyzed using IMARIS (Oxford Instruments) to quantify presynaptic and postsynaptic spot densities on neuronal dendrites and somata. To analyze all synapses in the network, synaptic signals were assigned to a mask of MAP2-positive neurons. Synaptic markers detected within a mask of GFP-positive neurons were assigned to NGN2 neurons. Synapse densities on AD2 neurons were calculated by subtraction of both values.

2.6 Statistics

Statistical analysis was performed using GraphPad Prism 10 (Graphpad Software). Outliers were identified using Prism's 'Robust regression and Outlier removal' (ROUT) method, with a ROUT coefficient Q = 1 %. All data were tested for Gaussian distribution using the D'Agostino-Pearson test, Anderson-Darling test, Shapiro-Wilk test, and Kolmogorov-Smirnov test. If data were tested negative for Gaussian distribution by any of the tests, the data were regarded as being non-normally distributed and non-parametric statistical tests were employed.

For comparison of two samples, normally distributed data were analyzed using an unpaired two-tailed t-test. Non-normally distributed data were analyzed using an unpaired two-tailed Mann-Whitney U test.

To compare three or more groups, normally distributed data were analyzed using an unpaired One-way ANOVA with Tukey's multiple comparison test. Non-normally distributed data were analyzed with an unpaired Kruskal-Wallis test with Dunn's multiple comparison test.

For experiments with more than one variable, data were analyzed with a 2way ANOVA and Šídák's or Tukey's multiple comparisons test. In case there were missing values in any of the samples, mixed-effects analysis with Šídák's multiple comparisons test was performed.

N numbers and statistical details for each experiment can be found in the respective figure legend. A p-value of <0.05 was considered as statistically significant.

3. Results

3.1 Patient-derived NPC show early neurodevelopmental aberrations

The notion that SCZ can be categorized as a neurodevelopmental disorder is widely accepted in the field (138). Therefore, the study of early disease-related neurodevelopmental phenotypes in NPC or immature neurons is of particular interest to identify early emerging aberrations. To study such phenotypes in NPC derived from CTR and SCZ iPSC lines, neurite outgrowth; neuronal differentiation efficiency and cell cycle dynamics were assessed.

3.3.1 Neurite outgrowth is reduced in SCZ NPC

To study neurite outgrowth of developing iPSC-derived neurons from CTR and SCZ patient iPSC lines, iPSC were first differentiated into NPC. NPC were then differentiated into immature neurons by directed and undirected differentiation.

First, two control (CTR2, CTR3) and four SCZ (SCZ1, SCZ2, SCZ4, SCZ5) NPC lines were differentiated by transduction with either NGN2 or AD2 (directed differentiation) to induce differentiation towards the glutamatergic and GABAergic lineage and differentiated for three days. Beta-III-tubulin staining of neurites did not show differences in mean neurite outgrowth per cell when comparing CTR and SCZ (**Figure 4A, B, Suppl. Figure 1**). Since subtle differences in early neurite development might be undetectable with this form of accelerated differentiation by forced transcription factor overexpression, undirected differentiation was performed by timed addition of growth factors. Outgrowing neurites of three control NPC lines (CTR1, CTR2, CTR3) and the four SCZ patient lines were tracked over a period of 40 h in the live cell imaging incubator IncuCyte (**Figure 4C, C'**). Starting 24 h after neural induction, the mean neurite length of SCZ cells was significantly reduced compared to CTR (**Figure 4D**). This deficit persisted with increasing magnitude until the end of the experiment, indicating early deficits in neurite outgrowth occurring in diseased cells, which confirms previous results from iPSC-based studies (139, 140).

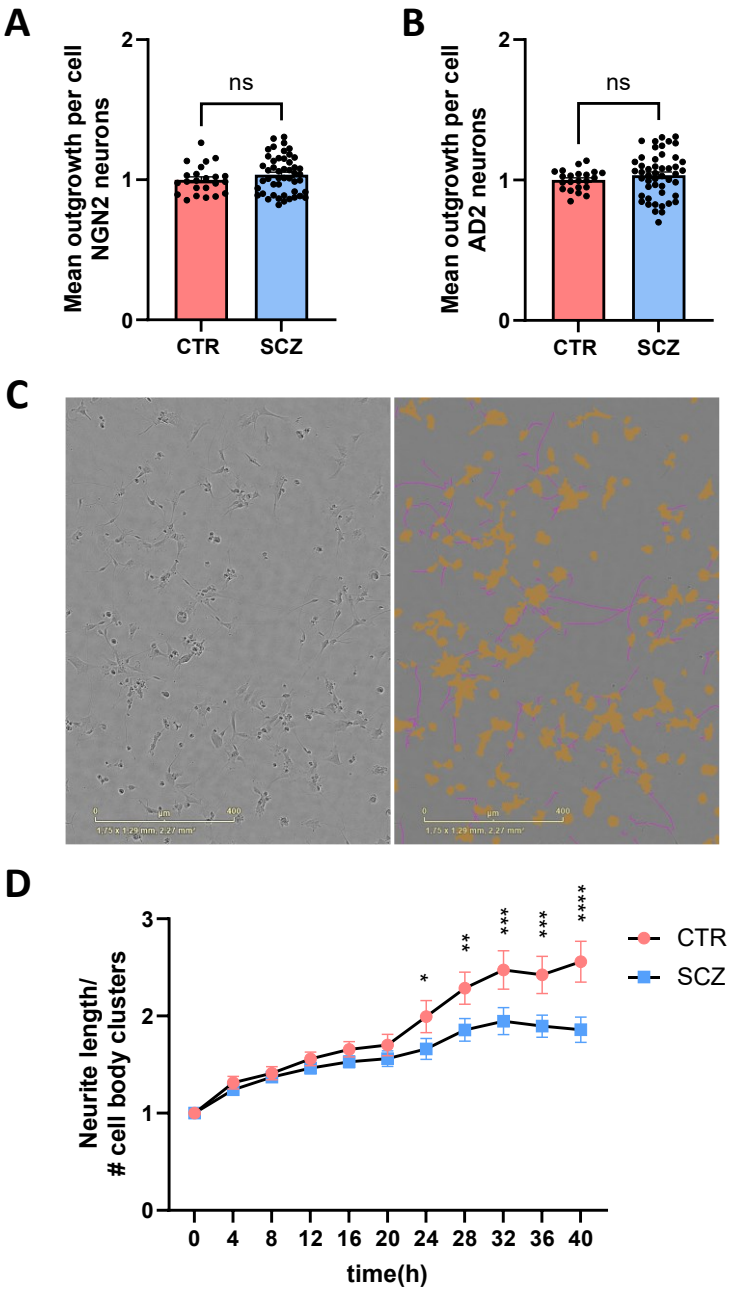

Figure 4 Neurite length is reduced in immature SCZ neurons generated by undirected differentiation.

(A-B) Mean neurite outgrowth per cell in DIV 3 neurons, generated by direct differentiation via overexpression of NGN2 **(A)** or AD2 **(B)**. Values are normalized to CTR. Data points represent individual wells analyzed. Unpaired, two-tailed t-test, ns= not significant, n>21, error bars: S.E.M. **(C)** Exemplary phase contrast image showing outgrowing immature CTR neurons (left) in which with neurites (purple) and cell body clusters (orange) were detected by the IncuCyte Neurotrack analysis module (right). Scale bars: 400 µm. **(D)** Neurite length normalized to the number of detected cell body clusters was measured over a time period of 40 h in NPC, differentiated by undirected differentiation. Data were obtained from four independent differentiations, all values are normalized to t=0 h. 2-way ANOVA with Tukey's multiple comparisons test, CTR: n=24, SCZ: n= 32 per time point, p≤0.05*, p≤ 0.01**, p≤ 0.001***, p≤0.0001****. Error bars: S.E.M.

3.1.1 Restricted neuronal differentiation capacity of SCZ NPC

To test whether impaired neurite outgrowth might be related to a limited neuronal differentiation capacity of diseased cells, immunocytochemical analysis of selected differentiation markers was performed in CTR and SCZ iPSC and NPC. First, suitable markers to describe the differentiation process were determined by comparing cells at the iPSC and NPC stage regardless of genotype. Three independent rounds of differentiation of iPSC into NPC were carried out for all CTR and SCZ lines.

As expected, a significant downregulation of pluripotency-associated transcription factor OCT4 was observed in NPC. At the NPC stage, a significant upregulation of the neuronal cytoskeletal proteins microtubule-associated protein 2 (MAP2) and Vimentin was detected. Additionally, the neural cell adhesion molecule NCAM was upregulated in NPC when compared to iPSC (**Figure 5**).

The Wnt signaling pathway plays an important role in neural induction during brain development (141). Hence, expression of the transcription factors lymphoid enhancer-binding factor 1 (LEF1) and beta-catenin, which are involved in canonical Wnt signaling, were in addition quantified as markers of neuronal differentiation. Beta-catenin expression was detected in the cytoplasm of iPSC and NPC, and a slight upregulation of the area of beta-catenin positive cells was observed in NPC (**Figure 6A, C-F**). LEF1 signal on the other hand was absent in iPSC, while NPC showed a significant upregulation of nuclear LEF1 staining (**Figure 6B, C-F**).

Overall, a set of suitable cell-type specific markers to assess the differentiation efficiency from iPSC towards NPC in CTR and SCZ samples was identified.

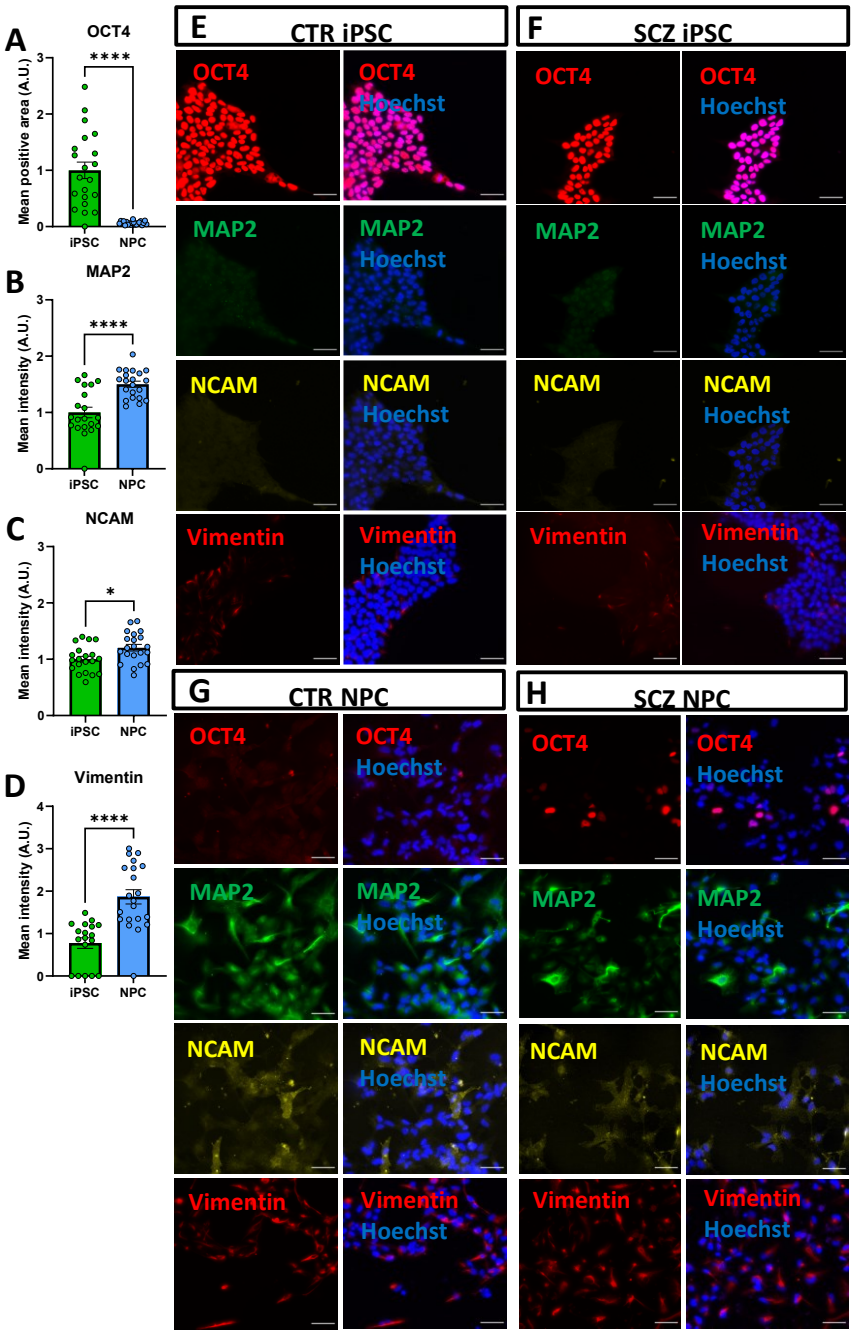

Figure 5 Evaluation of early neuronal differentiation markers during differentiation of iPSC into NPC.

(A-D) Quantification of markers specific for the iPSC and NPC stage in CTR and SCZ cells (all donors pooled). **(A)** Mean OCT4-positive area (unpaired, two-tailed t-test, n= 21), **(B)** mean intensity of MAP2 fluorescent signal (unpaired, two-tailed t-test, n≥20), **(C)** mean intensity of NCAM fluorescent signal (two-tailed Mann Whitney U test, n≥20) and **(D)** mean intensity of Vimentin fluorescent signal (two-tailed Mann Whitney U test, n≥18) in iPSC and NPC. Data points represent averages of multiple analyzed images within individual wells. Data were obtained from three independent NPC differentiations per line. Values are normalized to iPSC. p≤0.05*, p≤0.0001****. Error bars: S.E.M. **(E)** Exemplary images showing expression of OCT4, MAP2, NCAM and Vimentin in CTR iPSC, **(F)** SCZ iPSC, **(G)** CTR NPC and **(H)** SCZ NPC. Scale bars: 50 µm.

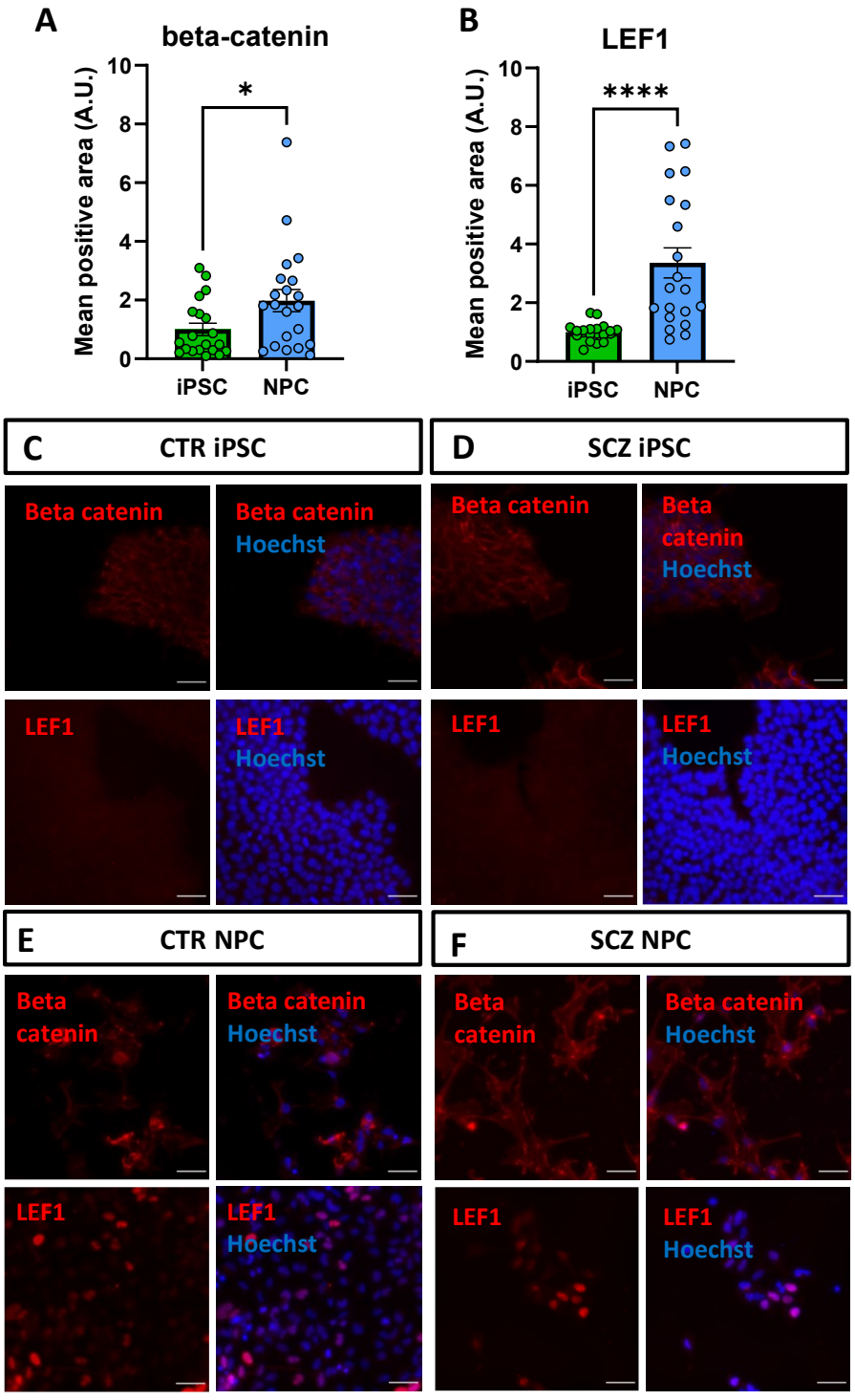

Figure 6 Upregulation of Wnt signaling proteins during the differentiation of iPSC to NPC.

Quantification of Wnt signaling proteins at the iPSC and NPC stage in CTR and SCZ samples. **(A)** Mean beta-catenin-positive area (two-tailed Mann Whitney U test, n≥20) and **(B)** Mean LEF1-positive area (two-tailed Mann Whitney U test, n=20). Data points represent averages of multiple analyzed images within individual wells. Data were obtained from three independent NPC differentiations per line. Values are normalized to iPSC. p≤0.05*, p≤0.0001****. Error bars: S.E.M. **(C)** Expression of beta-catenin and LEF1 in CTR iPSC, **(D)** SCZ iPSC, **(E)** CTR NPC and **(F)** SCZ NPC. Scale bars: 50 µm.

Next, the expression levels of the above-mentioned markers were compared in CTR and SCZ NPC to infer the relative amount of differentiated cells in the cultures. Interestingly, a significant increase of OCT4 expression was observed in SCZ NPC when compared to CTR, revealing a higher fraction of cells which remained in a pluripotent state (**Figure 7A, Figure 5G, H**). However, there was no change in NCAM, MAP2 and Vimentin expression between CTR and SCZ NPC (**Figure 7B-D, Figure 5G, H**). The expression of Wnt signaling protein beta-catenin was also unchanged (**Figure 7E, Figure 6E, F**). When analyzing the mean LEF1-positive area per image, as done before, no difference was detected between CTR and SCZ NPC (**Figure 7F**). However, the number of detected LEF-1 positive nuclei was significantly reduced in SCZ NPC (**Figure 7G**).

In summary, these data suggest that the efficiency of differentiation into NPC might be slightly restricted in diseased iPSC, indicated by higher expression levels of pluripotency marker OCT4 and lower levels of Wnt signaling protein LEF1.

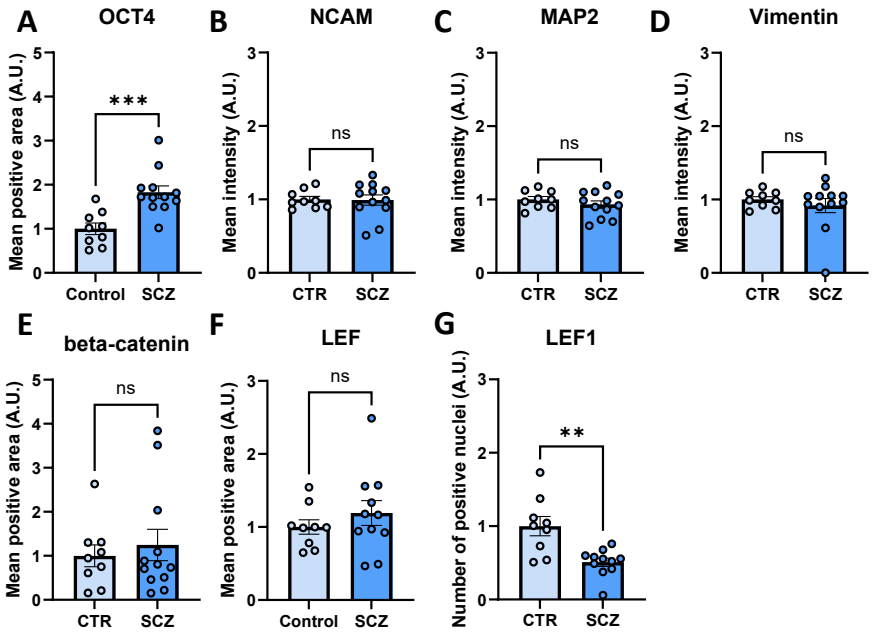

Figure 7 Limited neuronal differentiation capacity of SCZ iPSC.
Quantification of proteins indicative of differentiation status in CTR and SCZ NPC. **(A)** Mean OCT4-positive area (two-tailed Mann Whitney U test), **(B)** mean intensity of NCAM fluorescent signal (unpaired, two-tailed t-test), **(C)** mean intensity of MAP2 fluorescent signal (unpaired, two-tailed t-test), **(D)** mean intensity of Vimentin fluorescent signal (two-tailed Mann Whitney U test), **(E)** mean beta-catenin-positive area (two-tailed Mann Whitney U test), **(F)** mean LEF1-positive area (two-tailed Mann Whitney U test) and **(G)** relative number of LEF1-positive nuclei (two-tailed Mann Whitney U test). Data were obtained from three independent NPC differentiations per line. CTR: n= 9, SCZ: n= 12. Data points represent values of multiple images within individual wells. Values are normalized to CTR. p≤0.01**, p≤0.001***, ns= not significant. Error bars: S.E.M.

3.1.2 Altered cell cycle dynamics of SCZ patient-derived NPC

The limited neuronal differentiation efficiency that was observed in SCZ NPC could potentially be related to altered cell cycle dynamics such as arrest/delay in a particular cell cycle phase due to altered expression of cell-cycle regulating proteins, which has been reported by multiple studies in different cell types in SCZ (142-144). To explore this hypothesis, proliferation of CTR and SCZ NPC, using all three CTR and four SCZ lines, was tracked over a time period of 72 h with the live cell imaging incubator IncuCyte. Confluence of the cultures was calculated based on brightfield photographs of the cells, acquired every 4h. No significant differences were observed between CTR and SCZ NPC cultures at any of the time points analyzed (**Figure 8**).

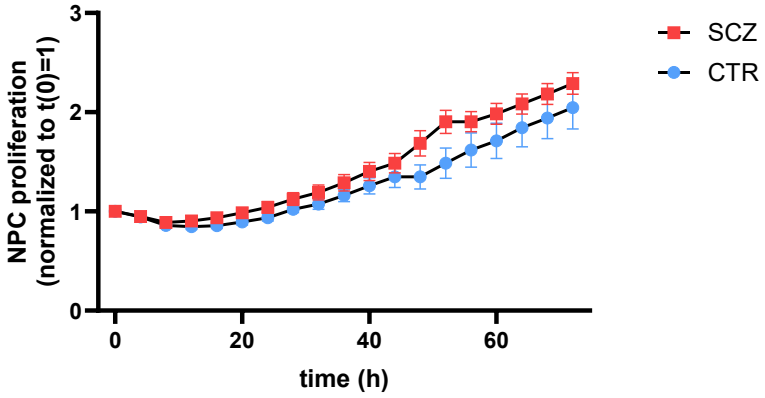

Figure 8 No differences of NPC proliferation between CTR and SCZ cultures.
Proliferation of CTR and SCZ NPC was measured every 4h over a period of 72h. All values were normalized to t=0h. Mixed-effects analysis with Šídák's multiple comparisons test did not reveal any statistically significant differences between CTR and SCZ. CTR: n=9 per time point, SCZ: n=12 per time point. Data were obtained from three independent experiments per line. Error bars: S.E.M.

To examine the cell cycle dynamics of NPC in more detail, CTR and SCZ NPC were analyzed with a propidium iodide (PI)-based cell cycle assay. PI stoichiometrically binds to the DNA of fixed cells, thereby indicating the relative amount of DNA within a cell by its fluorescence intensity (145). Single cells were analyzed by flow cytometry, to distinguish cells in G0/G1-phase from cells in S-phase, when the relative DNA content, and thereby PI intensity, increases during DNA synthesis. Cells in G2/M-phase have double the amount of DNA when compared to G0/G1 phase, and thereby fluoresce twice as bright. An exemplary outline of the gating strategy can be found in **Suppl. Figure 2.** Analysis of cell cycle phases was performed by applying the mathematical Dean-Jett-Fox model for univariate cell cycle analysis (137), for automated detection of all cell cycle phases (**Figure 9A-A'**). When comparing SCZ to CTR, the percentage of cells in G2/M phase was significantly increased, while the other phases were not significantly altered (**Figure 9A-A', B**). To confirm these findings, immunocytochemical staining of proteins associated with regulation of the G2/M-phase was performed. Aurora A

kinase, critically involved in the assembly of the mitotic spindle, was upregulated in SCZ NPC **(Figure 9C, F)**. Additionally, Cyclin B1, a cell cycle regulating protein of the G2-phase, was also upregulated in SCZ NPC (**Figure 9D, H**). Both effects were specific for the NPC stage, and not detected in iPSC (**Figure 9E, G**). In conclusion, these findings provide evidence for (temporary) arrest of SCZ NPC in the G2/M phase.

Overall, phenotypic analysis of NPC revealed reduced neurite outgrowth, impaired differentiation efficiency and altered cell cycle control in SCZ.

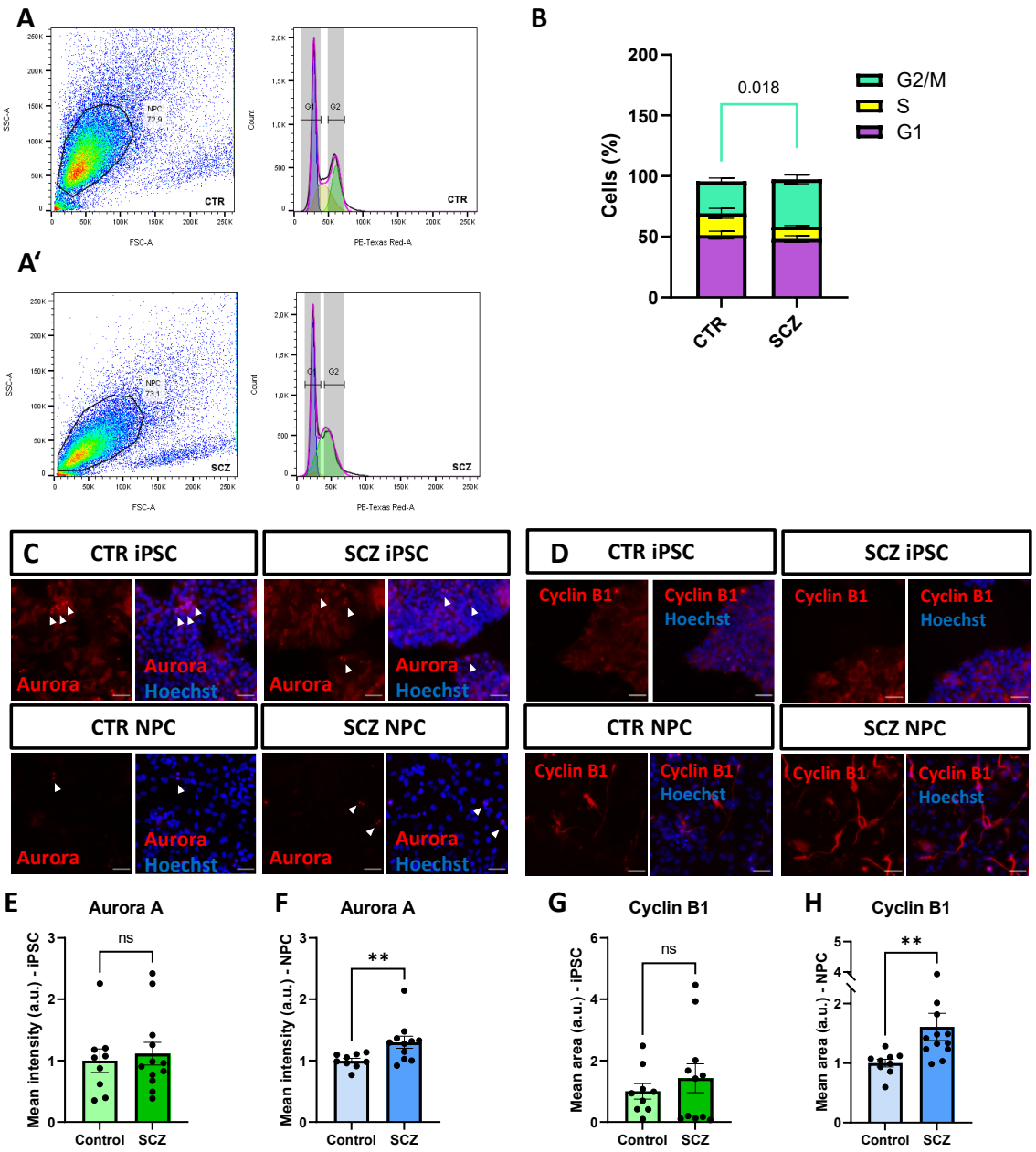

Figure 9 SCZ NPC arrest in G2/M cell cycle phase and show upregulation of G2/M-regulating proteins.

(A-A') Exemplary CTR **(A)** and SCZ **(A')** NPC populations stained with PI show characteristic G0/G1 (purple), S (yellow) and G2/M (green) cell cycle phases. **(B)** Quantification of cell phase distribution of CTR and SCZ NPC in percent. CTR: n= 5 wells, SCZ: 8 wells. A minimum of 15,000 events was recorded per well. 2-Way ANOVA with Tukey's multiple comparisons test, p-value as indicated, all others non-significant. Error bars: S.E.M. **(C-D)** Exemplary immunocytochemical staining of Aurora A Kinase **(C)**, Cyclin B1 **(D)** and Hoechst in CTR and SCZ iPSC and NPC. Scale bars: 50 µm. **(E-H)** Quantification of Aurora A mean fluorescence intensity in iPSC **(E)** and NPC **(F)** and Cyclin B1 mean stained area in iPSC **(G)** and NPC **(H)**. Two-tailed Mann Whitney U tests, CTR: n=9, SCZ: n= >10. Data points represent averaged values of multiple images within individual wells. Data were obtained from three independent experiments per line. Values are normalized to CTR. p≤0.01**, ns= not significant. Error bars: S.E.M.

3.2 Characterization of an iPSC-derived excitatory-inhibitory neuron co-culture model

Following the study of NPC, phenotypic characterization of differentiated neurons was performed next. To investigate synapse formation, neuronal activity and E-I balance in SCZ in a model of the cortical microcircuitry, an iPSC-derived E-I neuron co-culture system, comprising defined ratios of glutamatergic and GABAergic neurons, was employed. The chosen culture system represents a more physiological, complex model system, compared to traditional monocultures containing just one individual cell type, or heterogeneous neuronal cultures generate by undirected differentiation protocols.

The initial development and basal characterization of the E-I co-culture model was described in my Master's thesis (Johanna Heider, 2020). The co-culture system is comprised of iPSC-derived induced glutamatergic neurons, GABAergic interneurons, and murine astrocytes. In previous work performed by Dr. Ricarda Breitmeyer, the addition of functional primary astrocytes was found to be vital for neuronal maturity and proper synapse formation (Ricarda Breitmeyer, PhD thesis, 2021).

Neurons were generated via directed differentiation by lentiviral overexpression of lineage-specific transcription factors in iPSC-derived NPC, according to previously published protocols (122, 123). Directed differentiation protocols were chosen over undirected differentiation protocols due to their capacity to reproducibly generate homogenous populations of functional neurons in a short period of time, whilst rather heterogenous cultures are generated by undirected differentiation. Excitatory, glutamatergic neurons were differentiated by doxycycline-inducible overexpression of Neurogenin2 (NGN2 neurons) (122). Inhibitory GABAergic interneurons were generated by combined doxycycline-inducible overexpression of Achaete-scute homolog 1 (Ascl1) and Distal-Less homeobox 2 (Dlx2) (AD2 neurons) (123). Prior to seeding into E-I co-cultures, both types of immature neurons were selected by treatment with antibiotics for transgene-expressing cells, in order to maximize the purity of the cultures. NGN2 and AD2 neurons were combined into co-cultures at a ratio of 80:20, which is within the range of reported ratios of glutamatergic principal neurons to GABAergic interneurons in the cortex (48, 146, 147) (**Figure 10**).

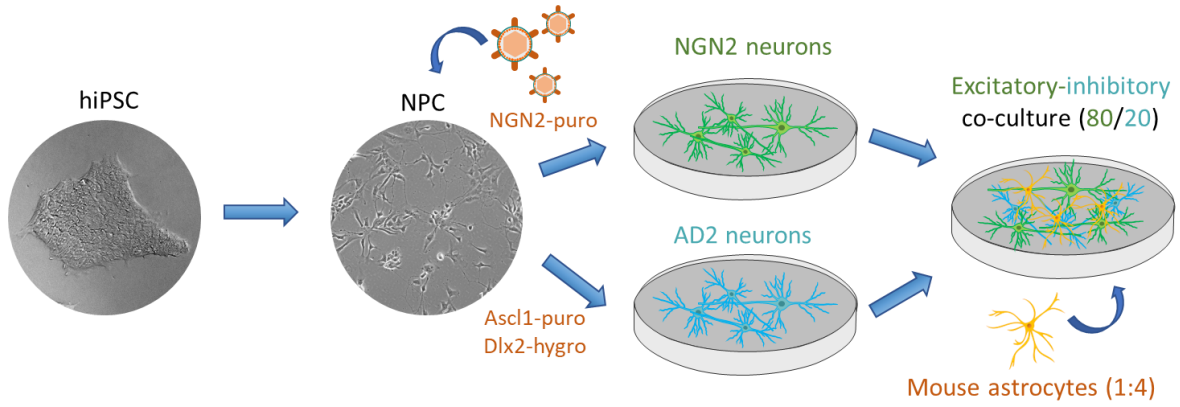

Figure 10 Schematic representation of E-I co-culture setup.
Human iPSC (hiPSC) are differentiated into NPC, which are transduced with NGN2-puromycine for differentiation into glutamatergic neurons (NGN2 neurons), or Ascl1-puromycine+Dlx2-hygromycine for differentiation into GABAergic (AD2) neurons by lentiviral infection. NGN2 and AD2 neurons are combined into co-cultures at a ratio of 80:20, and primary murine astrocytes are added at a ratio of 1:4.

3.2.1 NGN2 and AD2 neurons show characteristics of developing glutamatergic and GABAergic neurons

To evaluate whether both NGN2 and AD2 transduction of NPC reliably generated cultures enriched for glutamatergic and GABAergic neurons, respectively, immunocytochemical staining of cell type-specific markers was performed. After four weeks of differentiation (DIV28), immunocytochemical staining of subtype-specific neuronal markers was performed in CTR NGN2 and AD2 neurons cultured individually. NGN2 neurons showed robust expression of excitatory presynaptic marker vesicular glutamate transporter1 (vGLUT1), as well as postsynaptic markers Homer1 and postsynaptic density protein 95 (PSD95) (Johanna Heider, Master's thesis, 2020, **Figure 11A**). At the same time point, inhibitory synaptic markers were robustly expressed in AD2 neurons as well, including presynaptic markers vesicular GABA transporter (vGAT), glutamate decarboxylase 65 (GAD65), as well as postsynaptic markers Gephyrin and GABA-receptor subunit α2 (Johanna Heider, Master's thesis, 2020, **Figure 11B).** Pre- and postsynaptic markers in both types of neurons were observed to partially be in close apposition with each other, indicating the formation of structurally intact synapses (**Figure 11A, B**). GABAergic AD2 neurons also stained positive for the neurotransmitter GABA (**Figure 11C**), and a small fraction of neurons was found to express the peptide hormone somatostatin (SST), a marker of a subgroup of cortical interneurons which preferentially provides feedback inhibition to dendrites of cortical pyramidal neurons (148). No Parvalbumin (PV)-expressing interneurons were detected in AD2 cultures at this time point (**Figure 11D**).

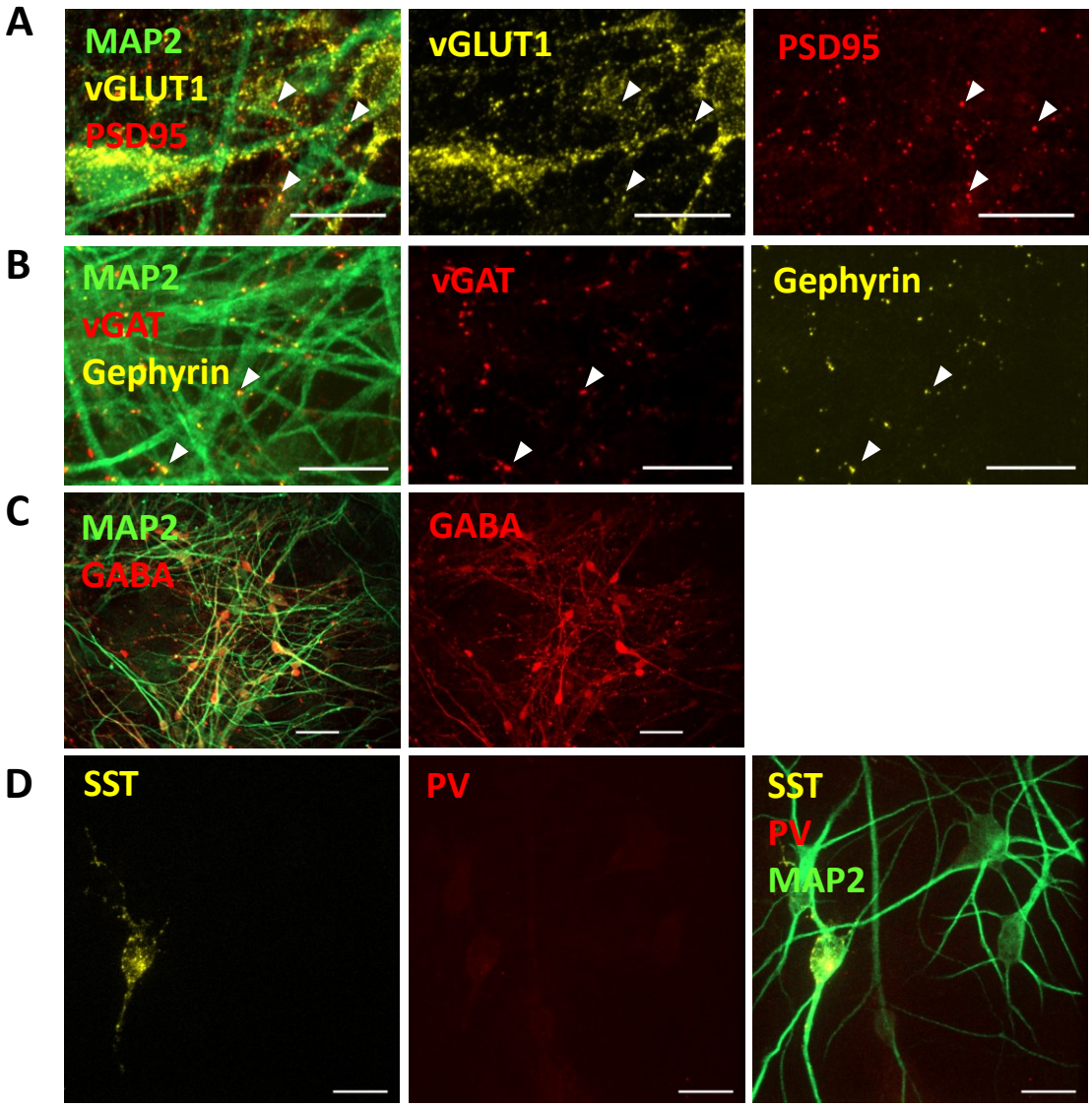

Figure 11 Expression of subtype-specific neuronal markers in NGN2 and AD2 monocultures.
(A) Expression of glutamatergic synaptic markers vGLUT1 and PSD95 by MAP2-positive NGN2 neurons (DIV28). Arrows indicate exemplary co-localizations of pre- and postsynaptic spots. Scale bars: 20 µm. **(B)** Expression of GABAergic synaptic markers vGAT and Gephyrin by MAP2-positive AD2 neurons (DIV28). Arrows indicate exemplary co-localizations of pre- and postsynaptic spots. Scale bars: 20 µm. **(C)** Expression of GABA by AD2 neurons (DIV28). Scale bars: 50 µm. **(D)** Immunocytochemical staining of somatostatin (SST) and Parvalbumin (PV) in AD2 neurons. Scale bars: 20 µm.

3.2.2 Fluorescent labelling of NGN2 neurons in E-I co-cultures allows the analysis of cell-type specific phenotypes

A further focus of this work was the cell-type specific analysis of disease phenotypes in co-cultured neurons. To allow the distinction of glutamatergic and GABAergic neurons in E-I co-cultures, fluorescent labeling of glutamatergic NGN2 neurons was performed. To this end, NPC were transduced with plasmids encoding NGN2 and GFP before seeding into co-culture. This allowed the distinction of GFP-positive NGN2 neurons from presumptive GFP-negative AD2 neurons for calcium imaging and synapse quantification experiments. Transduced neurons showed stable expression of GFP during the cultivation period up to DIV28, when assays were performed (**Figure 12A**). To exclude the possibility that GFP expression in NGN2 neurons impacts their functional and morphological properties, excitatory synapse formation and single-cell calcium activity was analyzed in monocultures of labeled and unlabeled NGN2 neurons, differentiated from three CTR lines (CTR1, CTR2, CTR3). Individual replicates of this experiment were performed by Sophia-Marie Hartmann.

Immunocytochemical analysis of co-localized vGLUT1 and PSD95 spots on MAP2-positive dendrites revealed no significant differences of excitatory synapse density nor the percentage of total vGLUT1 spots co-localizing with PSD95 (**Figure 12B-E**). To analyze spontaneous neuronal activity, cells were loaded with the red fluorescent chemical calcium indicator Calbryte 590 AM and recorded for 3 minutes after four weeks of differentiation (DIV28) to visualize neuronal activity. Specifically, somatic calcium traces of individual cells were analyzed as an approximation for action potential generation (149). Peak frequency as a measure of general activity and peak amplitude (ΔF/F) were analyzed, which indicates the relative amount of calcium entering the cell. Additionally, full width at half-maximum (FWHM) and area under the curve (AUC) were analyzed as a measure of calcium influx and efflux dynamics. For all parameters analyzed, no differences were detected between GFP-labeled and unlabeled NGN2 neurons (**Figure 12F-I).**

Overall, synapse quantification and neuronal activity measurements suggest that GFP expression does not markedly affect the properties of NGN2 neurons.

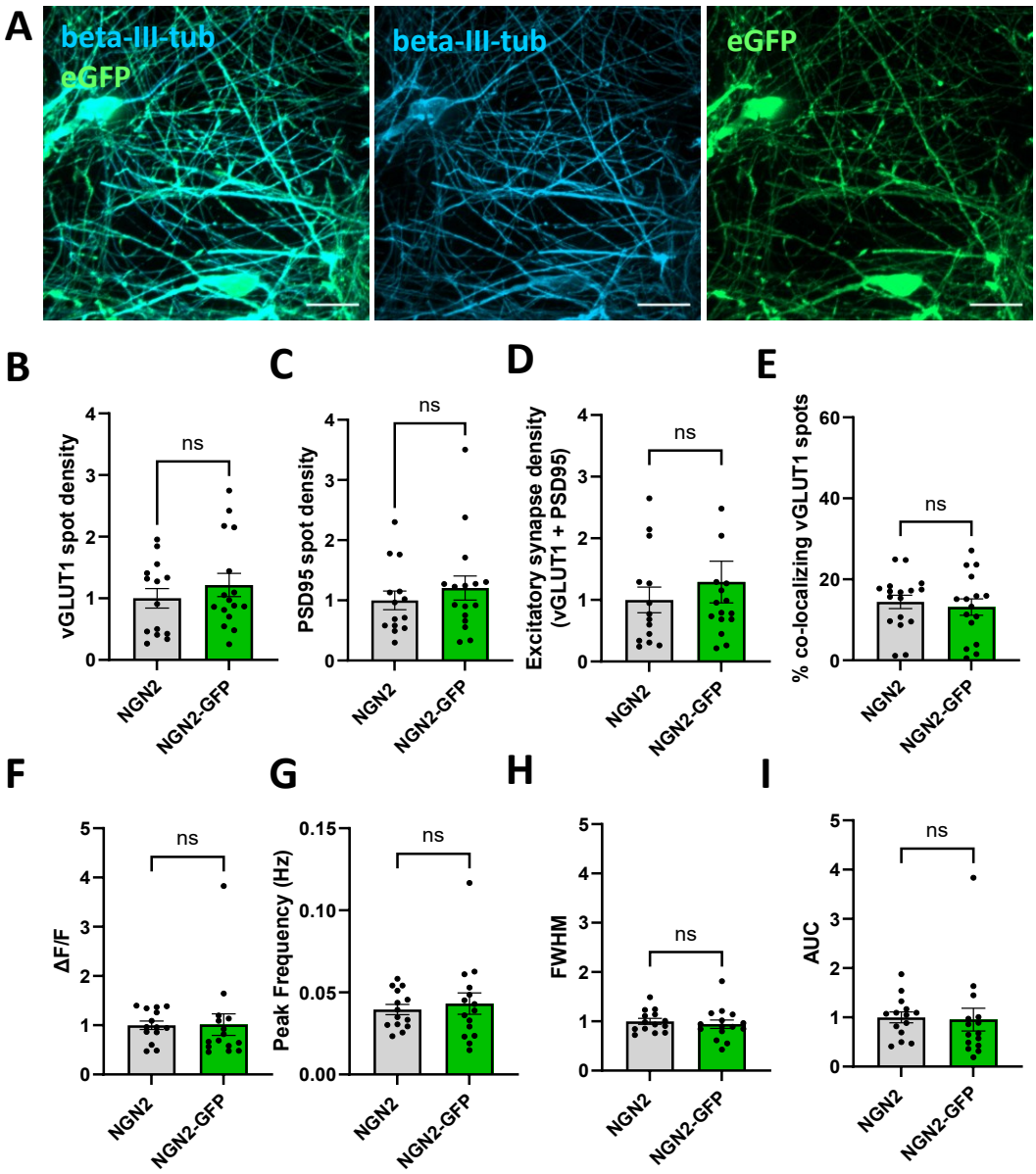

Figure 12 Expression of eGFP by NGN2 neurons does not alter their synapse expression and spontaneous neuronal activity.

(A) Beta-III-tubulin-positive neurons, differentiated by lentiviral transduction with NGN2-eGFP, strongly express GFP in their somata, axons and dendrites at DIV28. Scale bars: 20 µm. **(B-E)** Quantification of vGLUT1 presynaptic spot density **(B)**, PSD95 postsynaptic cluster density **(C)**, excitatory synapses (apposition of vGLUT1+PSD95) and the percentage of total vGLUT1 spots co-localizing with PSD95 **(E)** in monocultures of CTR NGN2 and NGN2-GFP neurons. All values are normalized to NGN2. Data points represent averaged values from multiple images within one well. Data were obtained from four independent experiments. Two-tailed Mann-Whitney U test, ns= not significant, n>13. **(F-I)** Analysis of peak amplitude (ΔF/F0) **(F)**, peak frequency (Hz) **(G)**, full-width half maximum (FWHM) **(H)** and area under the curve (AUC) **(I)** of single-cell calcium traces in monocultures of CTR NGN2 and NGN2-GFP neurons. All values are normalized to NGN2. Data points represent averaged values from multiple neurons within one well. Data were obtained from three independent experiments. Two-tailed Mann-Whitney U test, ns= not significant, n>13. Error bars: S.E.M.

3.3 Synaptic phenotypes in SCZ patient-derived neurons

A central component of the pathology of SCZ is the developmental disturbance of neuronal networks, amongst others characterized by a loss of synapses (150). GWAS data has linked multiple genetic risk variants linked to synapse formation as well as complement proteins to SCZ (14, 151), suggesting that intrinsic neuronal deficits in synapse formation, as well as aberrant complement-mediated synaptic pruning could be involved in the disease. Using the established E-I co-culture system, both aspects will be addressed in the following. In this first part, excitatory and inhibitory synapse formation will be first studied in cultures comprising only NGN2 neurons or AD2 neurons individually, followed by the analysis of E-I co-cultures.

3.3.1 Excitatory synapse density is reduced in SCZ NGN2 neuron monocultures

To quantify the number of excitatory synapses on NGN2 neurons, immunocytochemical staining of presynaptic marker vGLUT1 and postsynaptic marker PSD95 was performed using the full set of three CTR and four SCZ lines. To classify as a synapse, only pre- and postsynaptic spots on MAP2-positive neurons, which were in close apposition to each other (≤ 0.2 µm, corresponding to the resolution limit of the confocal microscope), were considered for analysis (**Figure 13A**).

At DIV28, the density of vGLUT1-positive presynaptic terminals was significantly reduced in SCZ NGN2 neurons (**Figure 13B**). However, the density of PSD95-positive postsynaptic structures was unaltered in SCZ neurons (**Figure 13C**). When vGLUT1 and PSD95 spots were analyzed in apposition to each other (= excitatory synapse) a significant reduction of synapses was observed in SCZ NGN2 neurons (**Figure 13D**). During the development of excitatory synapses, presynaptic terminals make contact with neuronal dendrites, leading to the assembly of the postsynaptic density (152). Therefore, the percentage of vGLUT1 spots in co-localization with PSD95 spots was analyzed as a measure of the fraction of total available presynaptic terminals which (already) established contact with postsynaptic compartments. No significant change of this parameter was observed in SCZ neurons (**Figure 13E**). Quantification results for each individual CTR and SCZ line can be found in **Suppl. Figure 3A-D.**

Overall, these results confirm previous observations of reduced presynapse density in NGN2 neurons, obtained with the same set of patient lines (136). Additionally, SCZ NGN2 neurons showed a significant reduction of excitatory synapses when cultured individually.

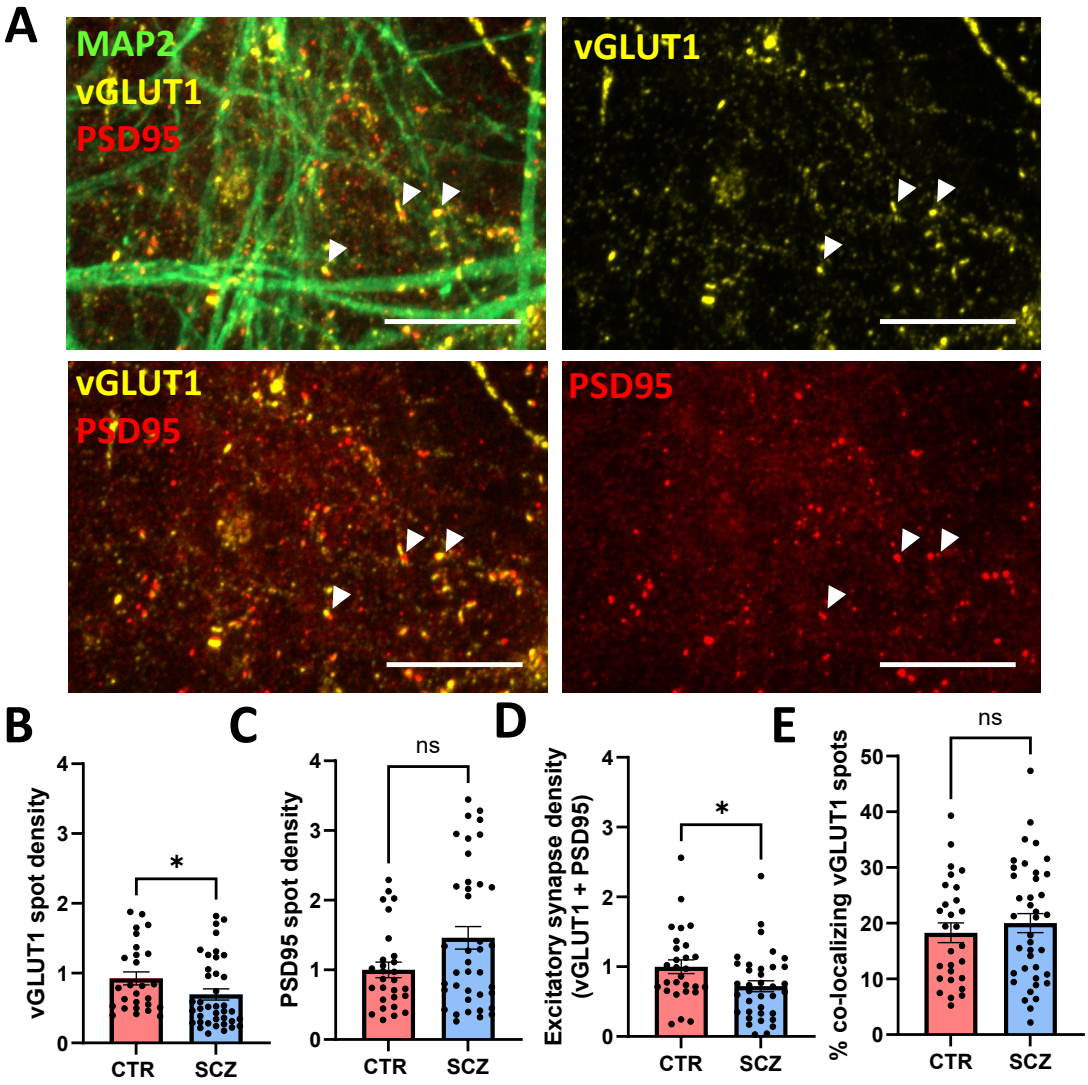

Figure 13 Excitatory synapse density is reduced in SCZ glutamatergic NGN2 neurons. **(A)** Apposition of presynaptic marker vGLUT1 and postsynaptic marker PSD95 on MAP2-positive dendrites in DIV28 NGN2 neuron monocultures. Exemplary co-localizing vGLUT1 and PSD95 spots are marked by arrows. Scale bars: 20 µm. **(B-E)** Quantification of synaptic markers on MAP2-positive dendrites of NGN2 neurons. Density of **(B)** VGLUT1 spots, **(C)** PSD95 spots, **(D)** excitatory synapses (apposition of vGLUT1+ PSD95 spots) and **(E)** percentage of vGLUT1 posts co-localizing with postsynaptic PSD95. All values are normalized to CTR. Data points represent averaged values from multiple images within one well. Data were obtained from four independent experiments per donor. Two-tailed Mann Whitney U test, p≤ 0.05*, ns= not significant, n >25, error bars: S.E.M.

3.3.2 Inhibitory synapse density is unchanged in SCZ AD2 neuron monocultures

Besides the well-characterized alterations of pyramidal neurons in SCZ, there is strong evidence for the involvement of cortical GABAergic neurons in the etiology of the disease (153). To this end, the number of inhibitory synapses formed by CTR and SCZ GABAergic AD2 neurons, cultured individually, was quantified.

The density of inhibitory synapses in the cultures was analyzed by quantification of apposing vGAT-positive presynaptic terminals and Gephyrin-positive postsynaptic terminals (**Figure 14A**). As described above, only pre- and postsynaptic spots in close apposition to each other (≤ 0.2 µm) were considered for analysis. DIV28 SCZ AD2 neurons showed a significant reduction of vGAT-positive terminals (**Figure 14B**), while no change of Gephyrin cluster density was observed (**Figure 14C**)**.** The density of inhibitory synapses was also not affected in SCZ neurons (**Figure 14D**). While these results suggest that synaptic vGAT seems to be largely unaffected, a significant increase of total vGAT spots co-localizing with Gephyrin clusters was observed in SCZ cultures (**Figure 14E**). Taking both of these findings into account, it can be concluded that the extrasynaptic rather than synaptic vGAT density is decreased in SCZ AD2 neurons. Quantification results for each individual CTR and SCZ line can be found in **Suppl. Figure 3E-H.**

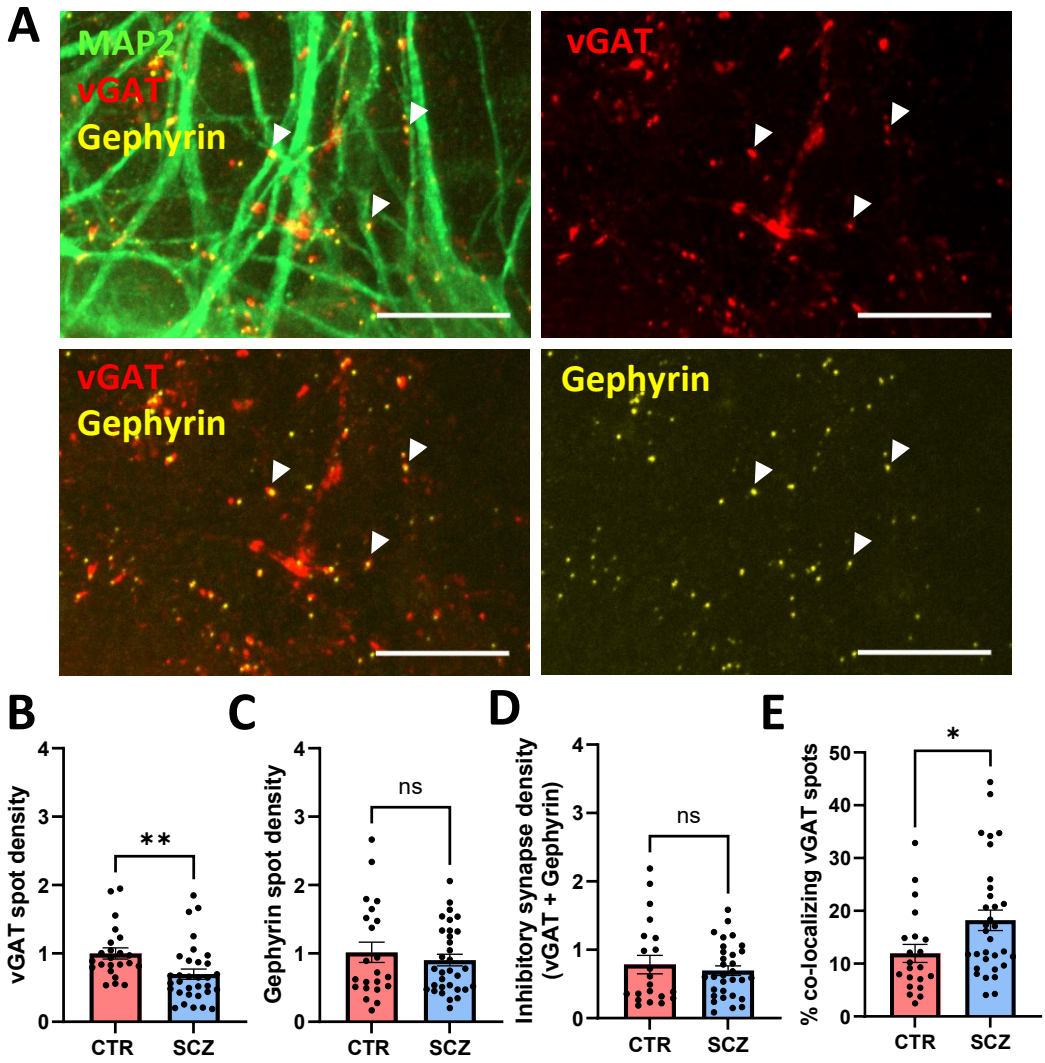

Figure 14 Inhibitory synapse density is unchanged in SCZ GABAergic AD2 neurons. **(A)** Apposition of presynaptic marker vGAT and postsynaptic marker Gephyrin on MAP2-positive dendrites in DIV28 AD2 neuron monocultures. Exemplary co-localizing vGAT and Gephyrin spots are marked by arrows. Scale bars: 20 µm. **(B-E)** Quantification of synaptic markers on MAP2-positive dendrites of AD2 neurons. Density of **(B)** VGAT spots, **(C)** Gephyrin spots, **(D)** inhibitory synapses (apposition of vGAT+Gephyrin spots) and **(E)** percentage of vGAT posts co-localizing with postsynaptic Gephyrin. All values are normalized to CTR. Data points represent averaged values from multiple images within one well. Data was obtained from four independent experiments per donor. Two-tailed Mann Whitney U test, p≤ 0.05*, p≤ 0.01**, ns= not significant, n >20, error bars: S.E.M.

3.3.3 Excitatory synapse numbers are increased in SCZ E-I co-cultures

Experiments with glutamatergic NGN2 and GABAergic AD2 neurons cultured individually revealed SCZ-specific synaptic alterations for both types of neurons, most importantly a decrease of presynaptic terminals (**3.3.1, 3.3.2**). These results help to shed light on intrinsic

mechanisms of synapse formation for the individual cell types. To investigate synapse formation in a more physiologically relevant, complex culture system, excitatory and inhibitory synapses were next quantified in E-I co-cultures, derived from CTR and SCZ NPC. NGN2 and AD2 neurons which were co-cultured were always derived from the same donor.

The number of presynaptic terminals, postsynaptic compartments, and pre- and posytsynaptic markers in apposition was quantified on MAP2-positive neurons. Importantly, GFP-labeled NGN2 neurons allowed the distinction of both types of neurons in the cultures**.** The present culture system therefore made it possible to distinguish between four types of synapses:

1) excitatory synapses (vGLUT1+PSD95) on NGN2 neurons (MAP2 +, GFP +)

2) excitatory synapses (vGLUT1+PSD95) on AD2 neurons (MAP2 +, GFP -)

3) inhibitory synapses (vGAT+Gephyrin) on NGN2 neurons (MAP2 +, GFP +)

4) inhibitory synapses (vGAT+Gephyrin) on AD2 neurons (MAP2 +, GFP -)

Contrary to NGN2 neurons cultured separately, quantification of vGLUT1-positive terminals in E-I co-cultures was unchanged between CTR and SCZ, regardless of their position on either NGN2 or AD2 neurons (**Figure 15B, F**). Interestingly however, a strongly significant increase (~ 1.8-fold) of PSD95 cluster density on both NGN2 and AD2 neurons was observed in SCZ cultures (**Figure 15C, G**). This increase of PSD95 density was also reflected in a significant increase of excitatory synapse density, specifically on AD2 neurons (~ 1.6-fold, **Figure 15H**). Excitatory synapses on NGN2 neurons were not significantly altered (**Figure 15D**). Finally, the percentage of total vGLUT1 spots co-localized with PSD95 spots was calculated. A significant increase of co-localizing vGLUT1 was detected on both NGN2 and AD2 neurons in SCZ cultures (**Figure 15E, I**). Quantification results for each individual CTR and SCZ line can be found in **Suppl. Figure 4**.

Next, inhibitory synapses on co-cultured NGN2 and AD2 neurons were studied by quantifying presynaptic vGAT-positive terminals and postsynaptic Gephyrin clusters (**Figure 16A**). Presynaptic vGAT density, postsynaptic Gephyrin cluster density and inhibitory synapse density on NGN2 and AD2 neurons were unaffected in SCZ cultures (**Figure 16B-D, F-H**). Solely the percentage of vGAT spots co-localizing with postsynaptic Gephyrin clusters was significantly elevated on SCZ AD2 neurons (**Figure 16I**). The same parameter remained unchanged when only NGN2 neurons were analyzed (**Figure 16E**). Quantification results for each individual CTR and SCZ line can be found in **Suppl. Figure 5**.

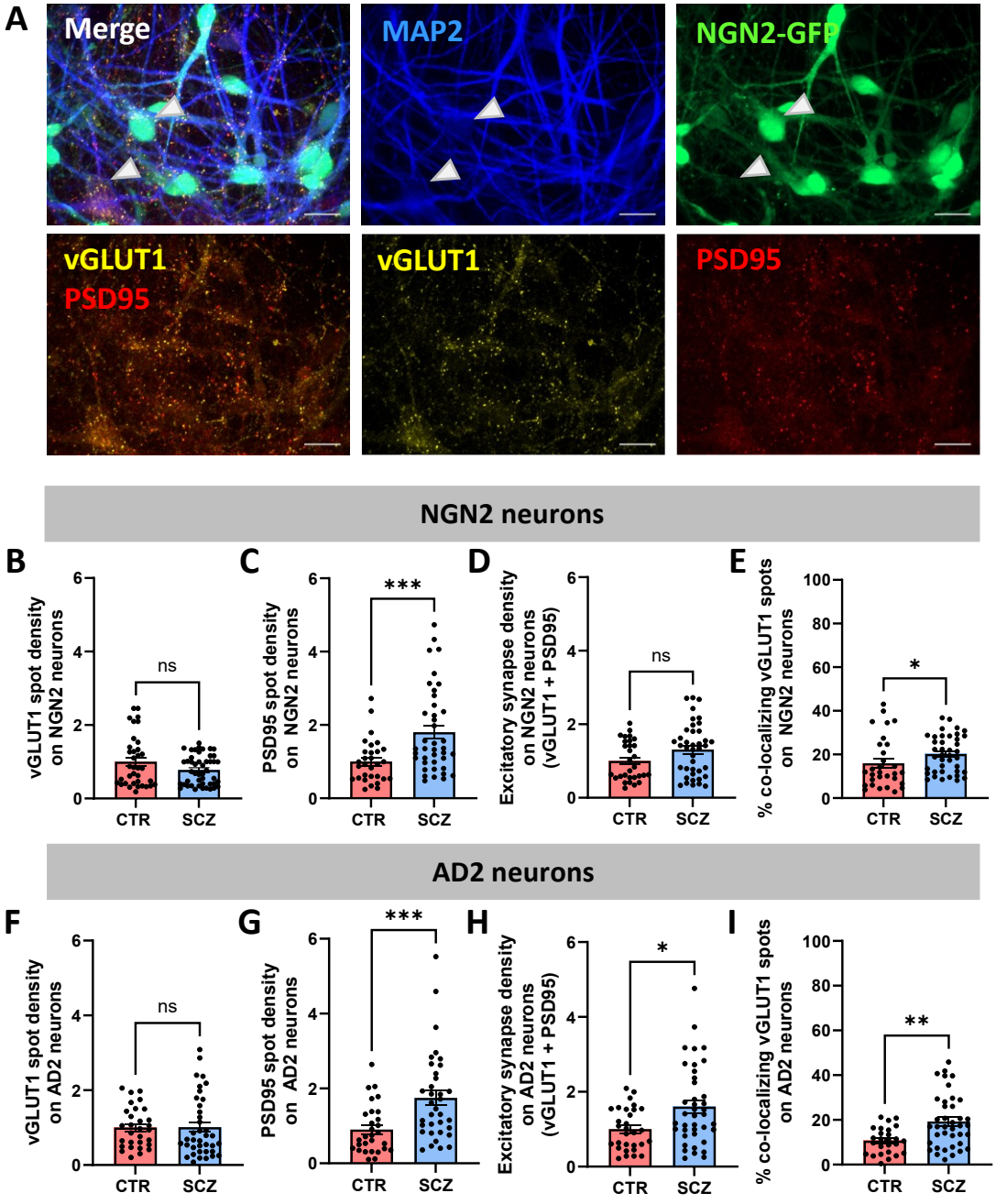

Figure 15 Increased excitatory synapse density in SCZ E-I co-cultures.
(A) Expression of vGLUT1-positive synaptic terminals and PSD95-positive postsynapses in DIV28 E-I co-cultures. Synapses were quantified on MAP2/GFP-double positive NGN2 neurons and MAP2-positive/GFP-negative AD2 neurons (examples indicated by arrows). **(B-E)** Quantification of excitatory synaptic markers on NGN2 neurons. Density of **(B)** VGLUT1 spots, **(C)** PSD95 spots, **(D)** excitatory synapses (apposition of vGLUT1+ PSD95 spots) and **(E)** percentage of vGLUT1 spots co-localizing with postsynaptic PSD95. **(F-I)** Quantification of excitatory synaptic markers on AD2 neurons. Density of **(F)** VGLUT1 spots, **(G)** PSD95 spots, **(H)** excitatory synapses and **(I)** percentage of vGLUT1 spots co-localizing with postsynaptic PSD95. All values are normalized to CTR. Data points represent averaged values from multiple images within one well. Data were obtained from five independent experiments per donor. Two-tailed Mann Whitney U test, p≤ 0.05*, p≤ 0.01**, p≤ 0.001***, ns= not significant, n >25, error bars: S.E.M.

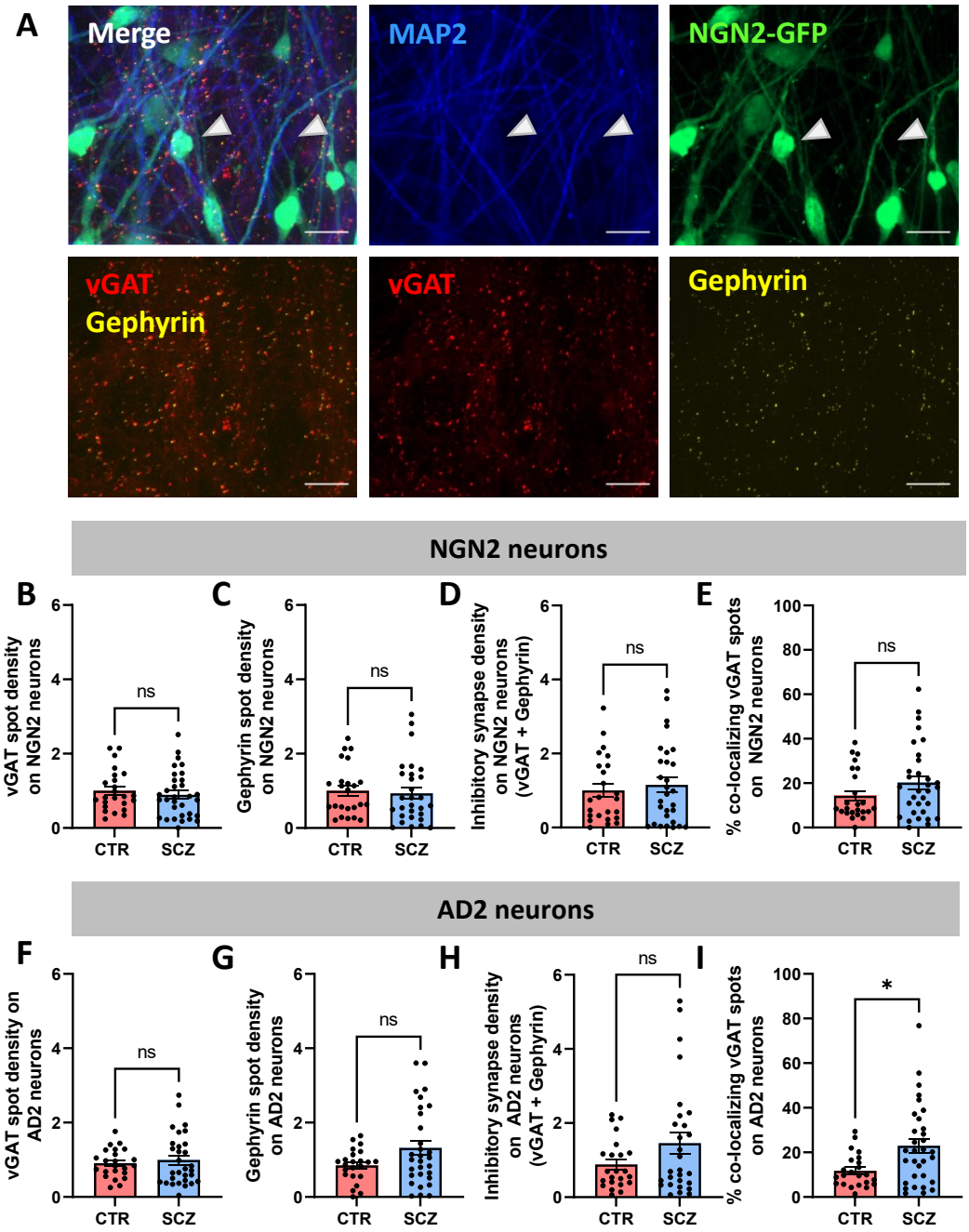

Figure 16 Inhibitory synapses are unaffected in SCZ E-I co-cultures.
(A) Expression of vGAT-positive synaptic terminals and Gephyrin-positive postsynapses in DIV28 E-I co-cultures. Synapses were quantified on MAP2/GFP-double positive NGN2 neurons and MAP2-positive/GFP-negative AD2 neurons (examples indicated by arrows). (B-E) Quantification of inhibitory synaptic markers on NGN2 neurons. Density of (B) vGAT spots, (C) Gephyrin spots, (D) inhibitory synapses (apposition of vGAT+Gephyrin spots) and (E) percentage of vGAT spots co-localizing with postsynaptic Gephyrin. (F-I) Quantification of inhibitory synaptic markers on AD2 neurons. Density of (F) VGAT spots, (G) Gephyrin spots, (H) inhibitory synapses and (I) percentage of vGAT spots co-localizing with Gephyrin. All values are normalized to CTR. Data points represent averaged values from multiple images within one well. Data were obtained from four independent experiments per donor. Two-tailed Mann Whitney U test, p≤ 0.05*, ns= not significant, n >22, error bars: S.E.M.

In summary, synapse quantifications in E-I co-cultures revealed diverging phenotypes when compared to NGN2 and AD2 neurons cultured separately, striking the importance of more physiologically relevant culture systems to study disease phenotypes. In general, excitatory synapses were more strongly affected in the present model system, with increased postsynaptic marker densities observed in SCZ cultures. Inhibitory synapses, on the contrary, showed only minor aberrations. The specificity of some of the reported alterations for just one cell type also underlines the importance of carrying out synaptic analyses of E-I co-cultures in a cell-type specific manner.

3.4 Spontaneous neuronal activity is altered in SCZ E-I co-cultures

As described in the previous chapter, aberrant synapse formation was observed in SCZ E-I co-cultures. To study whether there are functional consequences of altered synaptic connectivity and whether CTR and SCZ samples can be distinguished based on their basal neuronal activity patterns, calcium imaging of spontaneous single-cell and network activity was performed in E-I co-cultures.

3.4.1 Neurons in E-I co-cultures develop spontaneous single-cell and network burst activity

In vivo, the precisely timed interplay of cortical excitatory and inhibitory neurons is crucial for the generation of synchronized neuronal network oscillations, which emerge during brain development (71, 72). Therefore, the development of synchronized spiking activity in iPSC-derived neuronal cultures is regarded as an important indicator of neuronal network maturation (154).

In previous experiments, calcium imaging of neurons in E-I co-cultures revealed robust, spontaneous single-cell activity at DIV 21 and DIV 28. However, only 12.5 % of recorded wells showed synchronous network activity, indicative of functional synaptic connections (Johanna Heider, Master's thesis, 2020, (155)). Cultures were regarded as synchronous if either a larger fraction of cells showed coordinated neuronal activity (minimum of $\sim 1 / 4$ of the well) or if there was network activity observed throughout the whole well that was recorded from. To improve the maturity of E-I co-cultures for expanded analysis of neuronal activity in this thesis, the co-culture protocol was adapted. The addition of doxycycline to the neuronal medium at the end of the cultivation period (DIV24-28), inducing a second wave of transgene expression via the tetON system, was found to increase the fraction of cultures displaying spontaneous network

activity (**Figure 17**). Exemplary calcium traces of NGN2 and AD2 neurons in a culture with synchronized bursting behavior are displayed in **Figure 17A.** From a total of 120 wells, recorded from CTR (CTR1, CTR2, CTR3) and SCZ (SCZ1, SCZ2, SCZ4, SCZ5) cultures in seven independent neuronal differentiations, ~ 37 % of wells showed bursting activity (**Figure 17B**). When CTR and SCZ samples were analyzed separately, a higher proportion of CTR samples showed synchronized burst activity (~ 45 % of CTR wells and ~ 34 % of SCZ wells, **Figure 17C, D**). This difference was however not statistically significant (χ2- test, p= 0.23, CTR: n= 40, SCZ: n=80).

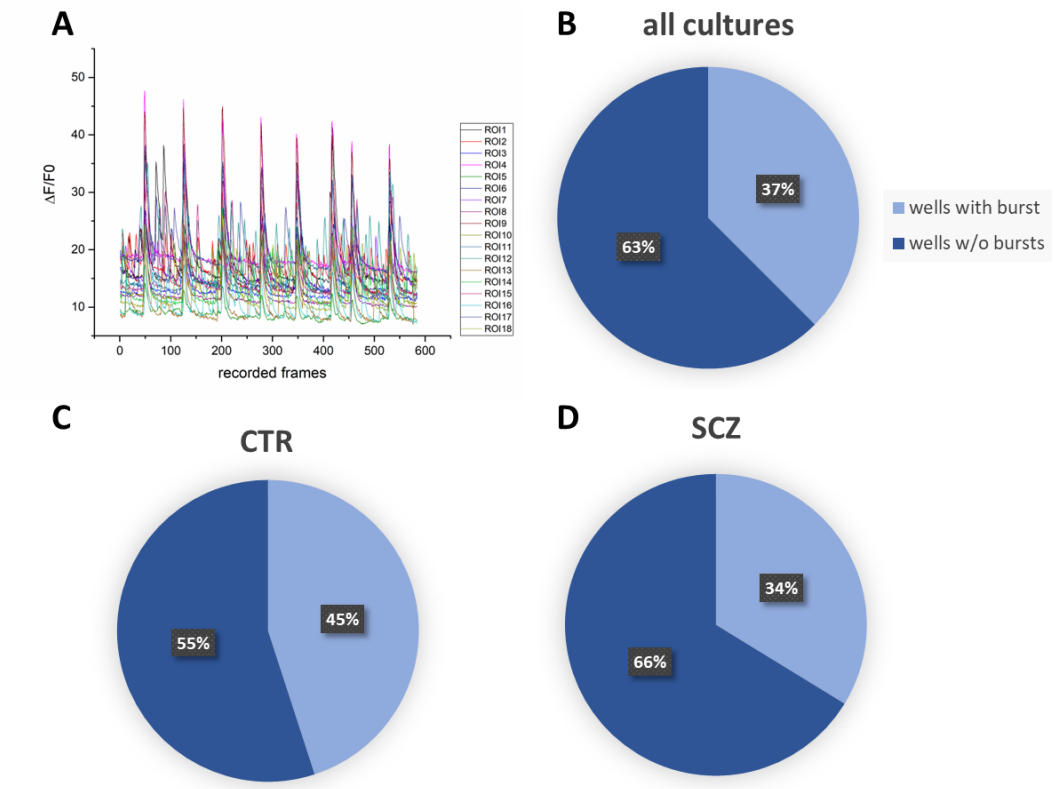

Figure 17 Characterization of synchronized network bursting in CTR and SCZ E-I co-cultures.
(A) Exemplary calcium traces, recorded over a period of 3 minutes, of 9 NGN2 (ROI 1-9) and 9 AD2 neurons (ROI 10-18) in a CTR E-I co-culture at DIV28 (ΔF/F0= amplitude). **(B)** Percentages of recorded wells with and without (w/o) synchronized network burst activity in all E-I co-cultures (n=120 from seven independent experiments, with bursts: n= 45, w/o bursts: n= 75), **(C)** CTR co-cultures (n= 40, with bursts: n= 18, w/o bursts: n= 22) and **(D)** SCZ co-cultures (n= 80, with bursts: n= 27, w/o bursts: n= 53).

3.4.2 NGN2 and AD2 neurons in E-I co-cultures show distinct activity patterns which are influenced by disease allocation

Primary rodent cortical glutamatergic and GABAergic neurons *in vitro* show clearly distinct spiking properties (156)**.** To study whether this also holds true for iPSC-derived NGN2 and AD2 neurons *in vitro* after a co-cultivation period of three weeks, the activity patterns of the two types of neurons were compared at DIV28. Somatic calcium traces were recorded and analyzed from CTR and SCZ neurons with a minimum of one calcium peak occurring during the recording period of 3 minutes. For this experiment, only neurons showing asynchronous spiking activity independent of network bursts were included, since the dynamics of asynchronous spiking were observed to be quite different to synchronous activity (e.g., higher bursting frequency of asynchronously active neurons). All neurons in the culture were stained with the red fluorescent chemical calcium indicator Calbryte 590 AM and NGN2 neurons were transduced with GFP to allow for cell-type specific analysis of calcium signals (**Figure 18A**). Peak amplitude (ΔF/F0), peak frequency, FWHM and AUC were analyzed.

Overall, NGN2 and AD2 neurons differed in multiple of the parameters analyzed, showing that the two types of neurons possess distinct functional properties in an unstimulated state. AD2 neurons in general showed increased amplitudes, reduced frequency, increased FWHM and increased AUC when compared to NGN2 neurons (**Figure 18B-K**). Interestingly, the distinction of NGN2 and AD2 based on these properties seemed to be even more prominent in SCZ cultures, in which the neurons differed significantly in all parameters analyzed (amplitude, frequency, FWHM and AUC, **Figure 18H-K**), while in CTR cultures, only peak frequency and AUC were significantly different between NGN2 and AD2 neurons (**Figure 18D-G**). To statistically analyze whether the differences between the two cell types are influenced by disease state, two-way ANOVA was performed for all four parameters. Besides the reported differences between NGN2 and AD2 neurons (cell type effect), an independent effect of disease allocation on the data sets for peak amplitude and FWHM was observed (ΔF/F0: $p= 0.005$, FWHM: $p= 0.03$). For the parameter AUC, an effect of disease state ($p= 0.003$), as well as an interactive effect of disease state and cell type ($p= 0.03$) was observed.

Taken together, these findings provide evidence for a potential influence of the SCZ phenotype on the basal calcium activity profile of NGN2 and/or AD2 neurons. Moreover, the analysis confirmed differential activity patterns (peak frequency, AUC) of glutamatergic NGN2 and GABAergic AD2 neurons in E-I co-cultures, emphasizing the importance to perform a separate analysis of each type of neuron rather than a broad analysis of all neurons in the cultures for the study of spontaneous desynchronized spiking activity.

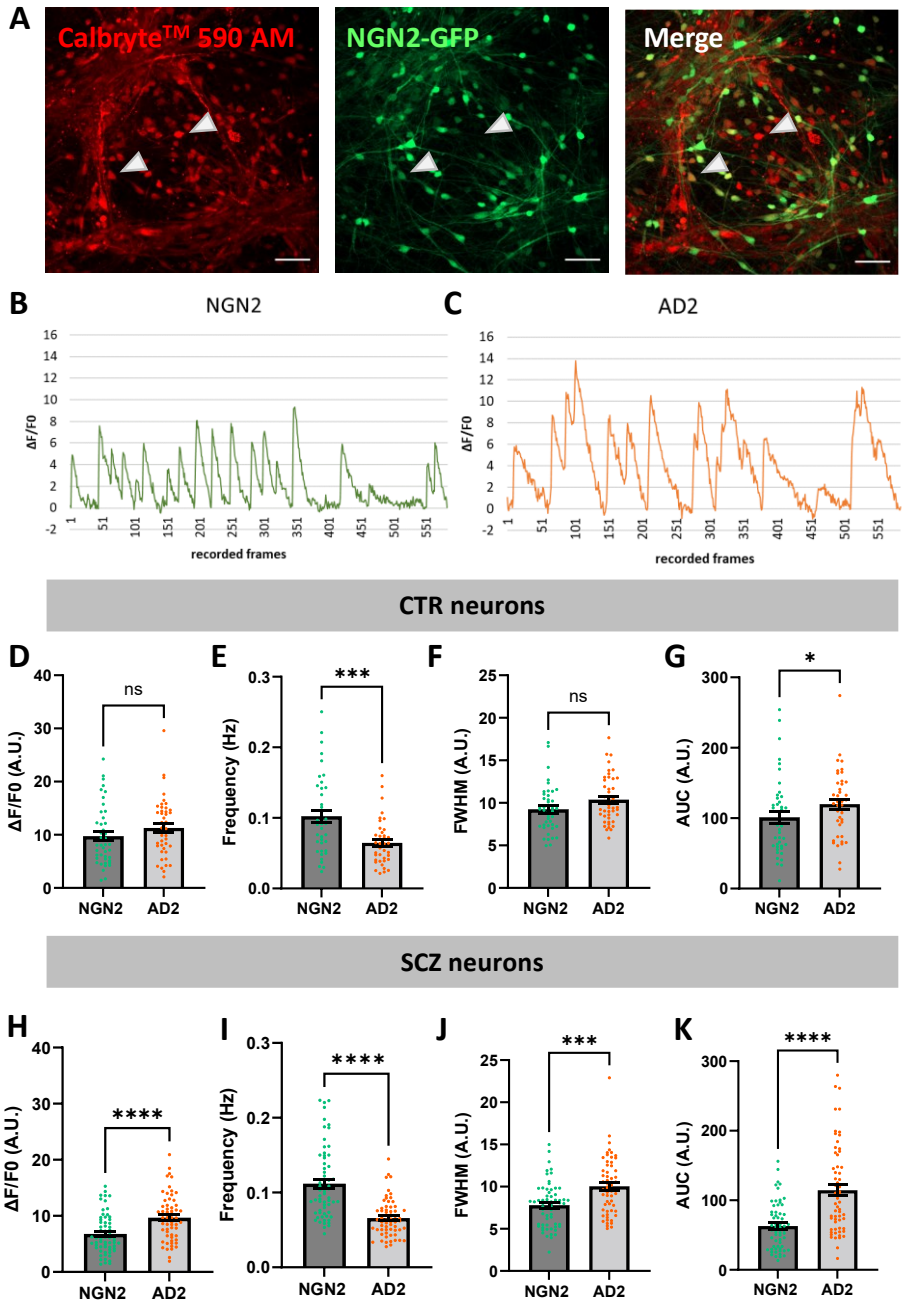

Figure 18 NGN2 and AD2 neurons in E-I co-cultures show differential activity patterns which are influenced by disease allocation.

(A) All neurons in E-I co-cultures are stained with the red fluorescent chemical calcium indicator Calbryte 590 AM and NGN2 neurons express GFP, allowing the cell type-specific analysis of calcium signals. Arrows indicate exemplary Calbryte/GFP-positive NGN2 and Calbryte-positive/GFP-negative AD2 neurons. Scale bars: 50 µm. **(B)** Exemplary somatic calcium traces of a NGN2 neuron and **(C)** an AD2 neuron, recorded over a period of 3 minutes. **(D-K)** Analysis of peak amplitude (ΔF/F0), peak frequency (Hz), full-width-half maximum (FWHM) and area under the curve (AUC) of NGN2 and AD2 CTR **(D-G)** and SCZ neurons **(H-K)**. Data points represent averaged values from multiple neurons within one well. Data were obtained from a minimum of three independent experiments per donor. Two-tailed Mann Whitney U test, p≤ 0.05*, p≤0.001***, p≤0.0001****, ns= not significant, n >40, error bars: S.E.M.

3.4.3 Differences in unsynchronized and synchronized single-cell activity in SCZ

Following up on the results described in **3.4.2**, spontaneous single-cell calcium activity of glutamatergic NGN2 and GABAergic AD2 neurons in E-I co-cultures of CTR and SCZ lines was compared. Recordings of somatic calcium signals in unstimulated GFP-positive NGN2 and GFP-negative AD2 neurons were performed at DIV28 over a time period of 3 minutes.

The analysis was first focused on non-bursting, unsynchronized neurons which are not or less influenced by synaptic connectivity. Altered activity patterns were only observed for glutamatergic NGN2 neurons in SCZ cultures, while the activity of SCZ AD2 GABAergic neurons was unchanged regarding all parameters analyzed (**Figure 19C, D, Suppl. Figure 6C, D**). SCZ NGN2 neurons presented a significantly reduced mean peak amplitude and FWHM, resulting in a lower AUC (**Figure 19A, Suppl. Figure 6A, B**). These findings suggest reduced calcium entry into the cells, as well as slower influx and/or efflux dynamics of calcium ions. The mean peak frequency of SCZ NGN2 neurons was not significantly different, compared to CTR (**Figure 19B**). Overall, a specific alteration of the basal spontaneous activity of NGN2 neurons was observed in SCZ samples, when the analysis was focused on neurons not or little influenced by synaptic connectivity.

Next, the functional consequences of altered synaptic connectivity in E-I co-cultures (**3.3.3**) were investigated by focusing the analysis of single-cell calcium activity on those neurons, which were involved in network burst activity. As in most cultures, both neurons with and without synchronized calcium activity were identified, this analysis offers the possibility to compare the activity patterns from neurons more influenced by their synaptic connections, to the basal activity of neurons more independent of their connectivity to neighboring neurons in the same samples. Again, cell-type specific analysis of CTR and SCZ NGN2 and AD2 neurons was performed.

Interestingly, the results obtained by the analysis of synchronous neurons differed considerably from the prior analysis of asynchronous neurons. The calcium peak amplitude of NGN2 neurons was unaffected this time, while it was significantly reduced in AD2 neurons. AD2 neurons also showed a concomitant reduction of AUC (**Figure 19E, G, Suppl. Figure 6H**). Additionally, the peak frequency of both synchronous NGN2 and AD2 neurons was significantly increased in SCZ (**Figure 19F, H**). FWHM remained unchanged in NGN2 and AD2 neurons (**Suppl. Figure 6E, G**). In summary, these observations, specific for synchronously firing neurons, suggest that altered synaptic connectivity or synapse function in SCZ alters the calcium response of the postsynaptic neuron.

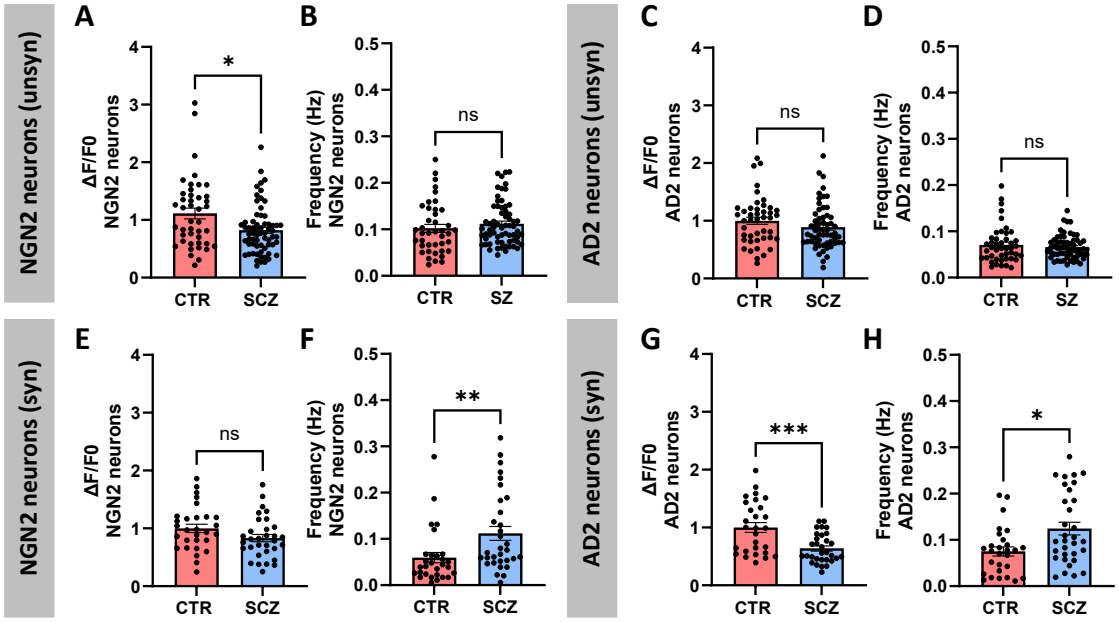

Figure 19 Altered calcium dynamics of unsynchronized and synchronized neuronal activity in SCZ.

(A-D) Analysis of calcium peak characteristics of DIV28 unsynchronized (=unsyn) NGN2 and AD2 neurons. Peak amplitude (ΔF/F0) and peak frequency (Hz) were analyzed in CTR and SCZ samples. Data points represent averaged values from multiple neurons within one well. Data were obtained from a minimum of three independent experiments per donor. Two-tailed Mann Whitney U tests, n >40, error bars: S.E.M. **(E-H)** Analysis of calcium peak characteristics (ΔF/F0, frequency) of DIV28 synchronized (=syn) NGN2 and AD2 neurons. Data points represent averaged values from multiple synchronous neurons within one recording across seven independent experiments. Two-tailed Mann Whitney U tests, ns= not significant, n >27, error bars: S.E.M. p< 0.05*, p≤0.01**, p≤0.001***.

Concluding the phenotypes observed in E-I co-cultures, aberrant synapse formation, network and single-cell calcium activity were identified in SCZ samples. The major synaptic phenotype was an elevated density of excitatory synapses targeting AD2 neurons, mediated by an overall increase in the number of postsynaptic PSD95 clusters. This finding was in contrast to the reduction of presynapses observed in both NGN2 and AD2 neurons cultured independently, suggesting an interaction of both types of neurons which influences synapse formation in the co-cultures. Functionally, the occurrence of spontaneous network burst activity was reduced in SCZ cultures. On a single cell level, NGN2 and AD2 neurons could be distinguished based on their basal spontaneous single-cell calcium dynamics, which also revealed a reduction of calcium activity specific for SCZ NGN2 neurons in E-I co-cultures. Finally, the analysis of synchronized single-cell activity showed alterations in both types of neurons, most strikingly an increase of peak frequency in NGN2 and AD2 SCZ neurons, as well as a decreased calcium amplitude of AD2 SCZ neurons.

3.5 Microglia derived from patients with SCZ influence synapse formation and neuronal activity in E-I co-cultures

Besides the intrinsic deficits of synapse formation and resultant aberrant neuronal network functionality which were discussed in the previous chapter, neuroinflammation is widely discussed as an important contributing factor to the pathology of SCZ. There is a growing body of evidence suggesting that microglia, the innate immune cells of the brain, show increased activation in SCZ and might contribute to synapse loss and thus excitation-inhibition imbalance in the cortex (85, 150).

To date, studies of synaptic pruning using iPSC-derived cell types have focused on the interaction of microglia with glutamatergic neurons and synaptosomes isolated from glutamatergic neurons (136, 157) and there are no studies of synaptic pruning in culture systems comprising both glutamatergic and GABAergic neurons in the context of SCZ. To study this aspect, iPSC-derived microglia were co-cultured with neurons in E-I co-cultures. Synapse quantification and measurements of neuronal activity by calcium imaging was performed to characterize cell-type specific neuron-microglia interactions.

3.5.1 Patient-derived microglia lead to reduced GABAergic presynapses in E-I co-cultures

Microglia were derived from CTR and SCZ iPSC lines and co-cultured with neurons as described previously (136). To specifically focus on microglia-mediated synaptic phenotypes, either CTR or SCZ microglia were added to CTR E-I co-cultures for 72h. Microglia were differentiated from three CTR iPSC lines (CTR2, CTR3, CTR4) and the four SCZ patient lines (SCZ1, SCZ2, SCZ4, SCZ5). Immunocytochemical staining of the microglial marker IBA1 showed an even distribution of microglia within E-I co-cultures at DIV28. Microglia were observed to be in direct contact with the neurons, wrapping their processes around MAP2-positive dendrites (**Figure 20A**). To investigate whether CTR and SCZ microglia exert a differential effect on synaptic density, presynaptic excitatory (vGLUT1) and inhibitory (vGAT) markers were stained and quantified. A small but significant reduction of vGAT-positive inhibitory terminals was observed in CTR E-I co-cultures in the presence of SCZ microglia (**Figure 20B**), when compared to cultures of CTR neurons and CTR microglia. Interestingly, no effect was observed for vGLUT1-positive excitatory synaptic terminals upon co-culture of CTR neurons with SCZ microglia (**Figure 20C**).

Since SCZ microglia showed a specific influence on inhibitory presynapses, the hypothesis that this effect was due to increased pro-inflammatory activation status of SCZ microglia was

explored. To this end, microglia were pre-treated with either the pro-inflammatory agent LPS or the anti-inflammatory antibiotic Minocycline for 60 minutes. Untreated or treated CTR (CTR2, CTR3) and SCZ (SCZ1, SCZ2, SCZ4, SCZ5) microglia were again co-cultured with CTR NGN2 and AD2 neurons for 72h, after which synapse numbers were assessed. When comparing the synapse densities of CTR neurons co-cultured with SCZ microglia, the previous observation of specifically reduced vGAT spot density was replicated in this separate set of experiments (**Suppl. Figure 7**). Interestingly, neither for pro-inflammatory nor anti-inflammatory treatments, an effect on vGAT or vGLUT1 spot density was observed (**Figure 20D, E**).

These findings contrast with previous observations obtained with the same iPSC lines used in this thesis, which demonstrated elevated inflammasome activation and inflammation-dependent synaptic pruning in a co-culture of patient iPSC-derived microglia and NGN2 neurons (136). The results presented here imply that in the presence of both glutamatergic and GABAergic neurons, microglia show a cell-type specific effect by reducing the density of inhibitory presynapses in E-I co-cultures in an inflammation-independent manner.

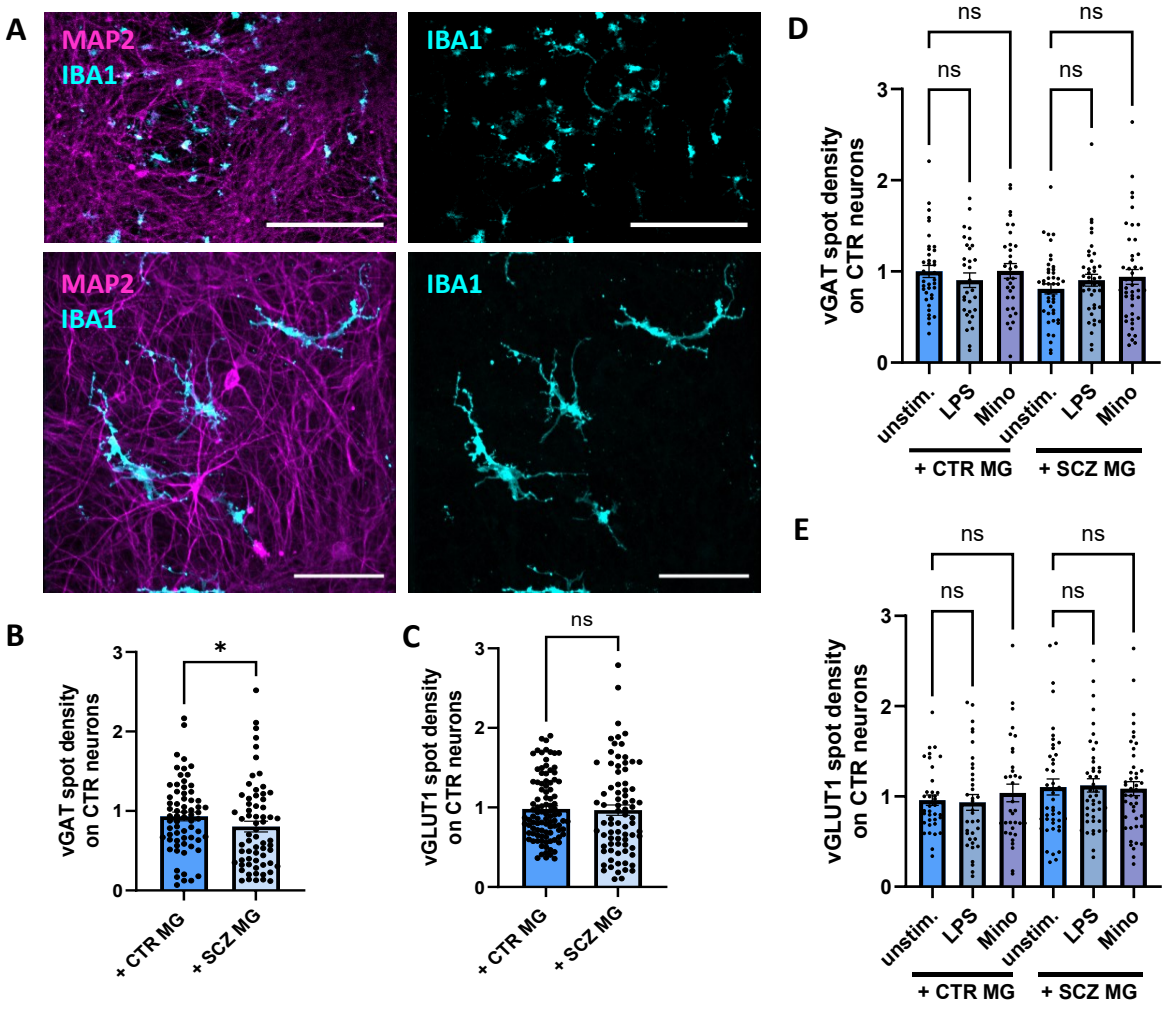

Figure 20 Reduced inhibitory presynapses in co-cultures of SCZ microglia and CTR NGN2 and AD2 neurons.

(A) Immunocytochemical staining of IBA1-positive microglia and DIV28 MAP2-positive neurons after 72 h in co-culture. Scale bars: 200 µm (top), 100 µm (bottom). **(B, C)** Quantification of vGAT-positive presynaptic density **(B)** and vGLUT1-positive presynaptic density **(C)** in CTR E-I co-cultures. Data points represent individual images analyzed. Values are normalized to CTR neurons + CTR microglia. Data were obtained from four independent differentiations. Two-tailed Mann-Whitney U test, n≥65, p≤0.05*, ns= not significant. Error bars: S.E.M. **(D, E)** Quantification of vGAT spot density **(D)** and vGLUT1 spot density **(E)** in CTR E-I cultures after co-culture with unstimulated, LPS-stimulated or Minocycline-stimulated CTR and SCZ microglia. Data points represent averaged values from multiple images per well. Values are normalized to unstimulated CTR neurons + CTR microglia. Data were obtained from a minimum of three independent microglial differentiations per donor. Kruskal-Wallis test with Dunn's multiple comparison, n≥32, ns= not significant. Error bars: S.E.M.

3.5.2 Patient-derived microglia influence spontaneous neuronal activity in E-I co-cultures

To evaluate whether the co-culture of E-I CTR neurons with SCZ microglia results in altered neuronal functionality, calcium imaging experiments were performed. Spontaneous single-cell somatic calcium transients were measured after 72 h of neuron-microglia co-culture. DIV28 neurons in E-I co-cultures were labeled with the chemical calcium indicator Cal-520 AM and recorded for 5 minutes. For improved neuronal activity, calcium imaging recordings were performed in neuronal medium.

The major disease-specific phenotype, observed in cultures of CTR neurons and SCZ microglia, was a significantly elevated amplitude of single-cell calcium signals and a concomitant increase of the AUC (**Figure 21A, C**). FWHM and frequency did not show differences after addition of SCZ microglia (**Figure 21E, G**). Since these alterations of neuronal activity could be related to the increased activation state of SCZ microglia, this possibility was evaluated by pro- and anti-inflammatory pre-treatment of microglia. Again, both pro-inflammatory treatment of CTR and SCZ microglia with LPS, as well as anti-inflammatory treatment with Minocycline, did not produce any major changes of any of the parameters measured (**Figure 21B, D, F, H).** Nevertheless, a significant increase of AUC was noted when CTR neurons were co-cultured with Minocycline-treated CTR microglia, when compared to co-cultures containing unstimulated microglia (**Figure 21D**).

Overall, only slight changes of spontaneous neuronal activity were observed as an effect of co-culture with SCZ microglia. These changes could not be replicated by pro-inflammatory treatment of CTR microglia, nor rescued by anti-inflammatory treatment of SCZ microglia, suggesting that these effects are most likely inflammation-independent.

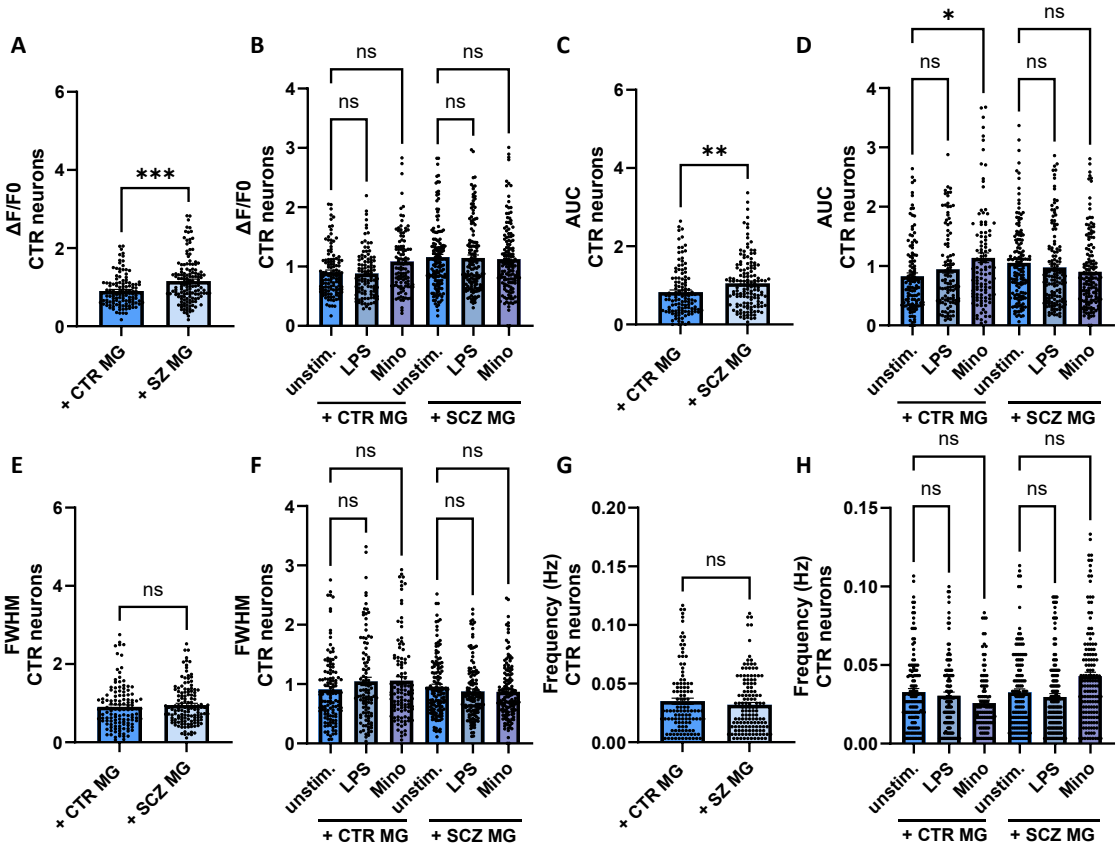

Figure 21 Increased amplitude of spontaneous calcium transients in the presence of SCZ microglia.

(A) Amplitude (ΔF/F0), **(C)** area under the curve (AUC), **(E)** full-width half-maximum (FWHM) and **(G)** peak frequency (Hz) of spontaneous somatic calcium transients of CTR neurons in E-I co-cultures in the presence of CTR or SCZ microglia at DIV28. Data points represent individual cells. Values are normalized to CTR neurons + CTR microglia. Data were obtained from a minimum of three microglial differentiations per line. Two-tailed Mann-Whitney U test, n≥120, p≤0.01**, p≤0.001***, ns= not significant. Error bars: S.E.M. **(B)** Amplitude, **(C)** AUC, **(E)** FWHM and **(H)** Frequency (Hz) of spontaneous somatic calcium transients of CTR neurons in E-I co-cultures in the presence of untreated, LPS-treated or Minocycline-treated CTR or SCZ microglia. Data points represent individual cells. Values are normalized to unstimulated CTR neurons + CTR microglia. Data were obtained from a minimum of three microglial differentiations per donor. Kruskal-Wallis test with Dunn's multiple comparison, n≥108, ns= not significant. Error bars: S.E.M.

3.6 Generation and characterization of iPSC carrying variants in the neuropsychiatric risk gene *DISC1*

When modeling diseases with iPSC, two main approaches can be pursued. iPSC can either be reprogrammed directly from patients to investigate sporadic disease phenotypes, as was described in the first part of this thesis. Another approach to disease modeling is the introduction of specific mutations in disease-relevant genes of healthy control cells, with the aim to study the impact of such mutations compared to the isogenic parental cell line.

In the second part of this thesis, the generation of iPSC carrying mutations in *DISC1*, a risk gene for SCZ; bipolar disorder and major depression, will be described. Synaptic phenotypes have been associated with DISC1 dysfunction in neurons (158). Therefore, in monocultures and E-I co-cultures of glutamatergic and GABAergic neurons, the effect of DISC1 mutations on excitatory and inhibitory synapse formation will be assessed.

Parts of this work were performed by Denise Sperlich during her Master's thesis, which was submitted in 2022. Examination of off-target effects, germ layer differentiation, FACS analysis and immunocytochemical staining of stem cell markers were part of this thesis. The generation and characterization of two *DISC1* mutant iPSC clones was published in Heider et al. (2021) in the journal Stem Cell Research (159).

3.6.1 Gene editing of iPSC using CRISPR/Cas9

For gene editing, the healthy iPSC line CTR 1 (see **Table 1**) was used. To affect as many DISC1 protein isoforms as possible, exon 2 of the *DISC1* gene was chosen to be the target for gene editing, since this exon is present in all previously identified DISC1 isoforms in the human brain (160). For gene editing, the Alt-R® CRISPR-Cas9 system from Integrated DNA Technologies was used. A crRNA targeting the anti-sense strand of DISC1 exon 2 was selected from a library of pre-designed crRNAs, provided by IDT (Hs.Cas9.DISC1.1.AC, PAM sequence: AGG, **Table 16**). The crRNA with the highest on-target and lowest off-target score was chosen. crRNA was fused to a fluorescently labeled tracrRNA which basepairs to the crRNA to form a functional gRNA complex. gRNAs are combined with a Cas9 nuclease to form a functional ribonucleoprotein (RNP) complex, which was introduced into the cells by nucleofection (**Figure 22A**). 24h after nucleofection, spot-like fluorescent signals were detected in the cytoplasm and nuclei of the majority of iPSC, indicating successful entry of the Atto550-labelled gRNA complex into the cells (**Figure 22B**).

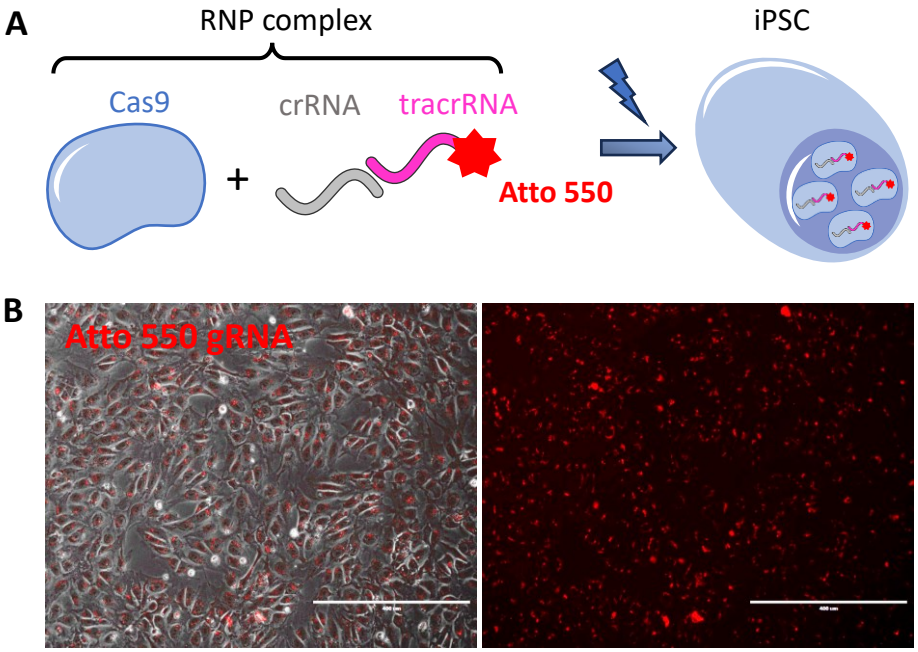

Figure 22 Nucleofection of iPSC with RNP complexes for CRISPR/Cas9 gene-editing. **(A)** Working principle of the IDT Alt-R® CRISPR-Cas9 system. A crRNA, complementary to the target DNA sequence, was fused to an Atto-550 fluorescently labeled tracrRNA. Together with the Cas9 endonuclease, a ribonucleoprotein (RNP) complex is formed which was introduced into iPSC by nucleofection. Figure created with BioRender.com. **(B)** iPSC show spot-like Atto-550 signals in cytoplasm and nucleus 24h after nucleofection, indicating entry of the RNP complex into the cells. Scale bars: 400 µm.

3.6.2 Selection of monoclonal mutant iPSC clones

To identify mutation carrying clones from the polyclonal population of nucleofected iPSC, single cells were sorted by FACS into individual wells of a 96-well plate. After expansion of clones arising from only a single cell, Sanger sequencing was performed to examine whether Indel mutations occurred in the targeted region in *DISC1* due to imprecise NHEJ. Allelic deconvolution identified one iPSC clone, carrying a heterozygous 5bp deletion (NC_000001.11: g.231,694,025–231,694,029delCTCGA, *DISC1 +/-*) and one homozygous clone with a 17 bp deletion on allele 1 (NC_000001.11: g.231,694,024–231,694,041delACTCGAGAGGCCTCTTG) and a 1 bp insertion on allele 2 (NC_000001.11: g.231,694,024_ 231,694,025insA, *DISC1 -/-*) (**Figure 23**). Both of these are frameshift mutations and were predicted to result in a preterminal stop codon (using https://web.expasy.org/translate/) after 38 codons for the heterozygous clone and 60 codons for the homozygous clone, respectively (159). The two mutant clones are registered in the Human Pluripotent Stem Cell registry (https://hpscreg.eu/) as TMOi001-A-5 (*DISC1 +/-)* and TMOi001-A-6 (*DISC1 -/-*).

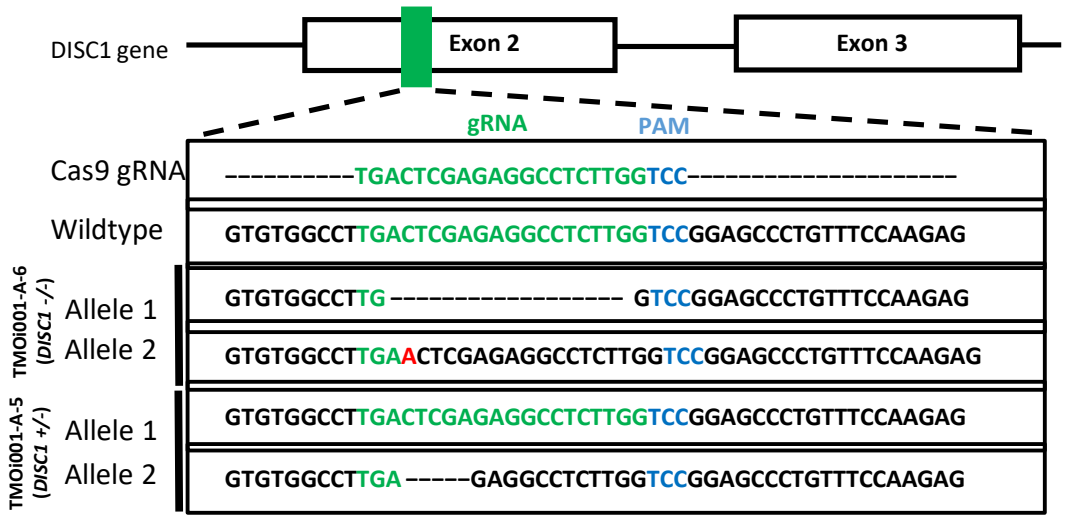

Figure 23 Sanger sequencing of monoclonal DISC1 mutant iPSC.
Deconvoluted DNA sequences of WT and mutant iPSC. TMOi001-A-5 (*DISC1 +/-*) carries a heterozygous 5 bp deletion ('CTCGA'). TMOi001-A-6 (DISC1 -/-) carries a heterozygous 17 bp ('ACTCGAGAGGCCTCTTG') deletion on allele 1 and a 1 bp insertion ('A') on allele 2 (**(159)**, Master's thesis Denise Sperlich, 2022).

3.6.3 Mutant iPSC clones show chromosomal integrity, are devoid of off-target mutations and show normal stem cell characteristics

Gene editing with CRISPR/Cas9 bears the risk of unwanted off-target effects in the form of smaller Indel mutations up to larger gains, losses or translocations of chromosomal material (161). To rule out larger chromosomal aberrations with a size of > 50-100kb, array CGH analysis of the mutant clones was performed by CeGaT GmbH, Tübingen. No major chromosomal aberrations were detected during the screen (Master' thesis Denise Sperlich, 2022, (159)). Analysis of smaller potential off-target insertions or deletions at the top 10 most likely genome wide off-target regions for the crRNA used (provided by IDT) was performed by Denise Sperlich. No mutations were detected in any of the regions examined for both clones (Master' thesis Denise Sperlich, 2022, (159)). Short tandem repeat (STR)-analysis of 16 loci was performed by Eurofins Genomics (Ebersberg, Germany) and confirmed a 100 % match between the isogenic parental iPSC line (CTR1) and the two mutant clones (**Suppl. Table 1**).

Afterwards, iPSC were screened for the expression of pluripotency-associated markers and their capacity to differentiate into all three germ layers, to ensure that the cells still show normal stem cell characteristics. Characterization of both mutant clones by immunocytochemistry and FACS was performed by Denise Sperlich (Master's thesis Denise Sperlich, 2022). Gene-edited iPSC showed characteristic stem cell morphology in culture (**Figure 24A**) and expressed the pluripotency markers NANOG, SOX2, OCT3/4, SOX2, Tra-1-60 and SSEA-4 as validated by

RT-PCR (**Figure 24B**), FACS analysis (**Figure 24C**) and immunocytochemistry (**Figure 24D**) (159). Trilineage differentiation demonstrated the capacity of both clones to differentiate into Pax6-positive ectodermal, Brachyury-positive mesodermal and Sox17-positive endodermal cells (**Figure 24E**) (159). For further experiments, only the heterozygous clone (*DISC1+/-*) was chosen to be included, as previously detected DISC1 mutations in patients are also heterozygous (16, 96).

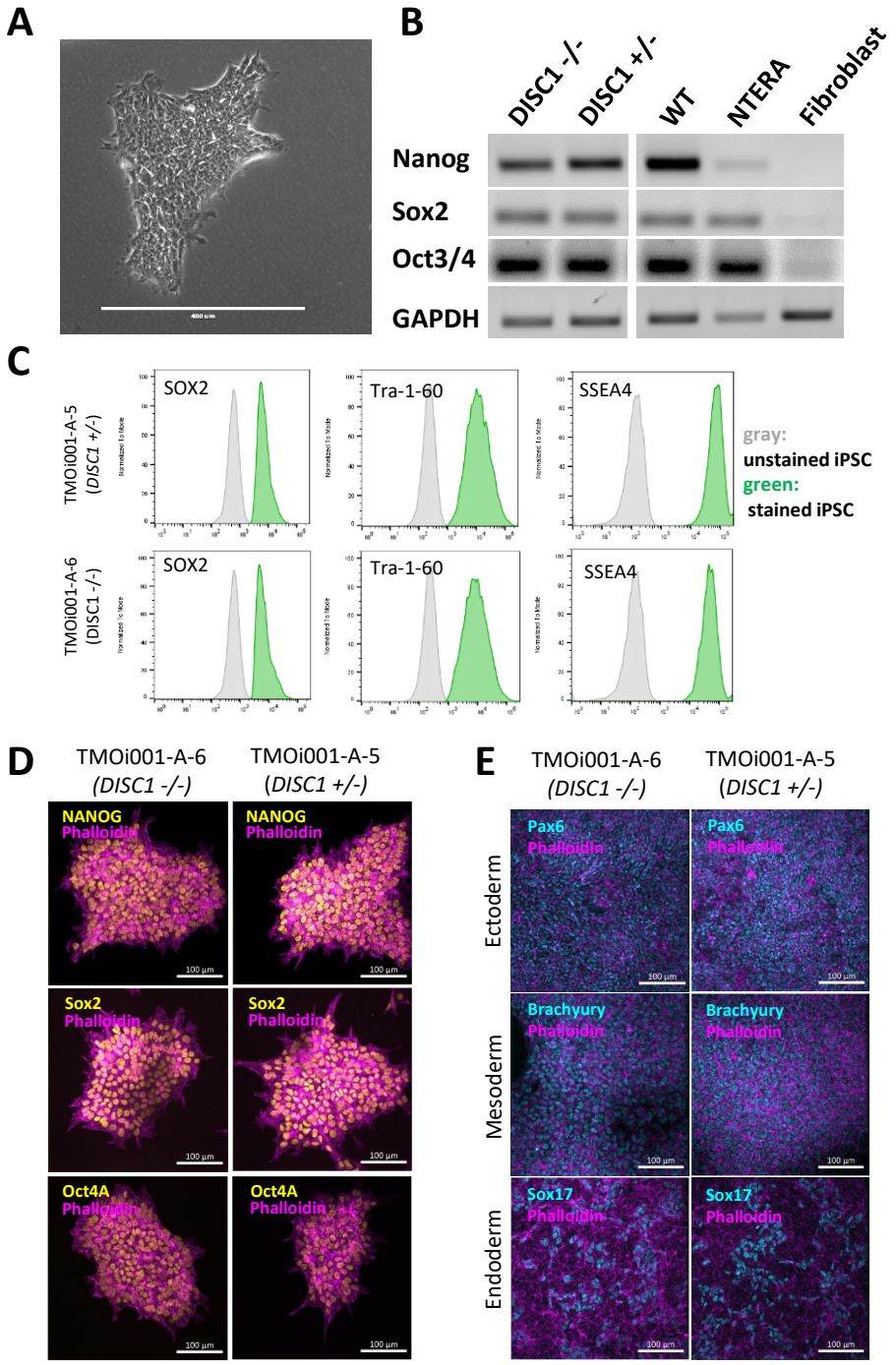

Figure 24 Characterization of the heterozygous (DISC1+/-, TMOi001-A-5) and homozygous (DISC1-/-, TMOi001-A-6) mutant iPSC clones.
(A) Characteristic stem cell morphology of gene-edited iPSC in culture. **(B)** Expression of the pluripotency-associated genes Nanog, Sox2 and Oct3/4 was assessed by RT-PCR. Loading control: GAPDH, pos. control: human teratocarcinoma cell line (NTERA), neg. control: fibroblasts. **(C)** Quantitative measurement of pluripotency markers Sox2, Tra-1-60 and SSEA4 by FACS. **(D)** Immunocytochemical staining of pluripotency markers Nanog, Sox2 and Oct4A in iPSC. Scale bars: 100 µm. **(E)** Immunocytochemical staining of ectodermal marker Pax6, mesodermal marker Brachyury and endodermal marker Sox17 in differentiated iPSC. Scale bars: 100 µm. Figure adapted from Heider et al. (159).

3.6.4 Reduced DISC1 protein expression in mutant iPSC and NPC

As described in **3.6.2**, the heterozygous 5 bp deletion in exon 2 that was introduced in one of the characterized clones was predicted to result in a frameshift and a pre-terminal stop codon. Preterminal stop codons might result in the expression of a truncated protein variant or potentially decreased expression of DISC1 from the mutated allele due to nonsense-mediated decay of the transcribed RNA (162). To analyze the expression level of DISC1, immunocytochemical staining was performed in iPSC and NPC, using an antibody directed against the C-terminus of the protein (**Figure 25A, B**). In OCT4-positive iPSC and partially PAX6-positive NPC, DISC1 expression was reduced by ~ 30 %, compared to wildtype (WT) (**Figure 25C, D**).

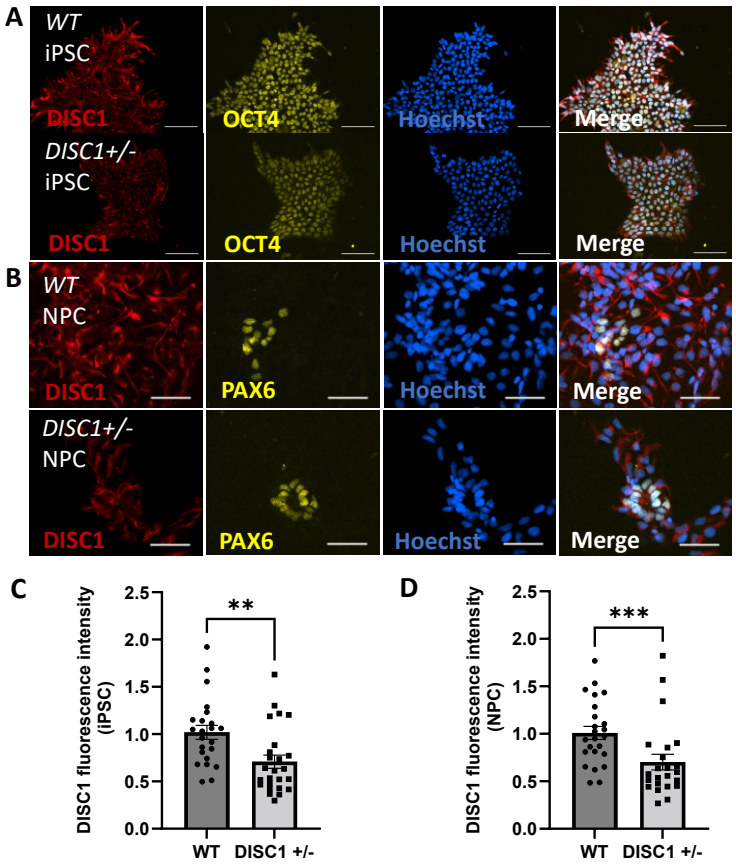

Figure 25 DISC1 protein expression is reduced in DISC1 +/- iPSC and NPC.
(A) Expression of DISC1 in WT and *DISC1 +/-* iPSC, which stain positive for the pluripotency marker OCT4. Scale bars: 100 µm. **(B)** Expression of DISC1 in WT and *DISC1 +/-* NPC, of which a fraction expresses NPC marker PAX6. Scale bars: 100 µm. **(C, D)** Quantification of DISC1 fluorescence intensity in WT and *DISC1+/-* iPSC **(C)** and NPC **(D).** Values are normalized to WT. Data points represent averaged values from multiple cells within individual images. Data were obtained from three independent experiments. Two-tailed Mann Whitney U test, n>22, p≤0.01**, p≤0.001***. Error bars: S.E.M.

3.7 Synaptic phenotypes in DISC1 +/- neurons

The DISC1 protein is involved in synaptic maintenance and functionality, and previous research on the effects of DISC1 disruption provided evidence for reduced spine density and altered synaptic plasticity in animal and iPSC models. However, the role of DISC1 in synaptic functions has not been described for iPSC-derived GABAergic neurons or in more complex, defined culture systems. Therefore, synapse formation was studied in NGN2/AD2 monocultures and in E-I co-cultures. The following results were published as part of Heider et al. (2024) in the journal BMC Neuroscience (163).

3.7.1 Reduced excitatory synapse density in DISC1+/- NGN2 neuron monocultures

To study intrinsic synaptic phenotypes associated with mutated *DISC1*, excitatory and inhibitory synapses were stained and quantified in monocultures of NGN2 and AD2 neurons, respectively (**Figure 26A, B, G, H**). Interestingly, the density of excitatory synapses was significantly reduced in *DISC1 +/-* NGN2 neurons, compared to WT (**Figure 26E**). The total density of vGLUT1 and PSD95 spots, comprising both synaptic and extrasynaptic spots, was not altered in mutant neurons (**Figure 26C, D**), neither was the percentage of total vGLUT1 spots co-localized with postsynaptic PSD95 (**Figure 26F**).

As markers of inhibitory synapses, presynaptic vGAT and postsynaptic Gephyrin clusters were quantified in cultures comprising only AD2 neurons (**Figure 26G, H**). In this case, neither inhibitory synapse density, nor total vGAT spot density, total Gephyrin spot density or percentage of vGAT spots co-localizing with Gephyrin clusters was altered in *DISC1+/-* AD2 neurons (**Figure 26I-L**).

In conclusion, only glutamatergic NGN2 neurons show aberrant synaptic phenotypes with the present *DISC1+/-* mutant model when cultured individually.

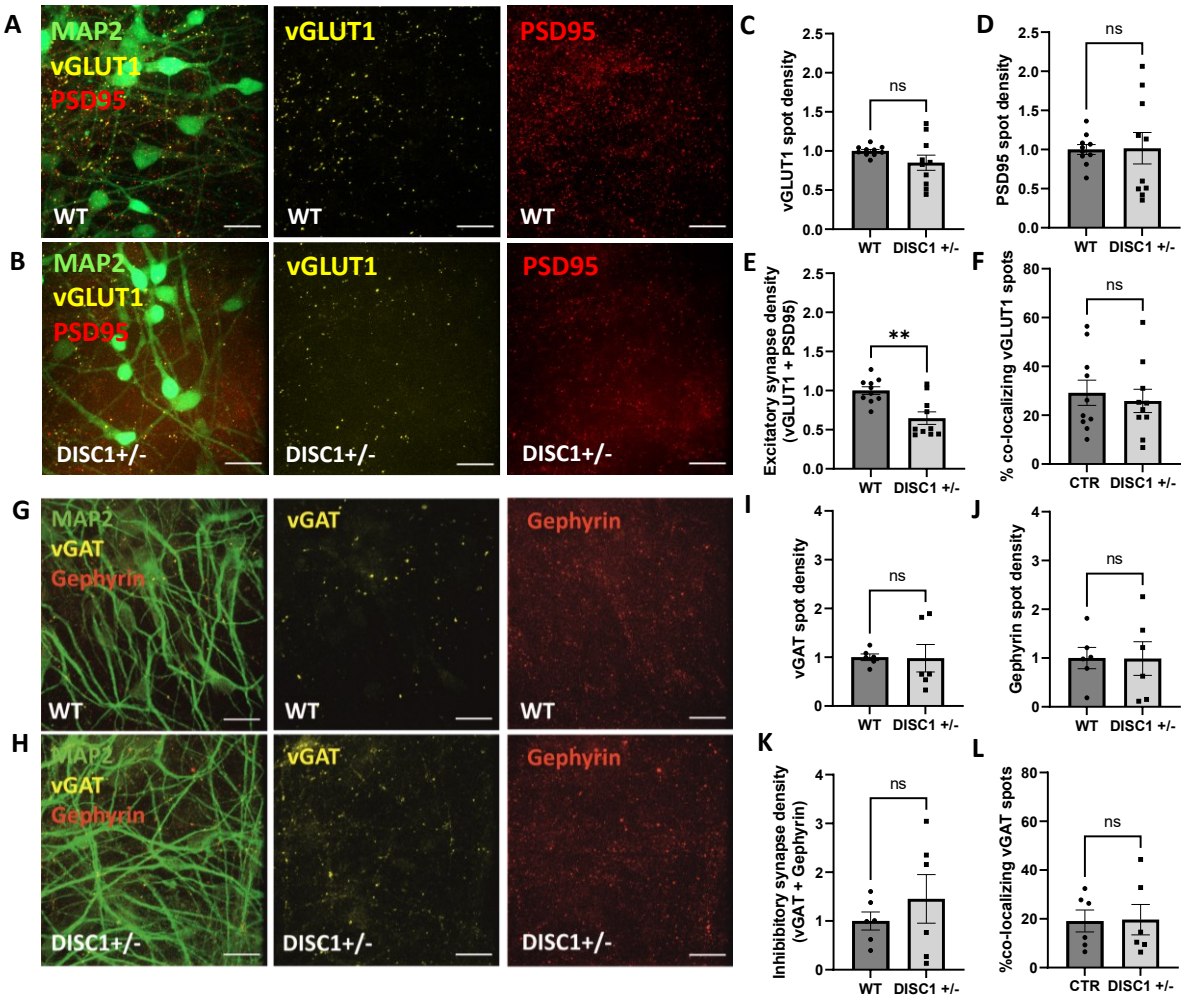

Figure 26 Excitatory synapses are reduced in DISC1+/- glutamatergic NGN2 neurons. **(A, B)** Expression of excitatory synaptic markers vGLUT1 and PSD95 on MAP2-positive WT **(A)** and *DISC1+/-* **(B)** NGN2 neurons (DIV28). Scale bars: 20 µm. **(C-F)** Quantification of synaptic marker densities in WT and *DISC1+/-* neurons. **(C)** Density of vGLUT1-positive presynaptic terminals**, (D)** density of PSD95 postsynaptic clusters, **(E)** excitatory synapse density (apposition of vGLUT1+PSD95) and **(F)** percentage of total vGLUT1 spots co-localizing with PSD95. Values are normalized to WT. Data points represent averaged values from multiple images within an individual well. Two-tailed Mann Whitney U test, n= 10, p≤0.01**, ns= not significant. **(G, H)** Expression of inhibitory synaptic markers vGAT and Gephyrin on MAP2-positive WT **(G)** and *DISC1+/-* **(H)** AD2 neurons (DIV28). Scale bars: 20 µm. **(I-L)** Quantification of synaptic marker densities in WT and *DISC1+/-* neurons. **(I)** Density of vGAT-positive presynaptic terminals, **(J)** density of Gephyrin cluster densities, **(K)** inhibitory synapse density (apposition of vGAT+Gephyrin) and **(L)** percentage of total vGAT spots co-localizing with Gephyrin. Values are normalized to WT. Data points represent averaged values from multiple images within an individual well. Data were obtained from a minimum of three independent experiments. Two-tailed Mann Whitney U test, n= 6, ns= not significant. Error bars: S.E.M.

3.7.2 Increased inhibitory presynapses in *DISC1+/-* E-I co-cultures

Following up on synapse quantification experiments performed with NGN2 and AD2 neurons cultured independently, excitatory and inhibitory synapses formed by WT and *DISC1+/-* neurons were quantified in the E-I co-culture system. Again, NGN2 neurons were GFP labeled to distinguish them from GFP-negative AD2 neurons in the co-cultures, making it possible to assign synaptic structures to one or the other type of neuron.

Strikingly, the major finding in *DISC1+/-* E-I co-cultures was a strong increase of vGAT-positive presynaptic terminals on both NGN2 and AD2 neurons by ~ 2.5 and ~ 4-fold, respectively (**Figure 27B, G**). These results reflected in a trend for increased inhibitory synapse densities on both types of neurons, which did not attain statistical significance (**Figure 27D, I**). Postsynaptic Gephyrin clusters and the percentage of vGAT spots co-localizing with Gephyrin were also not altered significantly in *DISC1 +/-* samples (**Figure 27C, E, H, J**).

For excitatory synaptic markers in WT and *DISC1 +/-* samples (**Figure 28A, F**), no overt differences were observed in E-I co-cultures, on both NGN2 and AD2 neurons. vGLUT1 and PSD95 densities (**Figure 28B, C, G, H**), as well as the percentage of co-localizing vGLUT1 spots were unaffected (**Figure 28E, J**). In line with the previous findings of reduced excitatory synapses in *DISC1+/-* NGN2 monocultures (see 3.7.1), a trend was observed for reduced excitatory synapse density specifically on NGN2 neurons (**Figure 28D,** p= 0.07).

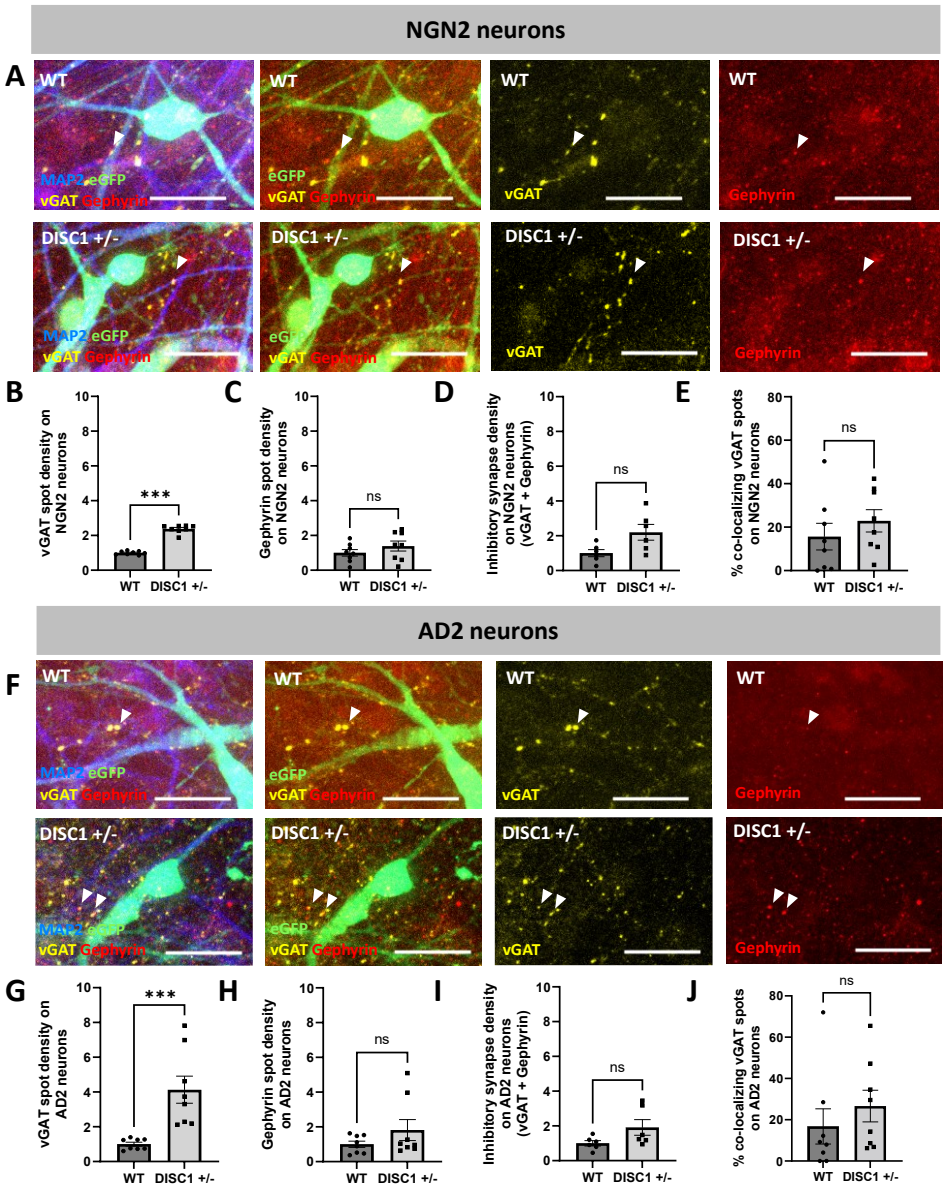

Figure 27 Inhibitory presynapses are increased on DISC1+/- NGN2 and AD2 neurons in E-I co-cultures.

(A) Immunocytochemical staining of inhibitory presynaptic marker vGAT and postsynaptic marker Gephyrin on eGFP-positive dendrites of MAP2-positive NGN2 neurons (DIV28). Arrows indicate exemplary co-localizations of pre- and postsynapses. Scale bars: 20 µm. **(B-E)** Quantification of inhibitory synaptic markers on NGN2 neurons. **(B)** vGAT spot density, **(C)** Gephyrin spot density, **(D)** inhibitory synapse density (apposition of vGAT+Gephyrin) and **(E)** percentage of total vGAT spots co-localizing with Gephyrin. **(F)** Immunocytochemical staining of vGAT and Gephyrin on eGFP-negative dendrites of MAP2-positive AD2 neurons (DIV28). Arrows indicate exemplary co-localizations of pre- and postsynapses. Scale bars: 20 µm. **(G-J)** Quantification of inhibitory synaptic markers on AD2 neurons. **(G)** vGAT spot density, **(H)** Gephyrin spot density, **(I)** inhibitory synapse density and **(J)** percentage of total vGAT spots co-localizing with Gephyrin. Values are normalized to WT. Data points represent averaged values from multiple images within an individual well. Data were obtained from four independent experiments. Two-tailed Mann Whitney U test, n≥6, p≤0.001***, ns= not significant. Error bars: S.E.M.

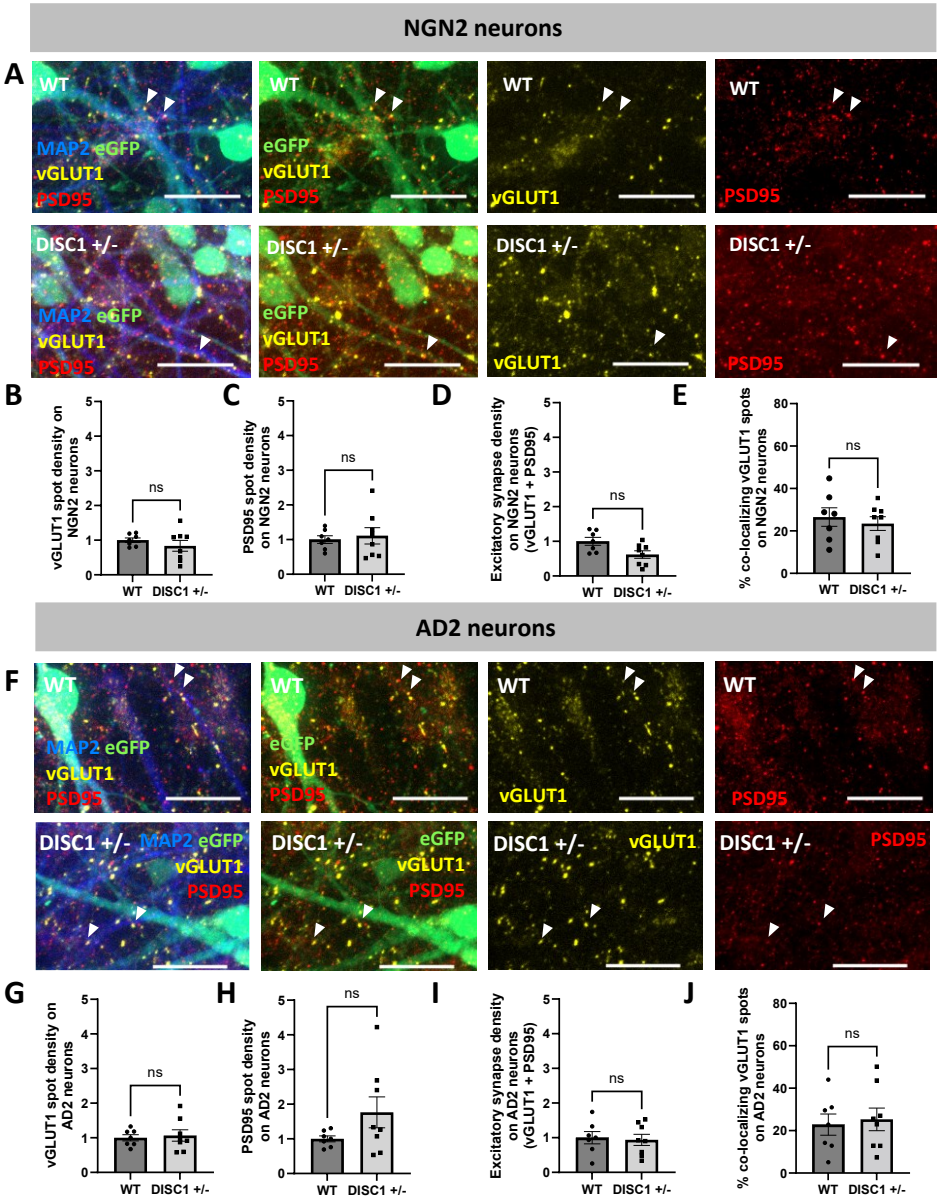

Figure 28 Excitatory synapses are unaltered in DISC1+/- co-cultured NGN2 and AD2 neurons.

(A) Immunocytochemical staining of excitatory presynaptic marker vGLUT1 and postsynaptic marker PSD95 on GFP-positive dendrites of MAP2-positive NGN2 neurons (DIV28). Arrows indicate exemplary co-localizations of pre- and postsynapses. Scale bars: 20 µm. **(B-E)** Quantification of excitatory synaptic markers on NGN2 neurons. **(B)** vGLUT1 spot density, **(C)** PSD95 spot density, **(D)** excitatory synapse density (apposition of vGLUT1+PSD95) and **(E)** percentage of total vGLUT1 spots co-localizing with PSD95. **(F)** Immunocytochemical staining of vGLUT1 and PSD95 on eGFP-negative dendrites of MAP2-positive AD2 neurons (DIV28). Arrows indicate exemplary co-localizations of pre- and postsynapses. Scale bars: 20 µm. **(G-J)** Quantification of excitatory synaptic markers on AD2 neurons. **(G)** vGLUT1 spot density, **(H)** PSD95 spot density, **(I)** excitatory synapse density and **(J)** percentage of total vGLUT1 spots co-localizing with PSD95. Values are normalized to WT. Data points represent averaged values from multiple images within an individual well. Data were obtained from four independent experiments. Two-tailed Mann Whitney U test, n≥7, ns= not significant. Error bars: S.E.M.

Taken together, these results suggest aberrant synapse formation or maintenance in neurons carrying heterozygous mutations in the *DISC1* gene. While excitatory synapses were reduced in monocultures of NGN2 neurons, this effect became less pronounced when NGN2 neurons were combined into co-cultures with AD2 neurons. On the other hand, a strong increase in the number of inhibitory presynapses was unique to co-cultured AD2 neurons, suggesting an interactive effect of glutamatergic and GABAergic neurons in co-cultures. When comparing the ratio of total excitatory to inhibitory synapses on all MAP2-positive neurons in WT and *DISC1+/-* E-I co-cultures, a significant increase in the relative proportion of inhibitory synapses was observed in mutant cultures, indicating a synaptic E-I imbalance (**Figure 29**).

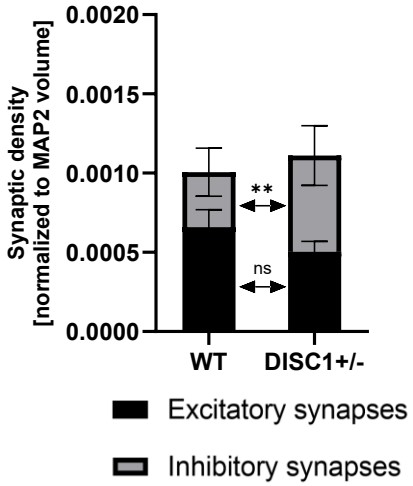

Figure 29 Altered ratio of excitatory and inhibitory synapses in DISC1+/- E-I co-cultures.
Quantification of excitatory and inhibitory synaptic densities, as defined by co-localized vGLUT1+PSD95 and vGAT+Gephyrin clusters, respectively, on all MAP2-positive neurons in WT and *DISC1+/-* E-I co-cultures. Y-axis values represent synaptic spot numbers normalized to the volume of the MAP2 mask. Data were obtained from a minimum of three independent experiments. Two-tailed Mann Whitney U tests, n≥6 (averages from multiple images within individual wells), p≤0.01**, ns= not significant. Error bars: S.E.M.

3.7.3 Increased GABAergic differentiation efficiency of DISC1+/- NPC

The major synaptic phenotype observed in *DISC1+/-* samples was a strong increase of inhibitory presynaptic terminals in E-I co-cultures. A possible explanation for these findings could be a generally increased differentiation efficiency of mutant neurons towards the GABAergic lineage, resulting in increased presynapse formation in the presence of glutamatergic neurons in a more complex neuronal network. To evaluate the GABAergic differentiation efficiency of *DISC1+/-* AD2 neurons, immunocytochemical staining of the inhibitory neurotransmitter GABA was performed in AD2 and NGN2 monocultures (**Figure**

30A). As expected, a significantly higher percentage of GABA-positive neurons in the total population of MAP2-positive neurons was observed in both WT and *DISC1+/-* AD2 cultures, compared to NGN2 cultures (CTR: ~ 42% GABA-positive, *DISC1+/-*: ~ 60 %, **Figure 30B**). In NGN2 cultures, no or very few GABA-positive neurons per image were observed, independent of genotype (WT: ~ 2 %, DISC1: ~ 5 %, **Figure 30B**), confirming the high degree of homogeneity in these cultures. Interestingly, a significantly increased percentage of GABA-positive neurons in *DISC1+/-* AD2 cultures was observed, when compared directly to WT AD2 cultures (**Figure 30C**).

Overall, these findings suggest that there seems to be a higher efficiency with which AD2-transduced *DISC1+/-* NPC convert into GABAergic neurons. While this phenotype is already present in AD2 neurons cultured independently, the phenotype of increased GABAergic synapses only manifests in the co-culture environment.

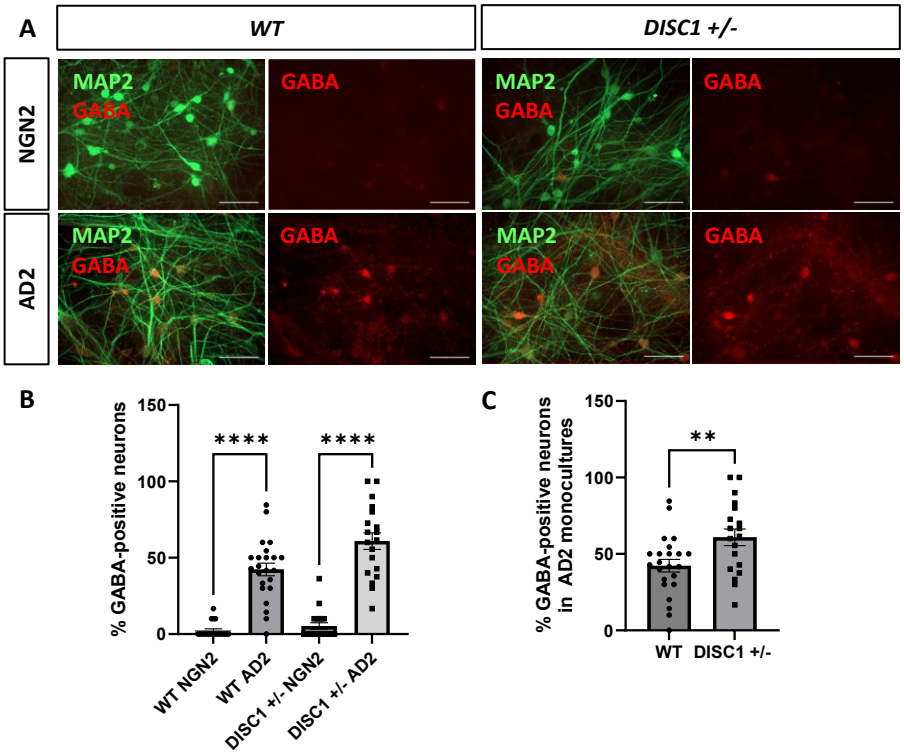

Figure 30 Increased GABAergic differentiation efficiency of DISC1+/- AD2-transduced neurons.
(A) Immunocytochemical staining for GABA and MAP2 in WT and *DISC1+/-* NGN2 and AD2 monocultures. Scale bars: 50 µm. **(B)** Percentage of GABA-positive neurons from the total population of MAP2-positive neurons in WT and *DISC1+/-* NGN2 and AD2 monocultures. Data points represent individual images. Kruskal-Wallis test with Dunn's multiple comparisons test, n≥20, p≤0.0001****. **(C)** Percentage of GABA-positive neurons from the total population of MAP2-positive neurons in WT and *DISC1+/-* AD2 cultures. Data points represent individual images. Data were obtained from two independent experiments. Unpaired, two-tailed t-test, n≥19, p≤0.01**, error bars: S.E.M.

4. Discussion

The major aim of this thesis was the identification and characterization of morphological and functional neuropsychiatric disease signatures using iPSC-derived neuronal model systems. For this purpose, neural progenitor cells and neurons, derived from SCZ patient iPSC or from iPSC carrying a mutation in the neuropsychiatric risk gene *DISC1*, were investigated.

Several potential disease-influencing aspects were addressed in this thesis:

1) *Analysis of early neurodevelopmental aberrations in SCZ*

Analysis of patient-derived NPC revealed restricted neuronal differentiation capacity, reduced neurite outgrowth and accumulation in the G2/M cell cycle phase already at an early developmental stage.

2) *Analysis of aberrant synaptic connectivity in the cortical microcircuitry in SCZ*

Analysis of synapse formation in patient-derived E-I co-cultures revealed that excitatory synapses are primarily affected in SCZ and might thus contribute to E-I imbalance in the cultures. The observed increased excitatory synapse density contrasted with the reduced density of presynaptic terminals formed by glutamatergic and GABAergic neurons when cultured individually.

3) *Analysis of aberrant neuronal activity as a consequence of synaptic phenotypes*

The occurrence of network activity was reduced in SCZ E-I co-cultures. However, in those cultures that did show synchronous activity, single-cell analysis revealed increased calcium activity of glutamatergic and GABAergic neurons involved in network bursting activity. On the other hand, basal unsychronized calcium activity was only affected in glutamatergic neurons.

4) *Analysis of the impact of neuroinflammation in SCZ*

Co-cultures of patient-derived microglia and healthy glutamatergic and GABAergic neurons revealed a specific decrease of inhibitory presynaptic terminals, suggesting that microglia in E-I co-cultures exert a cell-type specific effect. In addition, an increase of overall neuronal calcium signaling was observed. Both phenotypes were independent of microglial inflammation status.

5) Comparison of idiopathic and isogenic DISC1 mutant disease models

To generate a model of *DISC1* mutation, CRISPR-Cas9 gene editing was employed to introduce heterozygous frameshift mutations in the gene in iPSC. While previous observations of reduced excitatory synapse density were confirmed in monocultures of NGN2-transduced neurons, E-I co-cultures revealed a strong GABAergic phenotype, as shown by increased inhibitory presynapses and an overall increase of inhibitory synapses in the network. In line with these observations, the differentiation efficiency of mutant neurons towards the GABAergic lineage was increased. Overall, both the idiopathic, SCZ-specific, and more general isogenic *DISC1* model revealed synaptic aberrations and altered differentiation efficiency as shared phenotypes of neuropsychiatric diseases *in vitro,* however affecting different cell types.

4.1 Early neurodevelopmental aberrations in SCZ NPC

In a first step to investigate SCZ-associated phenotypes of NPC, neurite outgrowth of differentiating NPC was assessed. While initial measurements in immature neurons, generated by directed differentiation, did not reveal any differences, neurite outgrowth was found to be reduced in developing neurons generated by the addition of growth factors. Similar observations have been made by other groups, in which the same patient-derived iPSC lines showed diverging results regarding neurite outgrowth when differentiated by NGN2 overexpression (164) as compared to undirected differentiation (165). The finding of reduced neurite outgrowth in SCZ NPC is in line with multiple previous studies, reporting reduced neurite complexity, as well as decreased neuronal connectivity in SCZ postmortem brain tissue (166) and patient iPSC-derived neurons (139, 140). Moreover, decreased expression of neuronal cell adhesion molecules NCAM1, NLGN1 and NRXN1 have been observed in patient-derived NPC, which could be involved in aberrant outgrowth (167). The fact that neurite alterations are consistently observed in immature iPSC-derived neurons, as well as in mature neurons in postmortem tissue, suggests that this phenotype emerges early on during brain development where it could disturb the proper formation of neuronal networks.

To explore whether inefficient differentiation of SCZ iPSC towards the neuronal lineage might underlie this deficit at the NPC stage, neurodevelopmental markers were assessed in iPSC and NPC by immunocytochemistry. In accordance with this hypothesis, quantitative analysis revealed a higher proportion of pluripotent, OCT4-positive iPSC in SCZ NPC cultures, as well as lower expression levels of the transcription factor LEF1, involved in neurodevelopmental

Wnt signaling, suggesting impaired differentiation efficiency and impaired maturity of diseased iPSC and NPC, respectively. Impaired neuronal differentiation capacity of SCZ iPSC has previously been demonstrated by two studies, which reported reduced differentiation efficiency of 22q11.2 deletion iPSC, a CNV associated with SCZ (168), and impaired maturation of patient-derived glutamatergic neurons (169). The latter study also reported aberrant NPC marker expression in patient-derived samples, and gene expression analysis demonstrated DEG enrichment related to neuronal differentiation processes in NPC (169). However, both studies do not provide a clear indication of whether the differentiation capacity of SCZ NPC is improved or impaired. Furthermore, aberrant Wnt signaling has been linked to SCZ by patient studies (170) and in patient-derived NPC (171) and the overall evidence obtained in the field so far suggests hypoactivity of this pathway, which plays a critical role in neurodevelopment (172). Nevertheless, it is important to acknowledge that only two select analytes of the Wnt signaling pathway were investigated in this thesis, of which only LEF1 was altered. More detailed pathway analysis is required to provide a clearer picture of the putative relationship between altered Wnt signaling and impaired differentiation capacity.

The balance between cell proliferation and differentiation is tightly regulated by cell cycle dynamics (173). SCZ NPC showed accumulation in the G2/M phase of the cell cycle as indicated by flow cytometry analysis and NPC-specific increased expression of G2/M-associated regulating protein Cyclin B1 and Aurora A kinase, involved in mitotic spindle formation. These specific differences in the G2/M cell cycle phase did however not reflect in an aberrant overall proliferation rate. Increased proliferation and a shortened cell cycle were previously reported in SCZ olfactory cells (142) and proteomic alterations linked to cell cycle control were described in patient iPSC-derived neural stem cells (174). In accordance with our data and these reports, several genes associated with the cell cycle were found to be decreased in the blood of SCZ patients, supporting a role for altered cell cycle regulation in the pathogenesis of the disease (175).

While it remains to be addressed why SCZ NPC accumulate in G2/M and what the consequence of this accumulation might be, it can be speculated that it could be related to the observed impaired differentiation capacity of SCZ NPC, as it is well known that cell phase regulation is crucial for neurodevelopmental progression (176). There are multiple cell cycle check points, at which cells are screened for DNA damage, successful DNA replication and cell growth (177). At the G2/M checkpoint, cells with DNA damage or incompletely replicated DNA are inhibited from entering mitosis and DNA repair is initiated (178). Prolonged G2/M arrest due to increased DNA damage, which was previously linked to SCZ (179), or even failure to repair the damage and subsequent apoptosis, are two potential explanations for our observations. Consequently, DNA damage and DNA damage response, as well as the level of

apoptosis in SCZ samples should be investigated. To mechanistically study the relationship between aberrant cell cycle dynamics, Wnt signaling and differentiation efficiency, manipulation of cell cycle regulators or Wnt signaling proteins could be performed by application of specific antagonists and/or agonists in NPC and neurons.

4.2 Development of an optimized E-I co-culture system

Previous studies in the field of iPSC-based neuropsychiatric disease research have primarily made use of undirected differentiation protocols, which mostly yield heterogeneous cultures comprised of predominantly glutamatergic neurons (105, 139, 140, 165, 180, 181). In the past years, efforts were made to generate more homogenous populations of neurons by inducible overexpression of lineage-specific transcription factors. Since then, this technique has successfully been employed to study phenotypes of glutamatergic neurons in SCZ (136, 164). Overall, research on cortical GABAergic neurons in heavily underrepresented in the field, although it is well established that these neurons are involved in the pathogenesis of SCZ (182). In addition, there is also still a lack of research on the interaction of glutamatergic and GABAergic neurons, as there have only been two groups which so far employed a defined culture system, comprising glutamatergic NGN2 and GABAergic AD2-transduced neurons, to study E-I imbalance in a mutation model of the SCZ risk gene *SETD1A* and a 16p11.2 duplication model in a cell-type specific manner (183, 184).

In this thesis, such a defined co-culture system of NGN2-transduced NPC and AD2-transduced NPC was for the first time employed for the study of E-I imbalance in a patient model and in the context of *DISC1* mutation. Cell type specific analysis of synaptic and functional phenotypes via overexpression of GFP in NGN2 neurons was established, and confounding effects on these phenotypes by GFP overexpression were excluded. A second key adaptation of the protocol was the transient addition of doxycycline at the end of the cultivation period to induce a second wave of transgene expression in more mature neurons. This optimization resulted in improved maturity of the cultures, as indicated by the increased number of cultures with network activity and an increased number of postsynaptic sites, as well as intact synapses.

To conclude, the optimized NGN2/AD2 co-culture system presented in this thesis was employed for the first time to study cell-type specific aberrations in both glutamatergic and GABAergic neurons derived from patient iPSC and *DISC1* mutant iPSC.

4.3 Synaptic aberrations in SCZ patient-derived neurons

Synaptic aberrations are a pathological hallmark of SCZ and were thus investigated in detail using patient-derived neurons. In accordance with a previous report, using the same patient iPSC lines that were used in this thesis (136), a reduction of excitatory synapses (vGLUT1+PSD95) and presynaptic terminals (vGLUT1) was observed in cultures comprised of NGN2-transduced neurons. In line with this finding and a general reduction of presynapses in SCZ, a recent PET imaging study demonstrated decreased levels of the general presynaptic marker SV2A in the cortex of patients (46) and a meta-analysis of 13 studies revealed lower expression of the synaptic vesicle protein synaptophysin in postmortem brain tissue (47). Contrary to observations in SCZ patients, which have consistently reported a loss of cortical glutamatergic spines (45), the density of postsynaptic PSD95-positive clusters was not significantly affected in monocultures of NGN2 neurons. This difference might be related to the relative immaturity and low complexity of the NGN2 networks, in which postsynaptic phenotypes potentially do not yet manifest.

Concordant with this hypothesis, the synaptic phenotypes observed in the conceivably more mature E-I co-cultures differed considerably, with the major observation being a strong increase of PSD95-positive postsynaptic terminals and excitatory synapses on AD2 neurons, while presynaptic terminals were unaffected. The formation of synapses during development *in vivo* is usually initiated by presynaptic contact with the dendritic shaft which precedes the assembly of postsynaptic scaffolding proteins such as PSD95 (152, 185). Therefore, the observations made here might represent an aberrant developmental mechanism of synapse formation in which ectopic, extrasynaptic assembly of postsynaptic components could lead to increased, aberrant excitatory synapse formation. In addition, the percentage of total presynaptic terminals co-localizing with postsynaptic PSD95 was increased in SCZ cultures, suggesting that the precision with which targeting of the postsynaptic sites takes place is elevated and might thus also contribute to the observed increase of excitatory synapse density.

The role of PSD95 in SCZ remains to be elucidated in detail, however exome sequencing has associated variants in *PSD95* with the disease (151) and PSD95 protein was shown to be decreased in the PFC of SCZ patients (186). In support of our findings, a prior study using iPSC derived from patients with familial SCZ demonstrated increased presynapse formation and increased excitatory synaptic transmission (187). In contrast, a second study identified a decrease of PSD95 clusters and no change of excitatory synapse density in cultures of patient-derived glutamatergic neurons (140). While these results are contrary to our observations, both studies employed heterogeneous neuronal cultures generated by growth factor induction,

which might explain the different results observed. In addition, the upregulation of PSD95 observed in E-I co-cultures might only represent a transient phenotype, which still could result in a loss of spines at later stages, due to e.g. excess formation of premature, weak synapses which might be eliminated later. Finally, disease heterogeneity might further contribute the contrasting findings from different studies. Inter-donor variability was also observed in this thesis for the majority of experiments conducted with patient-derived iPSC lines, underlining the need for improved patient stratification and the generation of iPSC lines from specific cohorts, which could add to the understanding of the disease mechanisms in different subgroups of patients.

Overall, it can be concluded that the interaction of NGN2 with AD2-transduced GABAergic neurons in E-I co-cultures was necessary to produce an excitatory postsynaptic phenotype, which has not previously been observed and might help to gain insights into early synaptic aberrations in SCZ.

Next, the formation of inhibitory synapses was investigated in monocultures of AD2 neurons and in E-I co-cultures. When AD2 neurons were cultured separately, the density of vGAT-positive presynaptic terminals was reduced, in accordance with a previous report of reduced GAD67 in iPSC-derived cortical interneurons (188), which is also known to be decreased in patients (66). Interestingly, this reduction did not result in fewer inhibitory synapses (vGAT+Gephyrin) being formed and the percentage of presynaptic terminals in contact with postsynaptic Gephyrin was even increased, suggesting that extrasynaptic vGAT seems to be primarily affected. In E-I co-cultures however, the number of pre-, post- and total synapses was not different compared to CTR, while the increased percentage of co-localizing vGAT terminals was maintained. Previously, it has been reported that iPSC-derived GABAergic neurons show enhanced morphological and functional maturity upon co-culture with glutamatergic neurons (189, 190). Therefore, it is conceivable that intrinsic presynaptic deficits are rescued in the presence of NGN2 neurons, which might promote the maturity of AD2 neurons.

In summary, the analysis of synaptic phenotypes in E-I co-cultures revealed that excitatory synapses are mostly affected while inhibitory synapses are largely unchanged. Though the effects observed at the synaptic level are subtle, it would be interesting to study this phenotype in more mature cultures to see if it aggravates, changes over time or could provide a more clear indication of a potential E-I imbalance, which is likely implicated in SCZ pathology (72).

4.4 Altered neuronal activity in SCZ E-I co-cultures

As a next step, neuronal activity in E-I co-cultures was studied by calcium imaging to determine whether there are any alterations of single-cell and/or network activity, related to either the altered synaptic input or to intrinsic differences in calcium dynamics. A recent study on the development and maturation of neuronal activity patterns in iPSC-derived cultures suggests that monocultures of NGN2 and Ascl1-transduced neurons are unsuitable to study developing neuronal activity patterns, as only co-cultures of both depicted the emergence of network burst activity similar to developing networks *in vivo* (191). Therefore, measurements of intracellular calcium, which is crucial for the regulation of neuronal excitability, intracellular signaling and vesicle exocytosis (192), focused on co-cultured neurons only. In general, calcium imaging showed a mixture of spontaneous single-cell and coordinated synchronized network bursting. Network activity was observed to be either generalized throughout the entire well or restricted to smaller hubs of interconnected neurons. These observations are in line with a previous study, describing that iPSC-derived cultures exhibit a mixture of desynchronized and synchronized activity, with synchronous activity increasing during the cultivation period (193).

Upon direct comparison of CTR and SCZ neurons with a focus on unsynchronized activity, SCZ NGN2 neurons showed overall lower calcium activity, as depicted by a reduction of average peak amplitude (less calcium entering the cell), FWHM (altered influx/efflux dynamics) and concomitant reduction of the AUC, while AD2 neurons were unaffected. As the focus for this analysis were neurons not involved in network burst activity and thus less influenced by synaptic connections, these deficits might be related to differences in cellular calcium handling, which is tightly regulated by extra- and intracellular sources, such as receptors, transporters, and internal stores (194).

The number of studies addressing calcium signaling SCZ is still limited, however there is some evidence that this is a parameter affected in SCZ. A further study providing evidence for selective glutamatergic neuron dysfunction made use of isogenic 16p11.2 duplication iPSC lines to generate co-cultures of NGN2 and AD2-transduced neurons. Co-cultured neurons revealed downregulation of genes related to calcium binding, as well as reduced calcium signaling and synchronicity, which could be specifically attributed to NGN2 neurons (195). In a second study, primarily glutamatergic cortical neurons derived from patients with SCZ showed reduced peak frequency, increased FWHM and increased AUC (140). Finally, a third study reported decreased calcium activity in cortical 2D and 3D neuronal cultures, derived from patients with idiopathic SCZ (196). Therefore, there is accumulating evidence that single-cell calcium dynamics are a suitable parameter to distinguish CTR and SCZ neurons. In

accordance with deregulated calcium dynamics in SCZ, mutations and altered expression of voltage gated calcium channels were described in postmortem tissue (14, 197) and knockout of the calcium channel subunit *CACNA1* in mice, a risk gene for SCZ, resulted in lower calcium peak amplitudes of immature neurons (198).

Beside the study of unsychronized activity, synchronized burst activity was analyzed in E-I co-cultures at the network and single-cell level. The synchronized bursting activity of neuronal ensembles *in vivo* is controlled by the precise interplay of excitation and inhibition in the cortex (199). Network activity is generated as a result of increasing synaptic connectivity in iPSC-derived cultures, as both processes were previously shown to positively correlate (183, 195). In E-I co-cultures, a smaller proportion of synchronously active recorded wells was observed in SCZ samples as compared to CTR, indicating that SCZ cultures are less likely to develop network activity. In patients with SCZ, it is well known that cortical high-frequency network oscillations in the gamma-band range, which are involved in cognitive processing, are altered (200). However, there is variability in the findings from patient studies, which have reported both up- and downregulations of gamma-band activity (201). While the E-I co-culture is too reductionistic to inform on such high-frequency oscillations, the data obtained here, and other previous iPSC studies, suggest that network function is also altered in SCZ models *in vitro*. In agreement with our results, decreased network activity was previously reported using patient-derived and 16p11.2 duplication neurons (188, 195). On the contrary, increased network activity was observed in *SETD1A* mutant E-I co-cultures, comprised of NGN2 and AD2 neurons (184). In the present culture system, the reported increase of excitatory synapse density specifically on AD2 neurons could play a role in the decreased likelihood of a SCZ cultures to develop network burst activity due to increased inhibitory output, however this hypothesis needs to be explored in detail. Another possible explanation could be a delayed maturation of SCZ cultures, which would be in line with the reported differentiation deficits of SCZ iPSC (discussed in **4.1**).

To get more detailed insight into the contribution of glutamatergic and GABAergic neurons to the alteration of network activity in SCZ cultures, calcium signals of synchronized neurons were analyzed in a cell-type specific manner. Only one of the above-mentioned iPSC-based studies focused on single-cell calcium signals (16p11.2 duplication), which was confirmed by the application of synaptic blockers (195). However, this analysis was only performed in glutamatergic monocultures. With the present results, it is conceivable that while the likelihood of synchronous activity in SCZ E-I co-cultures is decreased, the frequency of burst activity is increased in those SCZ cultures that do develop network activity, as observed for both NGN2

and AD2 neurons. The cause behind the elevated calcium activity in SCZ neurons and the reduced calcium amplitude observed in AD2 neurons remains unclear, and could be related to altered synaptic input, neurotransmitter release probability, postsynaptic signal integration or altered calcium release from internal stores.

To address these questions, electrophysiological recordings of postsynaptic excitatory and inhibitory currents, as well as of miniature postsynaptic potentials as a measure of neurotransmitter release probability, could be performed. Mixed cultures comprising one CTR-derived and one SCZ-derived neuronal cell type could also be employed to study whether one type of neuron in particular is responsible for the observed alterations in network activity. Another important aspect to consider when interpreting the effects of single-cell calcium signals, is that it remains unclear whether GABA exerts a depolarizing or a hyperpolarizing effect with the present data set. There have been conflicting reports about when the GABA polarity switch happens in iPSC-derived cultures. While a polarity switch has been observed already in 2-week-old neurons (202), others have observed depolarizing GABA in 10-13-week old neurons (203). To study the timing of the GABA polarity switch, application of GABA receptor antagonists in E-I co-cultures at different time points could be performed to observed whether this induces a decrease or increase of network activity.

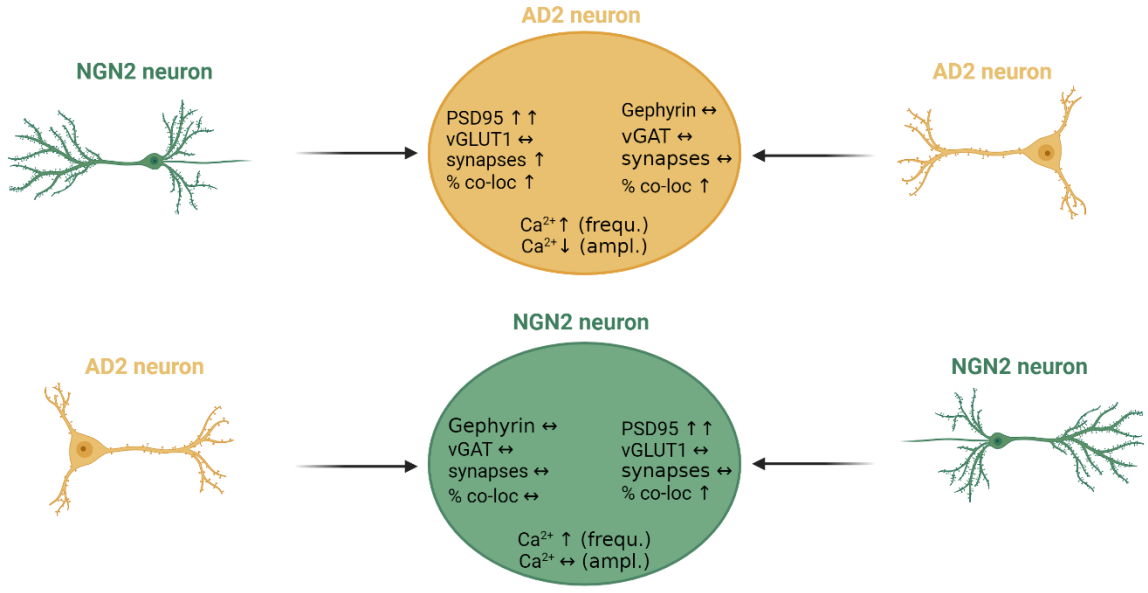

Figure 31 Summary of synaptic and functional phenotypes in patient-derived E-I co-cultures as discussed in sections 4.3 and 4.4.
Figure created with Biorender.com.

Figure 31 presents an overview of the synaptic and functional phenotypes observed in SCZ E-I co-cultures. Overall, the reported phenotypes support the view that synapse formation of developing neurons is altered in a cell type specific manner, which could contribute to excitation-inhibition imbalance in SCZ. Reduced neurite outgrowth and impaired neuronal differentiation efficiency of NPC might contribute to early alterations of synapse formation. Moreover, intrinsic deficits in calcium handling (measurement of unsynchronized activity) and in the calcium response to synaptic input (synchronized activity) might in turn influence the generation of aberrant network activity in SCZ.

4.5 Patient-derived microglia impact inhibitory synapse formation and neuronal activity

Accumulating evidence suggests a role for neuroinflammation in the pathogenesis of SCZ, which prompted us to study this aspect by co-culturing patient-derived microglia and healthy CTR neurons in E-I co-cultures. With this approach, the aim was to investigate if SCZ microglia impact neuronal synapse formation and activity and whether there is a selective impact on either glutamatergic or GABAergic neurons, which has not been investigated before.

Previous iPSC-based studies demonstrated excessive pruning of excitatory presynapses in co-culture with NGN2 neurons and of glutamatergic synaptosomes by SCZ microglia. Aberrant synaptic pruning was linked to inflammasome activation and increased C4A complement deposition at synapses, respectively. In addition, both studies successfully rescued altered microglia-mediated synapse uptake by anti-inflammatory treatment with minocycline (136, 157). While there is strong evidence for increased microglial activation and glutamatergic spine loss in patients with SCZ (45, 85), the hypothesis of altered synaptic pruning remains to be confirmed *in vivo*. Moreover, it is still unclear whether excess pruning only affects glutamatergic synapses, or if and to which extend GABAergic synapses are also affected. Recently, it has been proposed that ‘priming’ of microglia by environmental risk factors, combined with genetic vulnerability causing increased complement deposition at synapses, might lead to excess pruning of both excitatory and inhibitory synapses, contributing to E-I imbalance in SCZ (88).

The decrease of inhibitory presynapse density that was observed in this study could in principle be mediated by microglial synapse uptake (pruning) or the release of certain soluble factors by SCZ microglia such as cytokines or extracellular vesicles (204), which might impede initial presynapse formation or lead to loss of previously formed terminals via contact-independent mechanisms. Evidence of inhibitory synaptic pruning is limited, but one study reported specific pruning of inhibitory synapse in the somatosensory cortex of mice, in which it was

demonstrated that microglia expressing the $GABA_B$ receptor can sense GABA and leave excitatory synapses unaffected. This mechanism was also shown to be complement-dependent (205). Moreover, co-culture of iPSC-derived cortical interneurons with activated microglia previously showed impaired neuronal synapse formation, GABA release and metabolic function (206). Soluble factors released by microglia which could modulate neuronal function include cytokines, neurotrophic factors or extracellular vesicle carrying proteins and RNA, for which a role has been demonstrated in neurodegenerative diseases (204). Further experiments are required to determine whether microglia take up synaptic structures, or if treatment of co-cultures with microglia-conditioned medium would reproduce the observed effect.

Calcium imaging of neurons co-cultured with SCZ microglia revealed a slight increase in peak amplitude and AUC, which again was found to be an inflammation-independent mechanism. Abnormal regulation of neuronal activity by microglia has so far not been described in SCZ. However, it has been observed that microglia can provide negative feedback by suppressing neuronal activity in response to neuronal activation, and that ablation of microglia in the striatum can cause seizures (207). Potentially, this negative, ATP-mediated feedback mechanism could be deficient in SCZ microglia. In future experiments, it would be crucial to determine which type of neuron is affected specifically and whether the decrease of inhibitory presynaptic terminals also reflects in a decrease of synapses.

4.6 Generation of iPSC lines carrying mutations in the SCZ risk gene DISC1

To generate a second, more general model of neuropsychiatric diseases for the study of synaptic phenotypes, iPSC carrying a mutation in the gene *DISC1* were created by CRISPR-Cas9 gene-editing. Analysis of the *DISC1+/-* frameshift mutation predicted a preterminal stop codon after 39 irregular amino acids (163) . In line with this, immunocytochemical analysis with an antibody directed against the COOH terminus of DISC1 showed lower protein expression (30 %) in mutant iPSC and NPC, suggesting that expression of the long/long-variant isoform of DISC1 (which include the antibody target epitope) is reduced. In patients carrying the t(1;11) translocation which disrupts *DISC1*, expression of the protein was shown to be reduced by approximately 50 % (208). A possible mechanism by which the heterozygous mutation could lead to a reduction of protein expression is nonsense-mediated decay of the truncated RNA transcript. During this process, mRNA with a premature stop codon is degraded to avoid the production of truncated proteins (162) and due to haploinsufficiency, *DISC1+/-* cells might not be able to maintain a WT phenotype with just one remaining WT allele. To examine the effects

of the present mutation on the protein level in more detail, an antibody targeting the N-terminus of DISC1 should employed to determine if truncated variants of DISC1 are present. Overexpression of possible truncation variants in WT cells could then help to elucidate whether these can cause phenotypic changes in the cells.

4.7 Synaptic phenotypes in DISC1+/- neurons

DISC1 mutations in animal models suggest a strong implication of DISC1 in synapse formation and maintenance (see **1.4.2**). In support of this, aberrant synapse formation was observed in *DISC1+/-* neurons. In monocultures of NGN2-transduced neurons, the density of excitatory synapses was found to be reduced, concordant with the involvement of DISC1 in glutamatergic spine formation and maintenance (104, 105, 165). Strikingly however, *DISC1* mutation specifically impacted GABAergic neurons in E-I co-cultures. In accordance with a predominantly GABAergic phenotype in the co-cultures, an increase of AD2 neuron calcium activity, absent in NGN2 neurons, was observed with the same iPSC lines and the same culture system (163).

In contrast to these results, previous iPSC-based studies of mutant *DISC1* neurons identified a primarily glutamatergic phenotype. In iPSC-derived neurons in which a heterozygous patient mutation was introduced (4bp deletion in exon 12), excitatory synapses (SV2+/PSD95+) were reduced (105, 165, 181). In a second model, a frameshift mutation introduced into exon 2 of *DISC1* resulted in a reduction of presynaptic vGLUT1 expression (180). Importantly however, these studies employed heterogeneous cultures of human forebrain cortical neurons, primarily composed of glutamatergic neurons, in which an interaction effect of glutamatergic and only few GABAergic neurons might be less influential. In our model, the emergence of a primarily GABAergic phenotype in E-I co-cultures, which was completely absent in monocultures, suggests that NGN2 and AD2 neurons influence each other, as they mature together in the culture.

It is conceivable that the presence of NGN2 neurons in co-cultures could further reinforce the intrinsically increased GABAergic differentiation efficiency observed for *DISC1+/-* cells, leading to the strongly increased number of vGAT-positive presynapses formed by AD2 neurons. The average increase of vGAT density was ~ 1.5 times as high for terminals targeting AD2 neurons than NGN2 neurons, suggesting that there is, at least partially, a target-specific effect involved. The possibility that the maturation of GABAergic neurons can be influenced by glutamatergic modulation was described previously in a study, in which overexpression of mutant DISC1 in

cortical glutamatergic neurons caused a decrease of PV-positive interneurons in mice (209). An increase of GABAergic synaptic markers has also been described before in DISC1 mutant animal models. *DISC1* knockdown in interneurons, for example, was previously shown to account for increased formation of GAD65-positive inhibitory synaptic terminals targeting pyramidal neurons, as well as elevated excitability of PV-positive interneurons (210). In a second study, DISC1 disruption in immature granule cells resulted in increased formation of GABAergic synapses (211). As proposed by these studies and our data, DISC1 disruption results in an imbalance of excitatory and inhibitory synapses, a phenotype that has been described for multiple neuropsychiatric disorders including SCZ and ASD (212).

In future experiments, the effect of heightened inhibition on the activity of the neuronal network as a whole could be explored by measurements of network activity. Additionally, upregulation of Ascl1/Dlx2 downstream target genes could be monitored during GABAergic differentiation to potentially identify target(s) for drug intervention to rescue increased inhibitory synapse formation by mutant neurons.

4.8 Comparison of patient-derived and DISC1-related phenotypes

In this thesis, neurodevelopmental phenotypes were studied with idiopathic SCZ patient iPSC-derived neurons and *DISC1* mutant neurons with the aim to identify and compare common and diverging phenotypes of these two model systems.

For both models, initial experiments confirmed the results of previous studies reporting reduced neurite outgrowth of patient-derived (140) and DISC1 mutant neurons (164), generated with undirected differentiation protocols (reported in Heider et al. (2024) for the DISC1 model (163)). Another shared phenotype was the alteration of differentiation efficiency, however in different directions and concerning different cell types. While patient NPC showed reduced differentiation efficiency, *DISC1+/-* neurons showed enhanced GABAergic differentiation. Similar observations have been reported for patient-derived dopaminergic and glutamatergic neurons, which showed reduced differentiation efficiency and maturity (169), as well as for disruption of cortical neurogenesis in DISC1 exon 2 mutant cells (180). Regarding the formation of synapses in cultures comprised solely of NGN2-transduced neurons, both models showed a reduction of excitatory synapse density, consistent with previous iPSC-based studies (136, 165).

Following this first round of confirmatory experiments, gaps in current research regarding the involvement of GABAergic neurons and the interplay between both types of neurons were addressed, which was the point at which diverging phenotypes were observed.

In AD2 monocultures, inhibitory presynapses were reduced in patient-derived neurons and unchanged in *DISC1 +/-* neurons. Strikingly, E-I co-cultures revealed opposite synaptic phenotypes, as only excitatory synapses were affected in patient-derived cultures, and only inhibitory synapses were affected in DISC1 cultures. In both cases, an increase of synapses was observed, however in patient neurons due to an increase of postsynaptic interaction sites (PSD95), and in DISC1 neurons due to an increase of presynapse formation (vGAT). These findings suggest that different mechanisms of aberrant synapse formation/maintenance are likely at play in both models. In line with this, calcium imaging of basal, unsychronized activity revealed that only glutamatergic neurons are affected in patient-derived cultures, while only the activity of GABAergic neurons was altered in *DISC1+/-* cultures. As only one type of neuron in the co-cultures was observed to be primarily affected in both models, imbalanced E-I neurotransmission still emerges as an overarching phenotype in both systems, however manifesting in a different way. **Figure 32** presents a comparative graphical overview of all results obtained from synapse quantification and calcium imaging experiments in patient-derived and *DISC1+/-* E-I co-cultures.

Overall, shared phenotypes were especially observed in more simple culture systems, comprised of just one type of neuron. The emergence of diverging phenotypes in the more complex, physiologically relevant E-I co-cultures calls into question the usability of the here-presented *DISC1* mutant model to investigate phenotypes specific for SCZ. However, it still is a relevant model to investigate phenotypes related to DISC1 disruption, which occur in a subgroup of patients with neuropsychiatric diseases carrying mutations in the gene. SCZ is a highly complex disease with a large genetic component. However, the vast majority of cases are of idiopathic nature and single gene mutations, such as in the *DISC1*, are extremely rare. The mutation that was introduced into exon 2 has not been observed in patients and was chosen specifically to disturb as many protein isoforms as possible. Therefore, while the SCZ-specific idiopathic model can help to identify strong phenotypes that emerge even in the presence of inter-individual genetic variability, the mutation model can help to identify specific DISC1-related alterations without varying influences of the genetic background.

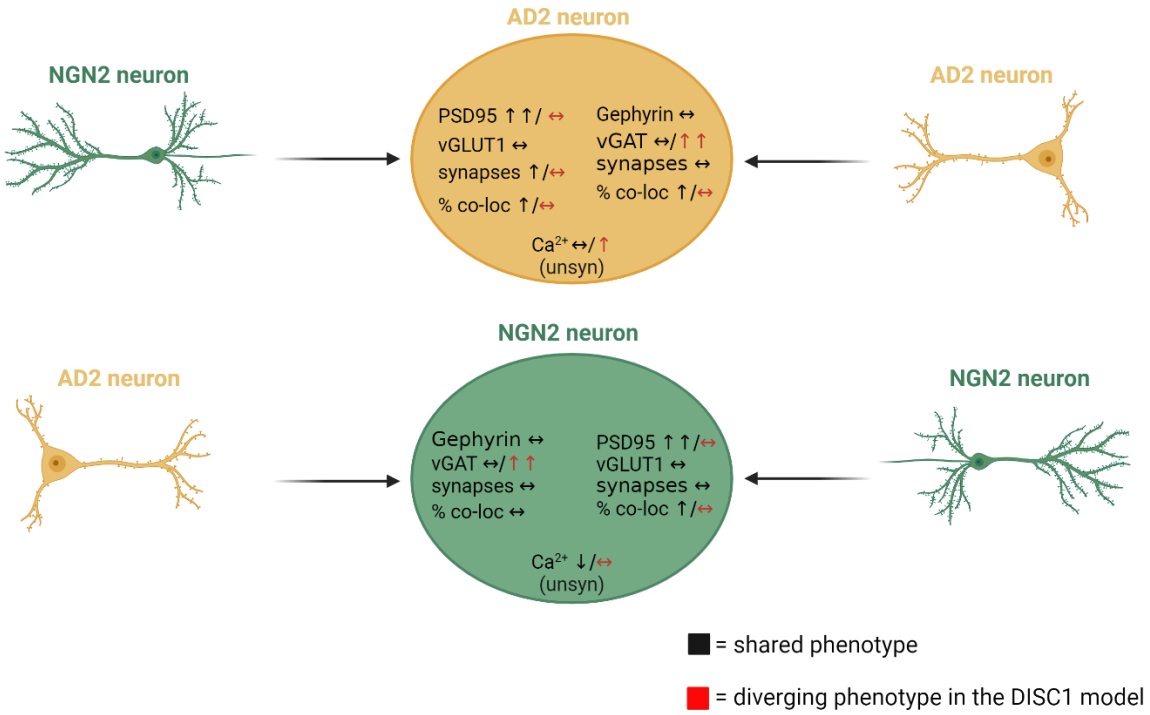

Figure 32 Comparison of synaptic and functional phenotypes observed in patient-derived and DISC1+/- E-I co-cultures.
Shared phenotypes observed in both models are marked in black. Phenotypes which showed diverging results in the DISC1+/- model are indicated in red. Figure created with Biorender.com.

4.9 Conclusion and Outlook

Deregulated synaptic connectivity and neuronal (network) activity in the PFC are strongly implicated in the pathogenesis of SCZ and related neuropsychiatric disorders. In this thesis, a highly defined co-culture system comprised of iPSC-derived, induced glutamatergic and GABAergic neurons, was employed to study disease-related neuronal aberrations in a SCZ patient-derived and a *DISC1* mutation model system.

Enhanced excitatory synaptic connectivity in patient-derived cultures and increased inhibitory connectivity in *DISC1+/-* cultures support the notion of synaptic disbalance as a shared phenotype of multiple neuropsychiatric disorders. Altered neuronal differentiation efficiency and spontaneous calcium activity were additionally identified in both models. Overall, the results presented in this thesis suggest that neuronal phenotypes can emerge early during brain development and differences are already visible at the neural progenitor stage, which agrees with previous literature and the neurodevelopmental hypothesis of SCZ. The present models support the notion that the process of neuronal network formation, governed by the establishment of precise synaptic connections between excitatory and inhibitory neurons,

seems to be disturbed in neuropsychiatric diseases. Altered connectivity at the circuit level might in turn contribute to aberrant cortical network activity and ultimately cognitive deficits in patients.

Despite the important insights that were gained with the present model systems, many open questions remain regarding the precise mechanisms behind the phenotypes observed. Cell type-specific interventions by the application of receptor agonists/antagonist or by implication of optogenetic and chemogenetic methods (213) can help to elucidate the cellular origin of a phenotype and which cells are directly influenced by it. Moreover, single-cell RNA sequencing can offer valuable insight into cell-type specific gene expression profiles, even in co-cultures composed of multiple cell types. Finally, in-depth electrophysiological characterization could be employed to study the direct functional impact of synaptic connectivity on synaptic transmission and network activity, as well as possible intrinsic alterations of neuronal excitability. All these methods can help to identify a target for drug intervention, which can be addressed by compound application in high-throughput format to explore whether a rescue can be achieved.

Importantly, 2D culture systems still lack complexity and maturity and need to be continuously adapted and improved to mimic the *in vivo* neurodevelopmental environment more closely. iPSC-derived 3D brain organoids offer the possibility to generate more complex neuronal cultures which self-assemble *in vitro* and thus more accurately represent neurodevelopmental processes (214). In addition, organoids can be cultured for extended periods of time to generate more mature neurons, and brain region-specific organoids can be combined to generate assembloids for the study of neuronal connectivity between different brain regions (215).

5. References

1. Adam D. Mental health: On the spectrum. Nature. 2013;496(7446):416-8.
2. Tandon R, Gaebel W, Barch DM, Bustillo J, Gur RE, Heckers S, et al. Definition and description of schizophrenia in the DSM-5. Schizophrenia Research. 2013;150(1):3-10.
3. Saha S, Chant D, Welham J, McGrath J. A systematic review of the prevalence of schizophrenia. PLoS Med. 2005;2(5):e141.
4. Solmi M, Radua J, Olivola M, Croce E, Soardo L, Salazar de Pablo G, et al. Age at onset of mental disorders worldwide: large-scale meta-analysis of 192 epidemiological studies. Molecular Psychiatry. 2022;27(1):281-95.
5. McGrath J, Saha S, Welham J, El Saadi O, MacCauley C, Chant D. A systematic review of the incidence of schizophrenia: the distribution of rates and the influence of sex, urbanicity, migrant status and methodology. BMC Med. 2004;2:13.
6. Hjorthoj C, Sturup AE, McGrath JJ, Nordentoft M. Years of potential life lost and life expectancy in schizophrenia: a systematic review and meta-analysis. Lancet Psychiatry. 2017;4(4):295-301.
7. Saha S, Chant D, McGrath J. A systematic review of mortality in schizophrenia: is the differential mortality gap worsening over time? Arch Gen Psychiatry. 2007;64(10):1123-31.
8. Sullivan PF, Kendler KS, Neale MC. Schizophrenia as a complex trait: evidence from a meta-analysis of twin studies. Arch Gen Psychiatry. 2003;60(12):1187-92.
9. Cardno AG, Gottesman, II. Twin studies of schizophrenia: from bow-and-arrow concordances to star wars Mx and functional genomics. Am J Med Genet. 2000;97(1):12-7.
10. Stefansson H, Ophoff RA, Steinberg S, Andreassen OA, Cichon S, Rujescu D, et al. Common variants conferring risk of schizophrenia. Nature. 2009;460(7256):744-7.
11. Ripke S, Sanders AR, Kendler KS, Levinson DF, Sklar P, Holmans PA, et al. Genome-wide association study identifies five new schizophrenia loci. Nature Genetics. 2011;43(10):969-76.
12. Ripke S, O'Dushlaine C, Chambert K, Moran JL, Kähler AK, Akterin S, et al. Genome-wide association analysis identifies 13 new risk loci for schizophrenia. Nature Genetics. 2013;45(10):1150-9.
13. Ripke S, Neale BM, Corvin A, Walters JTR, Farh K-H, Holmans PA, et al. Biological insights from 108 schizophrenia-associated genetic loci. Nature. 2014;511(7510):421-7.
14. Trubetskoy V, Pardiñas AF, Qi T, Panagiotaropoulou G, Awasthi S, Bigdeli TB, et al. Mapping genomic loci implicates genes and synaptic biology in schizophrenia. Nature. 2022;604(7906):502-8.
15. Singh T, Poterba T, Curtis D, Akil H, Al Eissa M, Barchas JD, et al. Rare coding variants in ten genes confer substantial risk for schizophrenia. Nature. 2022;604(7906):509-16.
16. Millar JK, Wilson-Annan JC, Anderson S, Christie S, Taylor MS, Semple CA, et al. Disruption of two novel genes by a translocation co-segregating with schizophrenia. Hum Mol Genet. 2000;9(9):1415-23.
17. St Clair D, Blackwood D, Muir W, Carothers A, Walker M, Spowart G, et al. Association within a family of a balanced autosomal translocation with major mental illness. Lancet. 1990;336(8706):13-6.
18. Takata A, Xu B, Ionita-Laza I, Roos JL, Gogos JA, Karayiorgou M. Loss-of-function variants in schizophrenia risk and SETD1A as a candidate susceptibility gene. Neuron. 2014;82(4):773-80.
19. Ohi K, Shimada M, Soda M, Nishizawa D, Fujikane D, Takai K, et al. Genome-wide DNA methylation risk scores for schizophrenia derived from blood and brain tissues further explain the genetic risk in patients stratified by polygenic risk scores for schizophrenia and bipolar disorder. BMJ Ment Health. 2024;27(1).
20. Williams NM, O'Donovan MC, Owen MJ. Chromosome 22 deletion syndrome and schizophrenia. Int Rev Neurobiol. 2006;73:1-27.
21. International Schizophrenia C. Rare chromosomal deletions and duplications increase risk of schizophrenia. Nature. 2008;455(7210):237-41.

22. Johnstone EC, Crow TJ, Frith CD, Husband J, Kreel L. Cerebral ventricular size and cognitive impairment in chronic schizophrenia. Lancet. 1976;2(7992):924-6.
23. Seidman LJ. Schizophrenia and brain dysfunction: An integration of recent neurodiagnostic findings. Psychological Bulletin. 1983;94(2):195-238.
24. Reveley AM, Reveley MA, Clifford CA, Murray RM. Cerebral ventricular size in twins discordant for schizophrenia. Lancet. 1982;1(8271):540-1.
25. Robinson N, Ploner A, Leone M, Lichtenstein P, Kendler KS, Bergen SE. Impact of Early-Life Factors on Risk for Schizophrenia and Bipolar Disorder. Schizophr Bull. 2023;49(3):768-77.
26. O'Callaghan E, Sham P, Takei N, Glover G, Murray RM. Schizophrenia after prenatal exposure to 1957 A2 influenza epidemic. Lancet. 1991;337(8752):1248-50.
27. Brown AS, Schaefer CA, Wyatt RJ, Begg MD, Goetz R, Bresnahan MA, et al. Paternal age and risk of schizophrenia in adult offspring. Am J Psychiatry. 2002;159(9):1528-33.
28. Stilo SA, Murray RM. Non-Genetic Factors in Schizophrenia. Curr Psychiatry Rep. 2019;21(10):100.
29. Harrison G, Gunnell D, Glazebrook C, Page K, Kwiecinski R. Association between schizophrenia and social inequality at birth: case-control study. Br J Psychiatry. 2001;179:346-50.
30. Marcelis M, Navarro-Mateu F, Murray R, Selten JP, Van Os J. Urbanization and psychosis: a study of 1942-1978 birth cohorts in The Netherlands. Psychol Med. 1998;28(4):871-9.
31. Arseneault L, Cannon M, Poulton R, Murray R, Caspi A, Moffitt TE. Cannabis use in adolescence and risk for adult psychosis: longitudinal prospective study. BMJ. 2002;325(7374):1212-3.
32. Creese I, Burt DR, Snyder SH. Dopamine receptor binding predicts clinical and pharmacological potencies of antischizophrenic drugs. Science. 1976;192(4238):481-3.
33. Seeman P, Lee T. Antipsychotic drugs: direct correlation between clinical potency and presynaptic action on dopamine neurons. Science. 1975;188(4194):1217-9.
34. Madras BK. History of the discovery of the antipsychotic dopamine D2 receptor: a basis for the dopamine hypothesis of schizophrenia. J Hist Neurosci. 2013;22(1):62-78.
35. Davis KL, Kahn RS, Ko G, Davidson M. Dopamine in schizophrenia: a review and reconceptualization. Am J Psychiatry. 1991;148(11):1474-86.
36. Stępnicki P, Kondej M, Kaczor AA. Current Concepts and Treatments of Schizophrenia. Molecules (Basel, Switzerland). 2018;23(8):2087.
37. Stepnicki P, Kondej M, Kaczor AA. Current Concepts and Treatments of Schizophrenia. Molecules. 2018;23(8).
38. Correll CU, Schooler NR. Negative Symptoms in Schizophrenia: A Review and Clinical Guide for Recognition, Assessment, and Treatment. Neuropsychiatr Dis Treat. 2020;16:519-34.
39. Lally J, MacCabe JH. Antipsychotic medication in schizophrenia: a review. British Medical Bulletin. 2015;114(1):169-79.
40. Samara MT, Nikolakopoulou A, Salanti G, Leucht S. How Many Patients With Schizophrenia Do Not Respond to Antipsychotic Drugs in the Short Term? An Analysis Based on Individual Patient Data From Randomized Controlled Trials. Schizophr Bull. 2019;45(3):639-46.
41. Fromer M, Roussos P, Sieberts SK, Johnson JS, Kavanagh DH, Perumal TM, et al. Gene expression elucidates functional impact of polygenic risk for schizophrenia. Nat Neurosci. 2016;19(11):1442-53.
42. Wilson CR, Gaffan D, Browning PG, Baxter MG. Functional localization within the prefrontal cortex: missing the forest for the trees? Trends Neurosci. 2010;33(12):533-40.
43. Mubarik A, Tohid H. Frontal lobe alterations in schizophrenia: a review. Trends Psychiatry Psychother. 2016;38(4):198-206.
44. Sun D, Phillips L, Velakoulis D, Yung A, McGorry PD, Wood SJ, et al. Progressive brain structural changes mapped as psychosis develops in 'at risk' individuals. Schizophr Res. 2009;108(1-3):85-92.

45. Moyer CE, Shelton MA, Sweet RA. Dendritic spine alterations in schizophrenia. Neurosci Lett. 2015;601:46-53.
46. Onwordi EC, Halff EF, Whitehurst T, Mansur A, Cotel MC, Wells L, et al. Synaptic density marker SV2A is reduced in schizophrenia patients and unaffected by antipsychotics in rats. Nat Commun. 2020;11(1):246.
47. Osimo EF, Beck K, Reis Marques T, Howes OD. Synaptic loss in schizophrenia: a meta-analysis and systematic review of synaptic protein and mRNA measures. Mol Psychiatry. 2019;24(4):549-61.
48. Sahara S, Yanagawa Y, O'Leary DD, Stevens CF. The fraction of cortical GABAergic neurons is constant from near the start of cortical neurogenesis to adulthood. J Neurosci. 2012;32(14):4755-61.
49. Tamamaki N, Yanagawa Y, Tomioka R, Miyazaki J, Obata K, Kaneko T. Green fluorescent protein expression and colocalization with calretinin, parvalbumin, and somatostatin in the GAD67-GFP knock-in mouse. J Comp Neurol. 2003;467(1):60-79.
50. Lim L, Mi D, Llorca A, Marin O. Development and Functional Diversification of Cortical Interneurons. Neuron. 2018;100(2):294-313.
51. Coyle JT, Ruzicka WB, Balu DT. Fifty Years of Research on Schizophrenia: The Ascendance of the Glutamatergic Synapse. Am J Psychiatry. 2020;177(12):1119-28.
52. Iasevoli F, Tomasetti C, Buonaguro EF, de Bartolomeis A. The glutamatergic aspects of schizophrenia molecular pathophysiology: role of the postsynaptic density, and implications for treatment. Curr Neuropharmacol. 2014;12(3):219-38.
53. Singh T, Walters JTR, Johnstone M, Curtis D, Suvisaari J, Torniainen M, et al. The contribution of rare variants to risk of schizophrenia in individuals with and without intellectual disability. Nat Genet. 2017;49(8):1167-73.
54. Moghaddam B, Javitt D. From revolution to evolution: the glutamate hypothesis of schizophrenia and its implication for treatment. Neuropsychopharmacology. 2012;37(1):4-15.
55. Catts VS, Lai YL, Weickert CS, Weickert TW, Catts SV. A quantitative review of the postmortem evidence for decreased cortical N-methyl-D-aspartate receptor expression levels in schizophrenia: How can we link molecular abnormalities to mismatch negativity deficits? Biol Psychol. 2016;116:57-67.
56. McCutcheon RA, Krystal JH, Howes OD. Dopamine and glutamate in schizophrenia: biology, symptoms and treatment. World Psychiatry. 2020;19(1):15-33.
57. Olney JW, Farber NB. Glutamate receptor dysfunction and schizophrenia. Arch Gen Psychiatry. 1995;52(12):998-1007.
58. Kruse AO, Bustillo JR. Glutamatergic dysfunction in Schizophrenia. Transl Psychiatry. 2022;12(1):500.
59. Mavroudis I, Petrides F, Kazis D, Chatzikonstantinou S, Karantali E, Ciobica A, et al. Morphological alterations of the pyramidal and stellate cells of the visual cortex in schizophrenia. Exp Ther Med. 2021;22(1):669.
60. Chung DW, Chung Y, Bazmi HH, Lewis DA. Altered ErbB4 splicing and cortical parvalbumin interneuron dysfunction in schizophrenia and mood disorders. Neuropsychopharmacology. 2018;43(12):2478-86.
61. Fung SJ, Webster MJ, Sivagnanasundaram S, Duncan C, Elashoff M, Weickert CS. Expression of interneuron markers in the dorsolateral prefrontal cortex of the developing human and in schizophrenia. Am J Psychiatry. 2010;167(12):1479-88.
62. Hashimoto T, Volk DW, Eggan SM, Mirnics K, Pierri JN, Sun Z, et al. Gene expression deficits in a subclass of GABA neurons in the prefrontal cortex of subjects with schizophrenia. J Neurosci. 2003;23(15):6315-26.
63. Enwright JF, Sanapala S, Foglio A, Berry R, Fish KN, Lewis DA. Reduced Labeling of Parvalbumin Neurons and Perineuronal Nets in the Dorsolateral Prefrontal Cortex of Subjects with Schizophrenia. Neuropsychopharmacology. 2016;41(9):2206-14.
64. Cotter D, Landau S, Beasley C, Stevenson R, Chana G, MacMillan L, et al. The density and spatial distribution of GABAergic neurons, labelled using calcium binding proteins, in the anterior cingulate cortex in major depressive disorder, bipolar disorder, and schizophrenia. Biol Psychiatry. 2002;51(5):377-86.

65. Glausier JR, Lewis DA. Selective pyramidal cell reduction of GABA(A) receptor alpha1 subunit messenger RNA expression in schizophrenia. Neuropsychopharmacology. 2011;36(10):2103-10.
66. Akbarian S, Kim JJ, Potkin SG, Hagman JO, Tafazzoli A, Bunney WE, Jr., et al. Gene expression for glutamic acid decarboxylase is reduced without loss of neurons in prefrontal cortex of schizophrenics. Arch Gen Psychiatry. 1995;52(4):258-66.
67. Curley AA, Arion D, Volk DW, Asafu-Adjei JK, Sampson AR, Fish KN, et al. Cortical deficits of glutamic acid decarboxylase 67 expression in schizophrenia: clinical, protein, and cell type-specific features. Am J Psychiatry. 2011;168(9):921-9.
68. Volk DW, Austin MC, Pierri JN, Sampson AR, Lewis DA. Decreased glutamic acid decarboxylase67 messenger RNA expression in a subset of prefrontal cortical gamma-aminobutyric acid neurons in subjects with schizophrenia. Arch Gen Psychiatry. 2000;57(3):237-45.
69. Morris HM, Hashimoto T, Lewis DA. Alterations in somatostatin mRNA expression in the dorsolateral prefrontal cortex of subjects with schizophrenia or schizoaffective disorder. Cereb Cortex. 2008;18(7):1575-87.
70. Tsubomoto M, Kawabata R, Zhu X, Minabe Y, Chen K, Lewis DA, et al. Expression of Transcripts Selective for GABA Neuron Subpopulations across the Cortical Visuospatial Working Memory Network in the Healthy State and Schizophrenia. Cereb Cortex. 2019;29(8):3540-50.
71. Buzsaki G, Draguhn A. Neuronal oscillations in cortical networks. Science. 2004;304(5679):1926-9.
72. Chung DW, Geramita MA, Lewis DA. Synaptic Variability and Cortical Gamma Oscillation Power in Schizophrenia. Am J Psychiatry. 2022;179(4):277-87.
73. Kwon JS, O'Donnell BF, Wallenstein GV, Greene RW, Hirayasu Y, Nestor PG, et al. Gamma frequency-range abnormalities to auditory stimulation in schizophrenia. Arch Gen Psychiatry. 1999;56(11):1001-5.
74. Wilson TW, Hernandez OO, Asherin RM, Teale PD, Reite ML, Rojas DC. Cortical Gamma Generators Suggest Abnormal Auditory Circuitry in Early-Onset Psychosis. Cerebral Cortex. 2007;18(2):371-8.
75. Williams S, Boksa P. Gamma oscillations and schizophrenia. Journal of Psychiatry and Neuroscience. 2010;35(2):75-7.
76. Bruining H, Hardstone R, Juarez-Martinez EL, Sprengers J, Avramiea AE, Simpraga S, et al. Measurement of excitation-inhibition ratio in autism spectrum disorder using critical brain dynamics. Sci Rep. 2020;10(1):9195.
77. Li W. Excitation and Inhibition Imbalance in Rett Syndrome. Front Neurosci. 2022;16:825063.
78. Bauer ME, Teixeira AL. Inflammation in psychiatric disorders: what comes first? Ann N Y Acad Sci. 2019;1437(1):57-67.
79. Di Nicola M, Cattaneo A, Hepgul N, Di Forti M, Aitchison KJ, Janiri L, et al. Serum and gene expression profile of cytokines in first-episode psychosis. Brain Behav Immun. 2013;31:90-5.
80. Miller BJ, Buckley P, Seabolt W, Mellor A, Kirkpatrick B. Meta-analysis of cytokine alterations in schizophrenia: clinical status and antipsychotic effects. Biol Psychiatry. 2011;70(7):663-71.
81. Heider J, Vogel S, Volkmer H, Breitmeyer R. Human iPSC-Derived Glia as a Tool for Neuropsychiatric Research and Drug Development. Int J Mol Sci. 2021;22(19).
82. Kettenmann H, Hanisch UK, Noda M, Verkhratsky A. Physiology of microglia. Physiol Rev. 2011;91(2):461-553.
83. Woodburn SC, Bollinger JL, Wohleb ES. The semantics of microglia activation: neuroinflammation, homeostasis, and stress. J Neuroinflammation. 2021;18(1):258.
84. Bloomfield PS, Selvaraj S, Veronese M, Rizzo G, Bertoldo A, Owen DR, et al. Microglial Activity in People at Ultra High Risk of Psychosis and in Schizophrenia: An [(11)C]PBR28 PET Brain Imaging Study. Am J Psychiatry. 2016;173(1):44-52.
85. Hartmann S-M, Heider J, Wüst R, Fallgatter AJ, Volkmer H. Microglia-neuron interactions in schizophrenia. Frontiers in Cellular Neuroscience. 2024;18.

86. Liu YJ, Spangenberg EE, Tang B, Holmes TC, Green KN, Xu X. Microglia Elimination Increases Neural Circuit Connectivity and Activity in Adult Mouse Cortex. J Neurosci. 2021;41(6):1274-87.
87. Faust TE, Gunner G, Schafer DP. Mechanisms governing activity-dependent synaptic pruning in the developing mammalian CNS. Nat Rev Neurosci. 2021;22(11):657-73.
88. Howes OD, Onwordi EC. The synaptic hypothesis of schizophrenia version III: a master mechanism. Mol Psychiatry. 2023;28(5):1843-56.
89. Sekar A, Bialas AR, de Rivera H, Davis A, Hammond TR, Kamitaki N, et al. Schizophrenia risk from complex variation of complement component 4. Nature. 2016;530(7589):177-83.
90. Sachs NA, Sawa A, Holmes SE, Ross CA, DeLisi LE, Margolis RL. A frameshift mutation in Disrupted in Schizophrenia 1 in an American family with schizophrenia and schizoaffective disorder. Mol Psychiatry. 2005;10(8):758-64.
91. Callicott JH, Straub RE, Pezawas L, Egan MF, Mattay VS, Hariri AR, et al. Variation in DISC1 affects hippocampal structure and function and increases risk for schizophrenia. Proceedings of the National Academy of Sciences. 2005;102(24):8627-32.
92. Hamshere ML, Bennett P, Williams N, Segurado R, Cardno A, Norton N, et al. Genomewide Linkage Scan in Schizoaffective Disorder: Significant Evidence for Linkage at 1q42 Close to DISC1, and Suggestive Evidence at 22q11 and 19p13. Archives of General Psychiatry. 2005;62(10):1081-8.
93. Hennah W, Varilo T, Kestilä M, Paunio T, Arajärvi R, Haukka J, et al. Haplotype transmission analysis provides evidence of association for DISC1 to schizophrenia and suggests sex-dependent effects. Human Molecular Genetics. 2003;12(23):3151-9.
94. Hodgkinson CA, Goldman D, Jaeger J, Persaud S, Kane JM, Lipsky RH, et al. Disrupted in Schizophrenia 1 (DISC1): Association with Schizophrenia, Schizoaffective Disorder, and Bipolar Disorder. The American Journal of Human Genetics. 2004;75(5):862-72.
95. Soares DC, Carlyle BC, Bradshaw NJ, Porteous DJ. DISC1: Structure, Function, and Therapeutic Potential for Major Mental Illness. ACS Chemical Neuroscience. 2011;2(11):609-32.
96. Thomson PA, Malavasi EL, Grunewald E, Soares DC, Borkowska M, Millar JK. DISC1 genetics, biology and psychiatric illness. Front Biol (Beijing). 2013;8(1):1-31.
97. Pletnikov MV, Ayhan Y, Nikolskaia O, Xu Y, Ovanesov MV, Huang H, et al. Inducible expression of mutant human DISC1 in mice is associated with brain and behavioral abnormalities reminiscent of schizophrenia. Mol Psychiatry. 2008;13(2):173-86, 15.
98. Tropea D, Hardingham N, Millar K, Fox K. Mechanisms underlying the role of DISC1 in synaptic plasticity. J Physiol. 2018;596(14):2747-71.
99. Hattori T, Shimizu S, Koyama Y, Yamada K, Kuwahara R, Kumamoto N, et al. DISC1 regulates cell-cell adhesion, cell-matrix adhesion and neurite outgrowth. Mol Psychiatry. 2010;15(8):778, 98-809.
100. Kamiya A, Tomoda T, Chang J, Takaki M, Zhan C, Morita M, et al. DISC1-NDEL1/NUDEL protein interaction, an essential component for neurite outgrowth, is modulated by genetic variations of DISC1. Hum Mol Genet. 2006;15(22):3313-23.
101. Shinoda T, Taya S, Tsuboi D, Hikita T, Matsuzawa R, Kuroda S, et al. DISC1 regulates neurotrophin-induced axon elongation via interaction with Grb2. J Neurosci. 2007;27(1):4-14.
102. Wu Q, Tang W, Luo Z, Li Y, Shu Y, Yue Z, et al. DISC1 Regulates the Proliferation and Migration of Mouse Neural Stem/Progenitor Cells through Pax5, Sox2, Dll1 and Neurog2. Front Cell Neurosci. 2017;11:261.
103. Camargo LM, Collura V, Rain JC, Mizuguchi K, Hermjakob H, Kerrien S, et al. Disrupted in Schizophrenia 1 Interactome: evidence for the close connectivity of risk genes and a potential synaptic basis for schizophrenia. Mol Psychiatry. 2007;12(1):74-86.
104. Kvajo M, McKellar H, Arguello PA, Drew LJ, Moore H, MacDermott AB, et al. A mutation in mouse Disc1 that models a schizophrenia risk allele leads to specific alterations in neuronal architecture and cognition. Proc Natl Acad Sci U S A. 2008;105(19):7076-81.
105. Kim NS, Wen Z, Liu J, Zhou Y, Guo Z, Xu C, et al. Pharmacological rescue in patient iPSC and mouse models with a rare DISC1 mutation. Nat Commun. 2021;12(1):1398.

106. Crabtree GW, Sun Z, Kvajo M, Broek JA, Fenelon K, McKellar H, et al. Alteration of Neuronal Excitability and Short-Term Synaptic Plasticity in the Prefrontal Cortex of a Mouse Model of Mental Illness. J Neurosci. 2017;37(15):4158-80.
107. Chandran JS, Kazanis I, Clapcote SJ, Ogawa F, Millar JK, Porteous DJ, et al. Disc1 variation leads to specific alterations in adult neurogenesis. PLoS One. 2014;9(10):e108088.
108. Clapcote SJ, Lipina TV, Millar JK, Mackie S, Christie S, Ogawa F, et al. Behavioral phenotypes of Disc1 missense mutations in mice. Neuron. 2007;54(3):387-402.
109. Lipina TV, Zai C, Hlousek D, Roder JC, Wong AH. Maternal immune activation during gestation interacts with Disc1 point mutation to exacerbate schizophrenia-related behaviors in mice. J Neurosci. 2013;33(18):7654-66.
110. Thomas D MA, LaFever S. Clinical development success rates and contributing factors 2011–2020. 2021.
111. Takahashi K, Yamanaka S. Induction of pluripotent stem cells from mouse embryonic and adult fibroblast cultures by defined factors. Cell. 2006;126(4):663-76.
112. Aboul-Soud MAM, Alzahrani AJ, Mahmoud A. Induced Pluripotent Stem Cells (iPSCs)-Roles in Regenerative Therapies, Disease Modelling and Drug Screening. Cells. 2021;10(9).
113. Al Abbar A, Ngai SC, Nograles N, Alhaji SY, Abdullah S. Induced Pluripotent Stem Cells: Reprogramming Platforms and Applications in Cell Replacement Therapy. Biores Open Access. 2020;9(1):121-36.
114. Liu C, Oikonomopoulos A, Sayed N, Wu JC. Modeling human diseases with induced pluripotent stem cells: from 2D to 3D and beyond. Development. 2018;145(5).
115. Hoffman GE, Schrode N, Flaherty E, Brennand KJ. New considerations for hiPSC-based models of neuropsychiatric disorders. Mol Psychiatry. 2019;24(1):49-66.
116. Gaj T, Sirk SJ, Shui SL, Liu J. Genome-Editing Technologies: Principles and Applications. Cold Spring Harb Perspect Biol. 2016;8(12).
117. Agrawal N, Dasaradhi PV, Mohmmed A, Malhotra P, Bhatnagar RK, Mukherjee SK. RNA interference: biology, mechanism, and applications. Microbiol Mol Biol Rev. 2003;67(4):657-85.
118. Gasiunas G, Barrangou R, Horvath P, Siksnys V. Cas9–crRNA ribonucleoprotein complex mediates specific DNA cleavage for adaptive immunity in bacteria. Proceedings of the National Academy of Sciences. 2012;109(39):E2579-E86.
119. Rath D, Amlinger L, Rath A, Lundgren M. The CRISPR-Cas immune system: Biology, mechanisms and applications. Biochimie. 2015;117:119-28.
120. Ran FA, Hsu PD, Wright J, Agarwala V, Scott DA, Zhang F. Genome engineering using the CRISPR-Cas9 system. Nat Protoc. 2013;8(11):2281-308.
121. Telias M. Neural differentiation protocols: how to choose the correct approach. Neural Regeneration Research. 2023;18(6):1273-4.
122. Ho SM, Hartley BJ, Tcw J, Beaumont M, Stafford K, Slesinger PA, et al. Rapid Ngn2-induction of excitatory neurons from hiPSC-derived neural progenitor cells. Methods. 2016;101:113-24.
123. Barretto N, Zhang H, Powell SK, Fernando MB, Zhang S, Flaherty EK, et al. ASCL1- and DLX2-induced GABAergic neurons from hiPSC-derived NPCs. J Neurosci Methods. 2020;334:108548.
124. Das AT, Tenenbaum L, Berkhout B. Tet-On Systems For Doxycycline-inducible Gene Expression. Curr Gene Ther. 2016;16(3):156-67.
125. Powell SK, O'Shea C, Townsley K, Prytkova I, Dobrindt K, Elahi R, et al. Induction of dopaminergic neurons for neuronal subtype-specific modeling of psychiatric disease risk. Molecular Psychiatry. 2023;28(5):1970-82.
126. Speicher AM, Wiendl H, Meuth SG, Pawlowski M. Generating microglia from human pluripotent stem cells: novel in vitro models for the study of neurodegeneration. Mol Neurodegener. 2019;14(1):46.
127. Suga M, Kondo T, Inoue H. Modeling Neurological Disorders with Human Pluripotent Stem Cell-Derived Astrocytes. Int J Mol Sci. 2019;20(16).

128. Canals I, Ginisty A, Quist E, Timmerman R, Fritze J, Miskinyte G, et al. Rapid and efficient induction of functional astrocytes from human pluripotent stem cells. Nat Methods. 2018;15(9):693-6.
129. Chen SW, Wong YH. Directed Differentiation of Human iPSCs into Microglia-Like Cells Using Defined Transcription Factors. Methods Mol Biol. 2023;2683:53-68.
130. Doss MX, Sachinidis A. Current Challenges of iPSC-Based Disease Modeling and Therapeutic Implications. Cells. 2019;8(5).
131. Marenco S, Weinberger DR. The neurodevelopmental hypothesis of schizophrenia: following a trail of evidence from cradle to grave. Dev Psychopathol. 2000;12(3):501-27.
132. Stock R, Vogel S, Mau-Holzmann UA, Kriebel M, Wust R, Fallgatter AJ, et al. Generation and characterization of human induced pluripotent stem cells lines from four patients diagnosed with schizophrenia and one healthy control. Stem Cell Res. 2020;48:101961.
133. Burridge PW, Thompson S, Millrod MA, Weinberg S, Yuan X, Peters A, et al. A universal system for highly efficient cardiac differentiation of human induced pluripotent stem cells that eliminates interline variability. PLoS One. 2011;6(4):e18293.
134. Keller AL, Binner A, Breitmeyer R, Vogel S, Anderle N, Rothbauer U, et al. Generation and characterization of the human induced pluripotent stem cell line NMIi010-A from peripheral blood mononuclear cells of a healthy 49-year old male individual. Stem Cell Res. 2021;54:102427.
135. Marrone L, Bus C, Schondorf D, Fitzgerald JC, Kubler M, Schmid B, et al. Generation of iPSCs carrying a common LRRK2 risk allele for in vitro modeling of idiopathic Parkinson's disease. PLoS One. 2018;13(3):e0192497.
136. Breitmeyer R, Vogel S, Heider J, Hartmann SM, Wust R, Keller AL, et al. Regulation of synaptic connectivity in schizophrenia spectrum by mutual neuron-microglia interaction. Commun Biol. 2023;6(1):472.
137. Fox MH. A model for the computer analysis of synchronous DNA distributions obtained by flow cytometry. Cytometry. 1980;1(1):71-7.
138. Murray RM, Bhavsar V, Tripoli G, Howes O. 30 Years on: How the Neurodevelopmental Hypothesis of Schizophrenia Morphed Into the Developmental Risk Factor Model of Psychosis. Schizophr Bull. 2017;43(6):1190-6.
139. Brennand KJ, Simone A, Jou J, Gelboin-Burkhart C, Tran N, Sangar S, et al. Modelling schizophrenia using human induced pluripotent stem cells. Nature. 2011;473(7346):221-5.
140. Grunwald LM, Stock R, Haag K, Buckenmaier S, Eberle MC, Wildgruber D, et al. Comparative characterization of human induced pluripotent stem cells (hiPSC) derived from patients with schizophrenia and autism. Transl Psychiatry. 2019;9(1):179.
141. Mulligan KA, Cheyette BN. Wnt signaling in vertebrate neural development and function. J Neuroimmune Pharmacol. 2012;7(4):774-87.
142. Fan Y, Abrahamsen G, McGrath JJ, Mackay-Sim A. Altered cell cycle dynamics in schizophrenia. Biol Psychiatry. 2012;71(2):129-35.
143. Katsel P, Davis KL, Li C, Tan W, Greenstein E, Kleiner Hoffman LB, et al. Abnormal Indices of Cell Cycle Activity in Schizophrenia and their Potential Association with Oligodendrocytes. Neuropsychopharmacology. 2008;33(12):2993-3009.
144. McCurdy RD, Féron F, Perry C, Chant DC, McLean D, Matigian N, et al. Cell cycle alterations in biopsied olfactory neuroepithelium in schizophrenia and bipolar I disorder using cell culture and gene expression analyses. Schizophrenia Research. 2006;82(2):163-73.
145. Shen Y, Vignali P, Wang R. Rapid Profiling Cell Cycle by Flow Cytometry Using Concurrent Staining of DNA and Mitotic Markers. Bio Protoc. 2017;7(16).
146. Hendry SH, Schwark HD, Jones EG, Yan J. Numbers and proportions of GABA-immunoreactive neurons in different areas of monkey cerebral cortex. J Neurosci. 1987;7(5):1503-19.
147. Tamamaki N, Yanagawa Y, Tomioka R, Miyazaki J-I, Obata K, Kaneko T. Green fluorescent protein expression and colocalization with calretinin, parvalbumin, and somatostatin in the GAD67-GFP knock-in mouse. Journal of Comparative Neurology. 2003;467(1):60-79.

148. Paz JT, Huguenard JR. Microcircuits and their interactions in epilepsy: is the focus out of focus? Nature Neuroscience. 2015;18(3):351-9.
149. Ali F, Kwan AC. Interpreting in vivo calcium signals from neuronal cell bodies, axons, and dendrites: a review. Neurophotonics. 2020;7(1):011402.
150. Howes OD, Onwordi EC. The synaptic hypothesis of schizophrenia version III: a master mechanism. Molecular Psychiatry. 2023.
151. Purcell SM, Wray NR, Stone JL, Visscher PM, O'Donovan MC, Sullivan PF, et al. Common polygenic variation contributes to risk of schizophrenia and bipolar disorder. Nature. 2009;460(7256):748-52.
152. Sudhof TC. The cell biology of synapse formation. J Cell Biol. 2021;220(7).
153. Gonzalez-Burgos G, Hashimoto T, Lewis DA. Alterations of cortical GABA neurons and network oscillations in schizophrenia. Curr Psychiatry Rep. 2010;12(4):335-44.
154. Iida S, Shimba K, Sakai K, Kotani K, Jimbo Y. Synchronous firing patterns of induced pluripotent stem cell-derived cortical neurons depend on the network structure consisting of excitatory and inhibitory neurons. Biochemical and Biophysical Research Communications. 2018;501(1):152-7.
155. Kuijlaars J, Oyelami T, Diels A, Rohrbacher J, Versweyveld S, Meneghello G, et al. Sustained synchronized neuronal network activity in a human astrocyte co-culture system. Sci Rep. 2016;6:36529.
156. Becchetti A, Gullo F, Bruno G, Dossi E, Lecchi M, Wanke E. Exact distinction of excitatory and inhibitory neurons in neural networks: a study with GFP-GAD67 neurons optically and electrophysiologically recognized on multielectrode arrays. Frontiers in Neural Circuits. 2012;6.
157. Sellgren CM, Gracias J, Watmuff B, Biag JD, Thanos JM, Whittredge PB, et al. Increased synapse elimination by microglia in schizophrenia patient-derived models of synaptic pruning. Nature Neuroscience. 2019;22(3):374-85.
158. Brandon NJ, Sawa A. Linking neurodevelopmental and synaptic theories of mental illness through DISC1. Nat Rev Neurosci. 2011;12(12):707-22.
159. Heider J, Sperlich D, Vogel S, Breitmeyer R, Volkmer H. Generation of two induced pluripotent stem cell lines (TMOi001-A-5, TMOi001-A-6) carrying variants in DISC1 exon 2 using CRISPR/Cas9 gene editing. Stem Cell Research. 2022;64:102925.
160. Nakata K, Lipska BK, Hyde TM, Ye T, Newburn EN, Morita Y, et al. DISC1 splice variants are upregulated in schizophrenia and associated with risk polymorphisms. Proceedings of the National Academy of Sciences. 2009;106(37):15873-8.
161. Hunt JMT, Samson CA, Rand Ad, Sheppard HM. Unintended CRISPR-Cas9 editing outcomes: a review of the detection and prevalence of structural variants generated by gene-editing in human cells. Human Genetics. 2023;142(6):705-20.
162. Kurosaki T, Maquat LE. Nonsense-mediated mRNA decay in humans at a glance. J Cell Sci. 2016;129(3):461-7.
163. Heider J, Stahl A, Sperlich D, Hartmann S-M, Vogel S, Breitmeyer R, et al. Defined co-cultures of glutamatergic and GABAergic neurons with a mutation in DISC1 reveal aberrant phenotypes in GABAergic neurons. BMC Neuroscience. 2024;25(1):12.
164. Srikanth P, Lagomarsino VN, Pearse RV, 2nd, Liao M, Ghosh S, Nehme R, et al. Convergence of independent DISC1 mutations on impaired neurite growth via decreased UNC5D expression. Transl Psychiatry. 2018;8(1):245.
165. Wen Z, Nguyen HN, Guo Z, Lalli MA, Wang X, Su Y, et al. Synaptic dysregulation in a human iPS cell model of mental disorders. Nature. 2014;515(7527):414-8.
166. Hu W, MacDonald ML, Elswick DE, Sweet RA. The glutamate hypothesis of schizophrenia: evidence from human brain tissue studies. Ann N Y Acad Sci. 2015;1338(1):38-57.
167. Brennand K, Savas JN, Kim Y, Tran N, Simone A, Hashimoto-Torii K, et al. Phenotypic differences in hiPSC NPCs derived from patients with schizophrenia. Molecular Psychiatry. 2015;20(3):361-8.
168. Toyoshima M, Akamatsu W, Okada Y, Ohnishi T, Balan S, Hisano Y, et al. Analysis of induced pluripotent stem cells carrying 22q11.2 deletion. Transl Psychiatry. 2016;6(11):e934.

169. Robicsek O, Karry R, Petit I, Salman-Kesner N, Müller FJ, Klein E, et al. Abnormal neuronal differentiation and mitochondrial dysfunction in hair follicle-derived induced pluripotent stem cells of schizophrenia patients. Molecular Psychiatry. 2013;18(10):1067-76.
170. Hoseth EZ, Krull F, Dieset I, Morch RH, Hope S, Gardsjord ES, et al. Exploring the Wnt signaling pathway in schizophrenia and bipolar disorder. Transl Psychiatry. 2018;8(1):55.
171. Topol A, Zhu S, Tran N, Simone A, Fang G, Brennand KJ. Altered WNT Signaling in Human Induced Pluripotent Stem Cell Neural Progenitor Cells Derived from Four Schizophrenia Patients. Biol Psychiatry. 2015;78(6):e29-34.
172. Kalkman HO. Altered growth factor signaling pathways as the basis of aberrant stem cell maturation in schizophrenia. Pharmacol Ther. 2009;121(1):115-22.
173. Hardwick LJ, Ali FR, Azzarelli R, Philpott A. Cell cycle regulation of proliferation versus differentiation in the central nervous system. Cell Tissue Res. 2015;359(1):187-200.
174. Zuccoli GS, Nascimento JM, Moraes-Vieira PM, Rehen SK, Martins-de-Souza D. Mitochondrial, cell cycle control and neuritogenesis alterations in an iPSC-based neurodevelopmental model for schizophrenia. European Archives of Psychiatry and Clinical Neuroscience. 2023;273(8):1649-64.
175. Okazaki S, Boku S, Otsuka I, Mouri K, Aoyama S, Shiroiwa K, et al. The cell cycle-related genes as biomarkers for schizophrenia. Prog Neuropsychopharmacol Biol Psychiatry. 2016;70:85-91.
176. Cremisi F, Philpott A, Ohnuma S. Cell cycle and cell fate interactions in neural development. Curr Opin Neurobiol. 2003;13(1):26-33.
177. Barnum KJ, O'Connell MJ. Cell cycle regulation by checkpoints. Methods Mol Biol. 2014;1170:29-40.
178. Jackson SP, Bartek J. The DNA-damage response in human biology and disease. Nature. 2009;461(7267):1071-8.
179. Markkanen E, Meyer U, Dianov GL. DNA Damage and Repair in Schizophrenia and Autism: Implications for Cancer Comorbidity and Beyond. Int J Mol Sci. 2016;17(6).
180. Srikanth P, Han K, Callahan DG, Makovkina E, Muratore CR, Lalli MA, et al. Genomic DISC1 Disruption in hiPSCs Alters Wnt Signaling and Neural Cell Fate. Cell Rep. 2015;12(9):1414-29.
181. Wang X, Ye F, Wen Z, Guo Z, Yu C, Huang WK, et al. Structural interaction between DISC1 and ATF4 underlying transcriptional and synaptic dysregulation in an iPSC model of mental disorders. Mol Psychiatry. 2021;26(4):1346-60.
182. Dienel SJ, Lewis DA. Alterations in cortical interneurons and cognitive function in schizophrenia. Neurobiol Dis. 2019;131:104208.
183. Wang S, Hesen R, Mossink B, Nadif Kasri N, Schubert D. Generation of glutamatergic/GABAergic neuronal co-cultures derived from human induced pluripotent stem cells for characterizing E/I balance in vitro. STAR Protoc. 2023;4(1):101967.
184. Wang S, Rhijn JV, Akkouh I, Kogo N, Maas N, Bleeck A, et al. Loss-of-function variants in the schizophrenia risk gene SETD1A alter neuronal network activity in human neurons through the cAMP/PKA pathway. Cell Rep. 2022;39(5):110790.
185. Favuzzi E, Rico B. Molecular diversity underlying cortical excitatory and inhibitory synapse development. Current Opinion in Neurobiology. 2018;53:8-15.
186. Catts VS, Derminio DS, Hahn CG, Weickert CS. Postsynaptic density levels of the NMDA receptor NR1 subunit and PSD-95 protein in prefrontal cortex from people with schizophrenia. NPJ Schizophr. 2015;1:15037.
187. Yamamoto K, Kuriu T, Matsumura K, Nagayasu K, Tsurusaki Y, Miyake N, et al. Multiple alterations in glutamatergic transmission and dopamine D2 receptor splicing in induced pluripotent stem cell-derived neurons from patients with familial schizophrenia. Translational Psychiatry. 2021;11(1):548.
188. Kathuria A, Lopez-Lengowski K, Watmuff B, McPhie D, Cohen BM, Karmacharya R. Synaptic deficits in iPSC-derived cortical interneurons in schizophrenia are mediated by NLGN2 and rescued by N-acetylcysteine. Transl Psychiatry. 2019;9(1):321.
189. Yang N, Chanda S, Marro S, Ng YH, Janas JA, Haag D, et al. Generation of pure GABAergic neurons by transcription factor programming. Nat Methods. 2017;14(6):621-8.

190. Mossink B, van Rhijn JR, Wang S, Linda K, Vitale MR, Zoller JEM, et al. Cadherin-13 is a critical regulator of GABAergic modulation in human stem-cell-derived neuronal networks. Mol Psychiatry. 2022;27(1):1-18.
191. Parodi G, Brofiga M, Pastore VP, Chiappalone M, Martinoia S. Deepening the role of excitation/inhibition balance in human iPSCs-derived neuronal networks coupled to MEAs during long-term development. J Neural Eng. 2023;20(5).
192. Marambaud P, Dreses-Werringloer U, Vingtdeux V. Calcium signaling in neurodegeneration. Molecular Neurodegeneration. 2009;4(1):20.
193. Estevez-Priego E, Moreno-Fina M, Monni E, Kokaia Z, Soriano J, Tornero D. Long-term calcium imaging reveals functional development in hiPSC-derived cultures comparable to human but not rat primary cultures. Stem Cell Reports. 2023;18(1):205-19.
194. Grienberger C, Konnerth A. Imaging calcium in neurons. Neuron. 2012;73(5):862-85.
195. Parnell E, Culotta L, Forrest MP, Jalloul HA, Eckman BL, Loizzo DD, et al. Excitatory Dysfunction Drives Network and Calcium Handling Deficits in 16p11.2 Duplication Schizophrenia Induced Pluripotent Stem Cell–Derived Neurons. Biological Psychiatry. 2023;94(2):153-63.
196. Naujock M, Speidel A, Fischer S, Kizner V, Dorner-Ciossek C, Gillardon F. Neuronal Differentiation of Induced Pluripotent Stem Cells from Schizophrenia Patients in Two-Dimensional and in Three-Dimensional Cultures Reveals Increased Expression of the Kv4.2 Subunit DPP6 That Contributes to Decreased Neuronal Activity. Stem Cells Dev. 2020;29(24):1577-87.
197. Schmitt A, Uhrig S, Spanagel R, von Wilmsdorff M, Kalman JL, Schneider-Axmann T, et al. Post-mortem gene expression of calcium channels Cav1.2 and Cav1.3 in schizophrenia. Eur Arch Psychiatry Clin Neurosci. 2022;272(7):1135-7.
198. Smedler E, Louhivuori L, Romanov RA, Masini D, Dehnisch Ellstrom I, Wang C, et al. Disrupted Cacna1c gene expression perturbs spontaneous Ca(2+) activity causing abnormal brain development and increased anxiety. Proc Natl Acad Sci U S A. 2022;119(7).
199. Yao Y, Wu M, Wang L, Lin L, Xu J. Phase Coupled Firing of Prefrontal Parvalbumin Interneuron With High Frequency Oscillations. Front Cell Neurosci. 2020;14:610741.
200. Uhlhaas PJ, Singer W. Abnormal neural oscillations and synchrony in schizophrenia. Nat Rev Neurosci. 2010;11(2):100-13.
201. Bianciardi B, Uhlhaas PJ. Do NMDA-R antagonists re-create patterns of spontaneous gamma-band activity in schizophrenia? A systematic review and perspective. Neurosci Biobehav Rev. 2021;124:308-23.
202. Rushton DJ, Mattis VB, Svendsen CN, Allen ND, Kemp PJ. Stimulation of GABA-Induced Ca2+ Influx Enhances Maturation of Human Induced Pluripotent Stem Cell-Derived Neurons. PLOS ONE. 2013;8(11):e81031.
203. Tiihonen J, Koskuvi M, Storvik M, Hyotylainen I, Gao Y, Puttonen KA, et al. Sex-specific transcriptional and proteomic signatures in schizophrenia. Nat Commun. 2019;10(1):3933.
204. Szepesi Z, Manouchehrian O, Bachiller S, Deierborg T. Bidirectional Microglia-Neuron Communication in Health and Disease. Front Cell Neurosci. 2018;12:323.
205. Favuzzi E, Huang S, Saldi GA, Binan L, Ibrahim LA, Fernandez-Otero M, et al. GABA-receptive microglia selectively sculpt developing inhibitory circuits. Cell. 2021;184(15):4048-63 e32.
206. Park GH, Noh H, Shao Z, Ni P, Qin Y, Liu D, et al. Activated microglia cause metabolic disruptions in developmental cortical interneurons that persist in interneurons from individuals with schizophrenia. Nat Neurosci. 2020;23(11):1352-64.
207. Badimon A, Strasburger HJ, Ayata P, Chen X, Nair A, Ikegami A, et al. Negative feedback control of neuronal activity by microglia. Nature. 2020;586(7829):417-23.
208. Millar JK, Pickard BS, Mackie S, James R, Christie S, Buchanan SR, et al. DISC1 and PDE4B are interacting genetic factors in schizophrenia that regulate cAMP signaling. Science. 2005;310(5751):1187-91.
209. Borkowska M, Millar JK, Price DJ. Altered Disrupted-in-Schizophrenia-1 Function Affects the Development of Cortical Parvalbumin Interneurons by an Indirect Mechanism. PLoS One. 2016;11(5):e0156082.

210. Seshadri S, Faust T, Ishizuka K, Delevich K, Chung Y, Kim SH, et al. Interneuronal DISC1 regulates NRG1-ErbB4 signalling and excitatory-inhibitory synapse formation in the mature cortex. Nat Commun. 2015;6:10118.
211. Kang E, Song J, Lin Y, Park J, Lee JH, Hussani Q, et al. Interplay between a Mental Disorder Risk Gene and Developmental Polarity Switch of GABA Action Leads to Excitation-Inhibition Imbalance. Cell Rep. 2019;28(6):1419-28 e3.
212. Canitano R, Pallagrosi M. Autism Spectrum Disorders and Schizophrenia Spectrum Disorders: Excitation/Inhibition Imbalance and Developmental Trajectories. Front Psychiatry. 2017;8:69.
213. Bang J, Kim HY, Lee H. Optogenetic and Chemogenetic Approaches for Studying Astrocytes and Gliotransmitters. Exp Neurobiol. 2016;25(5):205-21.
214. Kim SH, Chang MY. Application of Human Brain Organoids-Opportunities and Challenges in Modeling Human Brain Development and Neurodevelopmental Diseases. Int J Mol Sci. 2023;24(15).
215. Jang H, Kim SH, Koh Y, Yoon KJ. Engineering Brain Organoids: Toward Mature Neural Circuitry with an Intact Cytoarchitecture. Int J Stem Cells. 2022;15(1):41-59.

6. Supplementary Information

Supplementary Figure 1:

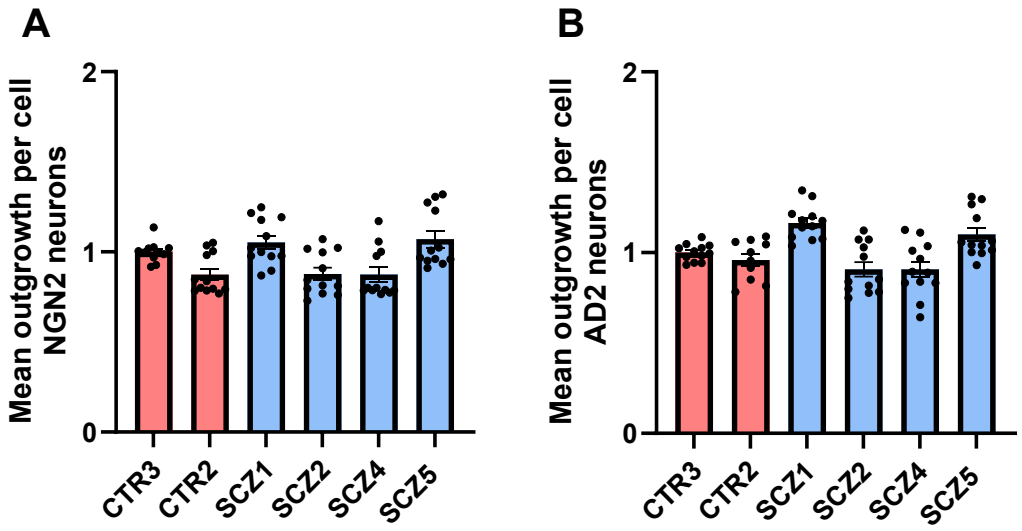

Suppl. Figure 1 Neurite outgrowth of immature neurons generated by directed differentiation.

(A-B) Mean neurite outgrowth per cell in DIV 3 neurons of two CTR and four SCZ donors, generated by direct differentiation via overexpression of NGN2 **(A)** or AD2 **(B)**. Values are normalized to CTR 3. Data points represent individual wells analyzed. Unpaired, two-tailed t-test, ns= not significant, n>10, error bars: S.E.M.

Supplementary Figure 2:

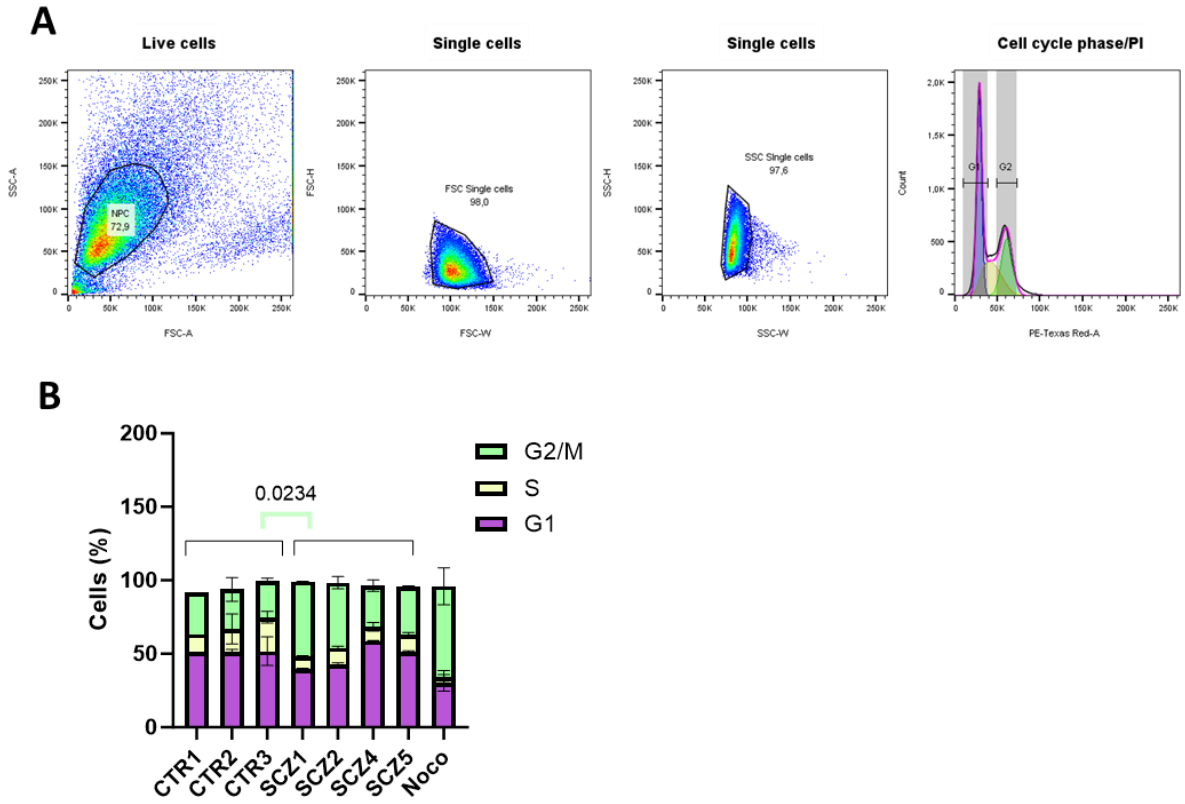

Suppl. Figure 2 Flow cytometry cell cycle analysis of CTR and SCZ NPC.
(A) Gating strategy applied for analysis of flow cytometry cell cycle data to exclude dead cells, doublets and determine cell cycle phases. **(B)** Percentage of NPC in each cell cycle phase for individual CTR and SCZ donors. Indicated significance is taken from statistics performed in Figure 9. Each bar represents > 15,000 events recorded from 1-2 wells per line. $p < 0.05$*. Error bars: S.E.M.

Supplementary Figure 3:

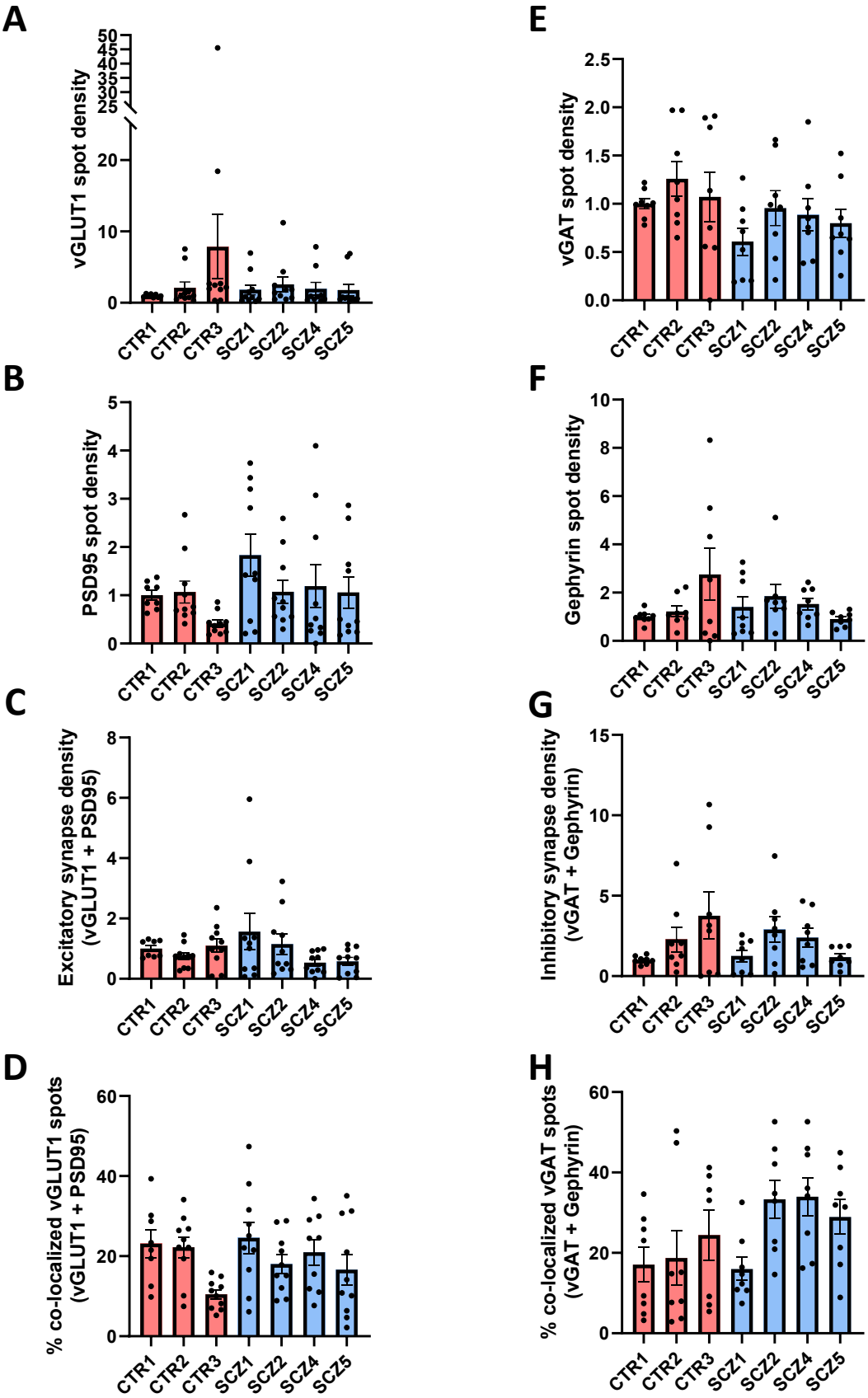

Figure legend on the next page.

Suppl. Figure 3 Quantification of excitatory and inhibitory synaptic markers in NGN2 and AD2 monocultures.

(A-D) Quantification of excitatory synaptic markers on NGN2 neurons from three CTR and four SCZ donors. Density of **(A)** vGLUT1 spots, **(B)** PSD95 spots, **(C)** excitatory synapses (apposition of vGLUT1+ PSD95 spots) and **(D)** percentage of vGLUT1 spots co-localizing with postsynaptic PSD95. **(E-H)** Quantification of inhibitory synaptic markers on AD2 neurons from three CTR and four SCZ donors. Density of **(E)** vGAT spots, **(F)** Gephyrin spots, **(G)** inhibitory synapses (apposition of vGAT+ Gephyrin spots) and **(H)** percentage of vGAT spots co-localizing with postsynaptic Gephyrin. All values are normalized to CTR1. Data points represent averaged values from multiple images within one well. Data were obtained from five independent experiments per donor. n >6, error bars: S.E.M.

Supplementary Figure 4:

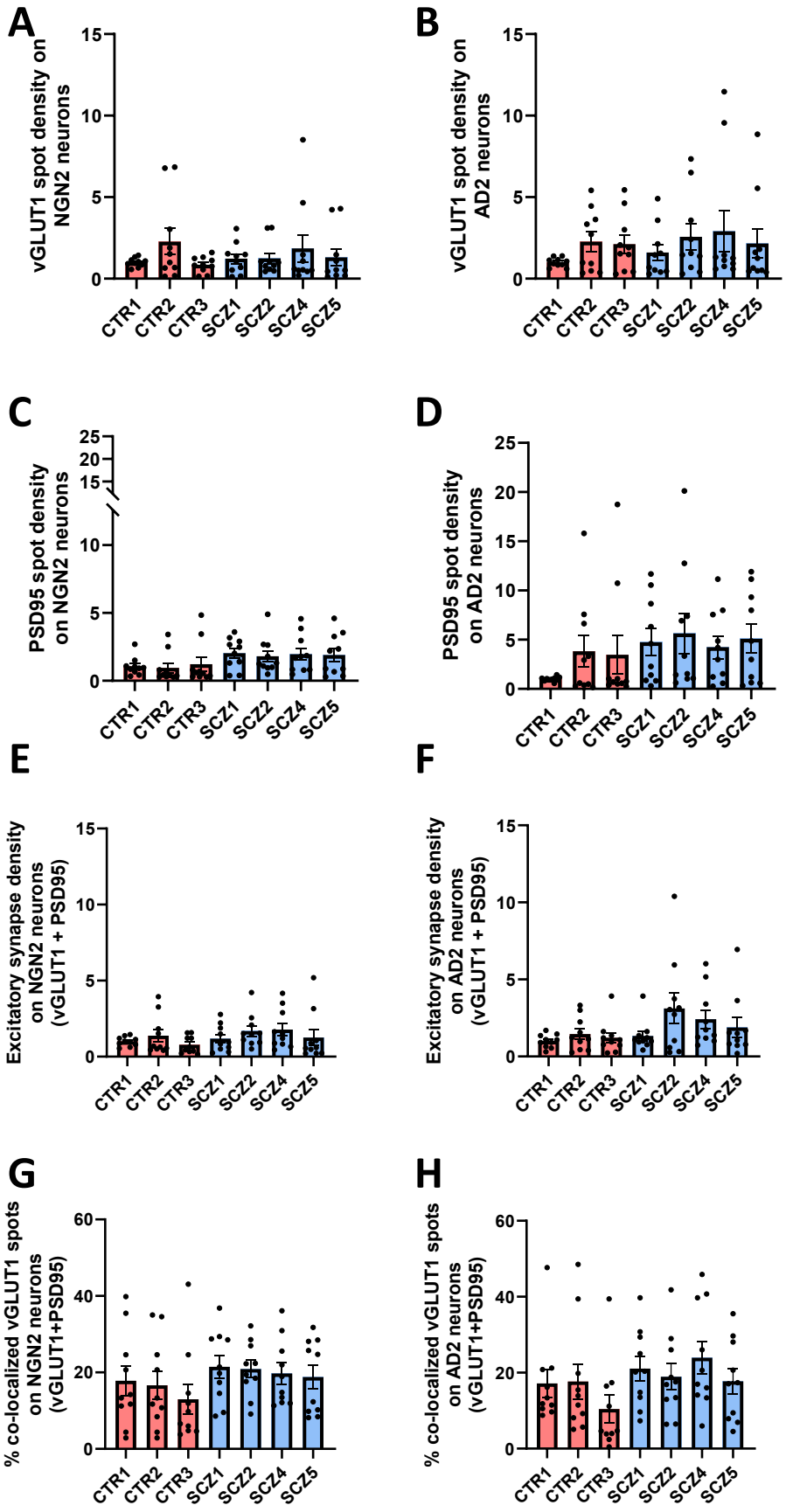

Figure legend on the next page.

Suppl. Figure 4 Quantification of excitatory synaptic markers in E-I co-cultures.

(A, C, E, G) Quantification of excitatory synaptic markers on NGN2 neuros from three CTR and four SCZ donors. Density of **(A)** vGLUT1 spots, **(C)** PSD95 spots, **(E)** excitatory synapses (apposition of vGLUT1+ PSD95 spots) and **(G)** percentage of vGLUT1 spots co-localizing with postsynaptic PSD95. **(B, D, F, H)** Quantification of excitatory synaptic markers on AD2 neuros from three CTR and four SCZ donors. Density of **(B)** VGLUT1 spots, **(D)** PSD95 spots, **(F)** excitatory synapses and **(H)** percentage of vGLUT1 spots co-localizing with postsynaptic PSD95. All values are normalized to CTR1. Data points represent averaged values from multiple images within one well. Data were obtained from five independent experiments per donor. n= 10, error bars: S.E.M.

Supplementary Figure 5:

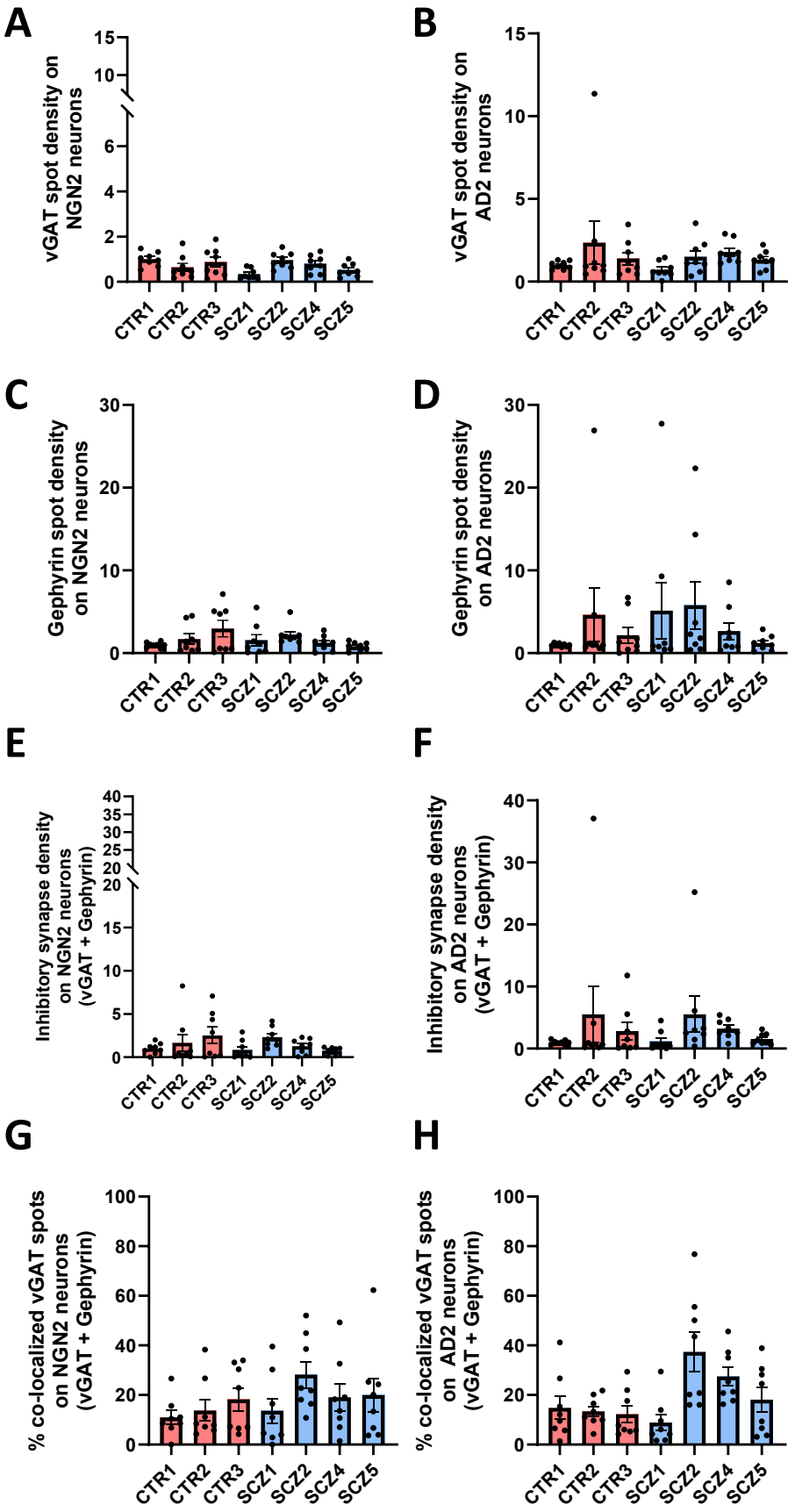

Figure legend on the next page.

Suppl. Figure 5 Quantification of inhibitory synaptic markers in E-I co-cultures.

(A, C, E, G) Quantification of inhibitory synaptic markers on NGN2 neurons from three CTR and four SCZ donors. Density of **(A)** VGAT spots, **(C)** Gephyrin spots, **(E)** inhibitory synapses (apposition of vGAT+Gephyrin spots) and **(G)** percentage of vGAT spots co-localizing with postsynaptic Gephyrin. **(B, D, F, H)** Quantification of inhibitory synaptic markers on AD2 neurons from three CTR and four SCZ donors. Density of **(B)** VGAT spots, **(D)** Gephyrin spots, **(F)** inhibitory synapses and **(H)** percentage of vGAT spots co-localizing with Gephyrin. All values are normalized to CTR1. Data points represent averaged values from multiple images within one well. Data were obtained from four independent experiments per donor. n= 8, error bars: S.E.M.

Supplementary Figure 6:

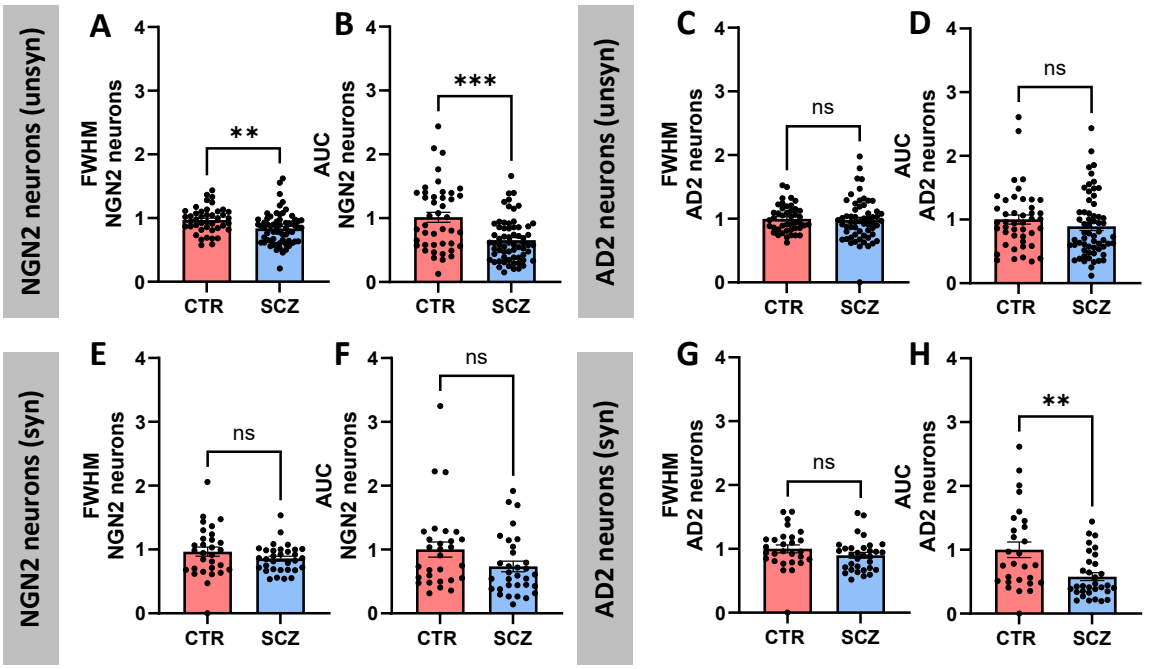

Suppl. Figure 6 Single-cell calcium imaging of unsychronized and synchronized neuronal activity.

(A-D) Analysis of calcium peak characteristics of DIV28 unsynchronized (=unsyn) NGN2 and AD2 neurons. FWHM and AUC were analyzed in CTR and SCZ samples. Data points represent averaged values from multiple neurons within one well. Data were obtained from a minimum of three independent experiments per donor. Two-tailed Mann Whitney U tests, n >40, error bars: S.E.M. **(E-H)** Analysis of calcium peak characteristics (FWHM, AUC) of DIV28 synchronized (=syn) NGN2 and AD2 neurons. Data points represent averaged values from multiple synchronous neurons within one recording across seven independent experiments. Two-tailed Mann Whitney U tests, ns= not significant, n >27, error bars: S.E.M. p≤0.01**, p≤0.001***.

Supplementary Figure 7:

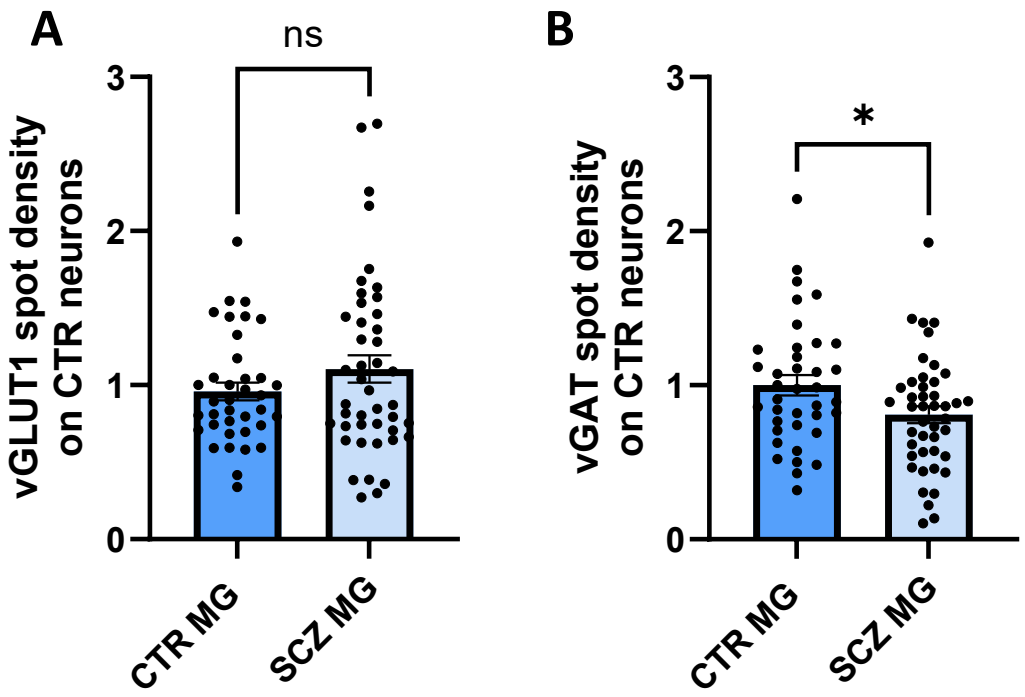

Suppl. Figure 7 Independent replication of presynaptic quantifications in neuron-microglia co-cultures.

(A, B) Quantification of vGLUT1-positive presynaptic density **(A)** and vGAT-positive presynaptic density **(B)** in CTR E-I co-cultures after 72 h co-cultivation with CTR/SCZ microglia. Data points represent individual images analyzed. Values are normalized to CTR neurons + CTR microglia. Data were obtained from three independent differentiations. Two-tailed Mann Whitney U test, n≥37, p≤0.05*, ns= not significant. Error bars: S.E.M.

Supplementary Table 1:

	Sample		
Locus	Isogenic control	DISC1+/-	DISC1 -/-
D8S1179	9,15	9,15	9,15
D21S11	29,29	29,29	29,29
D7S820	10,12	10,12	10,12
CSF1PO	11,11	11,11	11,11
D3S1358	15,18	15,18	15,18
TH01	9,9.3	9,9.3	9,9.3
D13S317	9,11	9,11	9,11
D16S539	11,13	11,13	11,13
D2S1338	17,24	17,24	17,24
D19S433	12,14	12,14	12,14
vWA	17,18	17,18	17,18
TPOX	8,8	8,8	8,8
D18S51	15,15	15,15	15,15
AMEL	X,X	X,X	X,X
D5S818	11,12	11,12	11,12
FGA	22,25	22,25	22,25

Suppl. Table 1 STR analysis DISC1 iPSC lines.

7. Publications

Parts of this thesis are published in:

Heider J, Sperlich D, Vogel S, Breitmeyer R, Volkmer H. Generation of two induced pluripotent stem cell lines (TMOi001-A-5, TMOi001-A-6) carrying variants in DISC1 exon 2 using CRISPR/Cas9 gene editing. *Stem Cell Res*. **2022**; 64:102925. doi:10.1016/j.scr.2022.102925

Breitmeyer R, Vogel S, **Heider J,** et al. Regulation of synaptic connectivity in schizophrenia spectrum by mutual neuron-microglia interaction. *Commun Biol.* 6, 472 (**2023**). doi:10.1038/s42003-023-04852-9

Heider J, Stahl A, Sperlich D, et al. Defined co-cultures of glutamatergic and GABAergic neurons with a mutation in DISC1 reveal aberrant phenotypes in GABAergic neurons. *BMC Neurosci*. **2024**;25(1):12. doi:10.1186/s12868-024-00858-z

Heider J*, Pardo González E*, et al. (2024). Aberrant neuronal connectivity and network activity of neurons derived from patients with idiopathic schizophrenia. *Neurobiol Dis.* Vol 201, 106678. doi: 10.1016/j.nbd.2024.106678

Published review articles:

Heider J, Vogel S, Volkmer H, Breitmeyer R. Human iPSC-Derived Glia as a Tool for Neuropsychiatric Research and Drug Development. *Int J Mol Sci*. **2021**;22(19):10254. Published 2021 Sep 23. doi:10.3390/ijms221910254

Heider J*, Hartmann S-M*, Wüst R*, Fallgatter AJ, Volkmer H. Microglia-neuron interactions in schizophrenia. *Frontiers in Cellular Neuroscience*. **2024**;18.

*= shared first authorship

8. Acknowledgements

An dieser Stelle möchte ich mich bei den vielen Personen bedanken, die mich bei der Anfertigung dieser Arbeit unterstützt haben.

Zunächst gilt mein größter Dank Prof. Hansjürgen Volkmer, der mir die Möglichkeit gegeben hat, meine Doktorarbeit in seiner Arbeitsgruppe anzufertigen. Ich danke dir für die stete Unterstützung, Beratung und all die spannenden wissenschaftlichen Diskussionen. Danke dass du mir immer so viel Freiraum gegeben hast, meine Ideen in die Tat umzusetzen und für die vielen Möglichkeiten meine Arbeit in Vorträgen und auf Konferenzen vorzustellen.

Danken möchte ich außerdem Prof. Andrea Burgalossi für die Betreuung und Begutachtung meiner Arbeit.

Ein ganz besonderer Dank gilt Sophia Hartmann, Sabrina Vogel und Lisa Wüstner. Danke für eure wunderbare Unterstützung und Zusammenarbeit nicht nur in Labor und Zellkultur, sondern ganz besonders eure großartigen Ratschläge zu allen wissenschaftlichen Belangen und natürlich euren emotionalen Support und eure Freundschaft, die mir sehr geholfen hat, wenn es mal nicht ganz so rund lief.

Außerdem möchte ich mich bei allen meinen Kollegen und Kolleginnen im 3. Stock bedanken. Viele von euch sind zu guten Freunden geworden und ich werde unsere gemeinsamen Mittagspausen und Ausflüge nach der Arbeit immer in sehr guter Erinnerung behalten.

Großer Dank gilt auch meiner Familie, die mir immer zur Seite stand und mich durch alle Höhen und Tiefen begleitet hat.

Zuletzt noch ein besonders großer Dank an Aaron Stahl. Du hast mich immer bedingungslos unterstützt, motiviert und wieder aufgebaut, wenn der Stress mal zu groß wurde. Ich bin sehr froh, dass wir sogar die Möglichkeiten hatten, zusammen an unserem eigenen Projekt zu arbeiten, und bin stolz was wir gemeinsam erreicht haben.